UNIVERSITY OF NATAL

THE USE OF INFRARED THERMOMETRY FOR IRRIGATION SCHEDULING OF CEREAL RYE (*Secale cereale* L.) AND ANNUAL RYEGRASS (*Lolium multiflorum* Lam.)

by

MICHAEL G. MENGISTU

B.Sc. Agric (Soil and Water Conservation), University of Asmara

Submitted in partial fulfilment of the requirement for the degree of

MASTER OF SCIENCE IN AGRICULTURE

(Agricultural and Environmental Instrumentation)

in Agrometeorology, SPACRU, School of Applied Environmental Sciences

Faculty of Science and Agriculture

University of Natal

Pietermaritzburg

South Africa

July 2003

DECLARATION

I ..MICHAEL MENGISTU... hereby certify that the research work reported in this thesis is the result of my own original investigations except where acknowledged.

Signed .Michael.....

Michael G. Mengistu

Signed .....

Professor Michael J. Savage

Professor of Agrometeorology

ACKNOWLEDGEMENTS

I would like to express my most sincere gratitude to:

Professor M. J. Savage, Agrometeorology Discipline, School of Applied Environmental Sciences, for his excellent supervision, patience, commitment and encouragement throughout my study period;

Dr CS Everson of the CSIR for his co-supervision;

Ms Jothimala Moodley and Mr. Peter Dovey, Agrometeorology Discipline, for the diversified help during field and laboratory work. Their contribution facilitated an excellent working environment;

Ms. Bezuidenhout from Cedara Department of Agricultural and Environmental Affairs for allowing use of facilities in her cereal rye field trial and providing soil data;

Mr. John Morisson from Cedara Department of Agricultural and Environmental Affairs, for allowing to utilise the annual ryegrass field trial;

Mr. E Abib of the Department of Soil Science Discipline for allowing use of laboratory equipment;

I would like to express my special thanks to my friends Michael Abraha, Mussie Gebregiorgis, Tesfalidet Ghebreab and Tekeste Abezgi for assistance during the field work;

the Water Research Commission and the National Research Foundation for previously funding the equipment used in this research;

the World Bank in agreement with the Human Resources Development of the University of Asmara, Eritrea funded the research and this support is gratefully acknowledged.

ABSTRACT

Limited water supplies are available to satisfy the increasing demands of crop production. It is therefore very important to conserve the water, which comes as rainfall, and water, which is used in irrigation. A proper irrigation water management system requires accurate, simple, automated, non-destructive method to schedule irrigations. Utilization of infrared thermometry to assess plant water stress provides a rapid, non-destructive, reliable estimate of plant water status which would be amenable to larger scale applications and would over-reach some of the sampling problems associated with point measurements. Several indices have been developed to time irrigation. The most useful is the crop water stress index (CWSI), which normalizes canopy to air temperature differential measurements, to atmospheric water vapour pressure deficit.

A field experiment was conducted at Cedara, KwaZulu-Natal, South Africa, to determine the non-water-stressed baselines, and CWSI of cereal rye (*Secale cereale* L.) from 22 July to 26 September 2002, and annual (Italian) ryegrass (*Lolium multiflorum* Lam.) from October 8 to December 4, 2002, when the crops completely covered the soil. An accurate measurement of canopy to air temperature differential is crucial for the determination of CWSI using the empirical (Idso *et al.*, 1981) and theoretical (Jackson *et al.*, 1981) methods. Calibrations of infrared thermometers, a Vaisala CS500 air temperature and relative humidity sensor and thermocouples were performed, and the reliability of the measured weather data were analysed.

The Everest and Apogee infrared thermometers require correction for temperatures less than 15 °C and greater than 35 °C. Although the calibration relationships were highly linearly significant the slopes and intercepts should be corrected for greater accuracy. Since the slopes of the thermocouples and Vaisala CS500 air temperature sensor were statistically different from 1, multipliers were used to correct the readings. The relative humidity sensor needs to be calibrated for RH values less than 25 % and greater than 75 %. The integrity of weather data showed that solar irradiance, net irradiance, wind speed and vapour pressure deficit were measured accurately. Calculated soil heat flux was underestimated and the calculated surface temperature was underestimated for most of the experimental period compared to measured canopy temperature. The CWSI was

determined using the empirical and theoretical methods. An investigation was made to determine if the CWSI could be used to schedule irrigation in cereal rye and annual rye grass to prevent water stress. Both the empirical and theoretical methods require an estimate or measurement of the canopy to air temperature differential, the non-water-stressed baseline, and the non-transpiring canopy to air temperature differential. The upper (stressed) and lower (non- stressed) baselines were calculated to quantify and monitor crop water stress for cereal rye and annual ryegrass. The non-water-stressed baselines were described by the linear equations $T_c - T_a = 2.0404 - 2.0424 * VPD$ for cereal rye and $T_c - T_a = 2.7377 - 1.2524 * VPD$ for annual ryegrass. The theoretical CWSI was greater than the empirical CWSI for most of the experimental days for both cereal rye and annual ryegrass. Variability of empirical $(CWSI)_E$ and theoretical $(CWSI)_T$ values followed soil water content as would be expected. The CWSI values responded predictably to rainfall and irrigation. CWSI values of 0.24 for cereal rye and 0.29 for annual ryegrass were found from this study, which can be used for timing irrigations to alleviate water stress and avoid excess irrigation water.

The non-water-stressed baseline can also be used alone if the aim of the irrigator is to obtain maximum yields. However the non-water-stressed baseline determined using the empirical method cannot be applied to another location and is only valid for clear sky conditions. And the non-water-stressed baseline determined using theoretical method requires computation of aerodynamic resistance and canopy resistances, as the knowledge of canopy resistance, however the values it can assume throughout the day is still scarce. The baseline was then determined using a new method by Alves and Pereira (2000), which overcomes these problems. This method evaluated the infrared surface temperature as a wet bulb temperature for cereal rye and annual ryegrass. From this study, it is concluded that the infrared surface temperature of fully irrigated cereal rye and annual ryegrass can be regarded as a surface wet bulb temperature. The value of infrared surface temperature can be computed from measured or estimated values of net irradiance, aerodynamic resistance and air temperature. The non-water-stressed baseline is a useful concept that can effectively guide the irrigator to obtain maximum yields and to schedule irrigation. Surface temperature can be used to monitor the crop water status at any time of the day even on cloudy days, which may greatly ease the task of the irrigator.

TABLE OF CONTENTS

LIST OF FIGURES

LIST OF TABLES

LIST OF APPENDICES

CHAPTER 1

INTRODUCTION

Limited water supplies are available to satisfy the increasing demands of crop production. It is therefore very important to conserve water, which comes as rainfall, and water, which is used in irrigation. Irrigation should be scheduled in order to increase yield per unit of water applied and to increase the quality of the product. If the irrigation scheduling method used does not provide sufficient warning, the crop yields will be reduced because of lack of water, while the other extreme could result in too much water applied and a waste of water and energy (Hatfield, 1983a). Methods currently used are soil water measurements, plant measurements, and evapotranspiration models (Hatfield, 1983a; Reginato, 1990). The role of remote sensing into these various approaches has been investigated in a number of studies (Jackson *et al.*, 1977; Ehrler *et al.*, 1978; Walker and Hatfield, 1979; Clawson and Blad, 1982).

The use of canopy temperature to detect water stress in plants is based upon the assumption that, as water becomes limiting, transpiration is reduced and the plant temperature increases (Hatfield, 1983b; Patel *et al.*, 2001). Early works largely ignored meteorological factors and concentrated by necessity of limited equipment, on measuring the temperature of individual leaves (Jackson *et al.*, 1988). With the development of infrared radiometers, the temperature of groups of leaves could be measured, the controversy concerning plant temperatures to quantify plant water stress investigated (Tanner, 1963). Canopy temperatures are determined by the water status of the plants and by ambient meteorological conditions (Human *et al.*, 1991). The crop water stress index (CWSI), defined by Idso et al. (1981), combines these factors and yields a measure of plant water stress (Human *et al.*, 1991).

Two approaches for scheduling irrigation using infrared thermometry have been proposed: an empirical approach and theoretical approach. Idso *et al.* (1981) presented an empirical method for quantifying crop water stress by determining "non-water-stressed baselines" for crops. These baselines represent the lower limit of temperature that a particular crop canopy would attain if the plants were transpiring at their potential

rate. In addition, estimation of the upper limit of temperature that a non-transpiring crop would attain is necessary (Jackson *et al.*, 1988). This empirical approach has received considerable attention because of its simplicity and the fact that one needs only to measure canopy temperature, air temperature, and the water vapour pressure deficit of the air (Hatfield, 1981; Jackson *et al.*, 1988). It has also, however, received some criticism concerning its inability to account for canopy temperature changes due to solar irradiance (Jackson *et al.*, 1988) and wind speed (O'Toole and Hatfield, 1983; Jackson *et al.*, 1988).

Shortly after the empirical approach was proposed, Jackson *et al.* (1981) presented a theoretical method for calculating the crop water stress index. This theoretical method used an estimate of net irradiance and an aerodynamic resistance factor, in addition to the surface temperature and water vapour pressure terms required by the empirical method of Idso *et al.* (1981). Although the theoretical approach specified how the upper and lower limits could be evaluated, the additional measurements of net irradiance and aerodynamic resistance, and perhaps some equations that appear more complex than they actually are, have resulted in this method not receiving the thorough field tests that the empirical method has undergone (Jackson *et al.*, 1988).

The CWSI method relies on two baselines: the non-water-stressed baseline, that represents a fully watered crop and the maximum stressed baseline, which corresponds to a non-transpiring crop (Idso *et al.*, 1981). The non-water-stressed baseline can also be used alone whenever the aim of the irrigator is to obtain maximum yields (Alves and Pereira, 2000). Alves and Pereira (2000) presented a new definition of a non-water-stressed baseline, theoretically-based and driven by weather variables such as net irradiance, aerodynamic resistance and air temperature that can easily be estimated. This method allows measurements at any time of the day and variable weather conditions, and evaluates the infrared surface temperature, as a wet bulb temperature for irrigation scheduling aiming at maximum yields. In their study, they concluded that the infrared temperature of fully irrigated crops can be regarded as a surface wet bulb temperature, which allows a theoretical derivation of its value when net irradiance, aerodynamic resistance and air temperature are known.

Utilization of infrared thermometry to assess plant water stress provides a rapid, non-destructive and reliable estimate of plant water status which would be amenable to larger scale applications and would overcome some of the sampling problems associated with point measurements. In this study the crop water stress index was determined using both the empirical and theoretical method. The infrared surface temperature was evaluated as a wet bulb temperature, to propose a procedure for the calculation of surface temperature that can be used for irrigation scheduling.

The main objectives of this study were:

i) To determine the non-water-stressed baselines and maximum-stressed baselines for cereal rye and annual ryegrass

ii) To determine the crop water stress index of cereal rye and annual ryegrass using the empirical and theoretical methods

iii) To investigate the use of the crop water stress index for scheduling irrigation of cereal rye and annual ryegrass

iv) To evaluate the infrared surface temperature, T_s, as a wet bulb temperature ($T_s = T_w$) and hence to propose a procedure for the calculation of surface temperature that can be used for irrigation scheduling aiming at maximum yields

In this thesis, the use of infrared thermometry for measuring canopy temperature is discussed in Chapter 2, and the use of crop water stress indices is reviewed in Chapter 3. Chapter 4 deals with general materials and methods and Chapter 5 with calibration of sensors and integrity weather data. Determination of crop water stress index using the empirical and theoretical methods is discussed in Chapter 6, and the infrared surface temperature is evaluated as a wet bulb temperature in Chapter 7.

CHAPTER 2

INFRARED THERMOMETRY FOR MEASURING CANOPY TEMPERATURE

2.1 INTRODUCTION

Accurate measurement of the leaf to air temperature differential is crucial for the determination of CWSI and other plant responses in both single leaves and plant canopies. This differential is often less than 1 °C, which means that the leaf temperature must be known to within about ± 0.1 °C (Bugbee *et al.*, 1999). Radiometric surface thermometers, more commonly known as infrared thermometers (IRT_s) can be calibrated to achieve this accuracy. Infrared thermometers measure the infrared irradiance emitted by an object that is beyond the wavelength sensitivity range of the human eye. Infrared irradiance is electromagnetic radiation within the wavelength interval from about 0.75 μm up to 1000 μm (Sammis, 1996).

Infrared thermometers are filtered to allow only a specific wave band, about 8 to 14 μm, to be transmitted to the IRT detector. This transmitted energy irradiance (E) is converted to temperature (T) *via* the Stefan-Boltzmann law which states $E = \varepsilon\sigma T^4$, where ϵ is the emissivity of the object and σ is the Stefan-Boltzmann constant which is $5.670*10^{-8}$ J m^{-2} s^{-1} K^{-4} (Wikipedia, 2003). Infrared thermometers only sense longwave irradiance, and the amount of long wave irradiance, as sensed by the thermometer is given by:

$$\sigma T^{4}_{measured} = \varepsilon\sigma T^{4}_{leaf} + rL_{d} \qquad 2.1$$

where $T_{measured}$ is the apparent temperature of the leaf, $\varepsilon\sigma T^4_{leaf}$ is the emittance from the leaf surface and rL_d is the amount of long wave irradiance reflected from the leaf surface (Savage, 2001a).

Infrared thermometers have many advantages over conventional thermometers for the measurement of surface temperatures, but they require consideration of target emissivity, field of view, and sensor body temperature (Bugbee *et al.*, 1999). Routine use of infrared thermometers to accurately measure the leaf, foliage, canopy or crop temperature requires that the user be able to estimate target dimensions based on the position of the sensor in relation to the surface being remotely sensed (O'Toole and Real, 1984).

2.2 HISTORICAL PERSPECTIVES

The literature concerning leaf temperature measurement started at least before the early part of the eighteenth century. Nearly a century and a half ago, Rameax (1843) as cited by Ehlers (1915), placed a number of leaves on top of one another and wrapped the stack around a mercury thermometer (Jackson *et al.*, 1988). This experiment may have been the beginning of research concerning the increase in plant temperature in response to water stress (Clawson and Blad, 1982). Later, Wallace and Clum (1938) as cited by Jackson *et al.* (1988), reported leaf temperatures as much as 7 ^{o}C less than air temperature. Curtis (1936, 1938) argued that transpirational cooling could not explain the results, but that erroneous air temperature measurements, radiative cooling, and other factors were the cause (Jackson *et al.*, 1988). Tanner (1963) may have been the first to use infrared thermometry to quantify the relationship of canopy temperature differences and plant water stress. He found a maximum temperature of 3 ^{o}C between irrigated and non-irrigated potatoes.

The work of Ehrler (1973) reported that leaf temperatures could be cooler than air temperature, and were a function of the water vapour pressure deficit of the air. He placed fine wire thermocouples in cotton leaves and measured the air temperature and the water vapour pressure at 1 m above the crop. His results showed plots of leaf-air temperature versus water vapour pressure deficit were linear. Idso *et al.* (1981) used infrared thermometers to measure canopy temperature and presented an empirical approach to develop the crop water stress index (CWSI), which is discussed in more detail in Chapter 3. They found a linear relationship of leaf to air temperature differential versus water vapour pressure deficit in their alfalfa. A review of canopy

temperature and crop water stress research was reported by Jackson *et al.* (1981) and re-examined in 1988 (Jackson *et al.*, 1988).

In the last two decades makers of infrared thermometers have incorporated software into instruments that automatically calculate CWSI for the user but for many growers, researchers, and extension agents the concept is still new and poorly understood (Nielsen *et al.*, 1992a).

2.3 METHODOLOGY

2.3.1 Principles of use of infrared thermometers

Infrared thermometers should be held at a 45-degree angle facing north in northern hemisphere and south in southern hemisphere to take measurements of canopy temperature in fields. Primary precautions that should be taken when using an IRT are the field of view (FOV) and the angle at which the IRT is positioned relative to the object (O'Toole and Real, 1984). A wide FOV, e.g., 15^{0}, will view a large target area and could possibly detect energy emitted by the soil, surrounding plants, or sky (Hatfield, 1990). These objects may be at temperatures different from the intended target and create an error that depends on the magnitude of the temperature difference between the intended target and other objects and the relative area of the FOV they occupy (O'Toole and Real, 1984; Hatfield, 1990).

The field of view of the IRT forms a right circular cone when it is held at an angle to a surface as shown in Fig. 2.1. The view area is a circle of radius given by the following relationship:

$$r = f \tan \frac{FOV}{2} \qquad 2.2$$

where r = radius of the circle, f = perpendicular distance of the view area from the instrument, FOV= field of view (Jackson *et al.*, 1981).

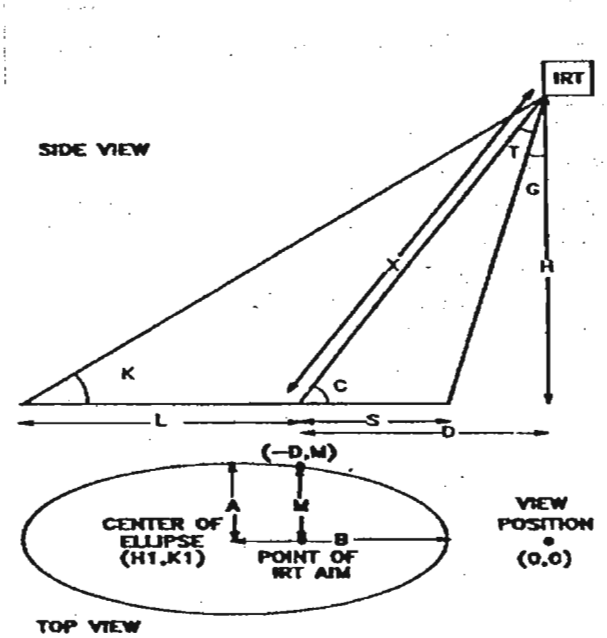

Fig. 2.1 Schematic representation of a spot viewed by an inclined infrared thermometer with angles and lengths noted (Nielson *et al.*, 1992b)

However, there are significant disadvantages to narrow field of view IRTs. The IRTs see less of the target and more of their own temperature, so the best approach is to use a sensor with the widest field of view possible and place it close to the target (Bugbee *et al.*, 1999).

2.3.2 Calibration of infrared thermometers

Like any other instrument, the IRT requires calibration to provide accurate and reliable readings. Calibration of infrared temperature transducers is carried out over a surface with known emissivity and for which actual surface temperatures can be accurately measured (Stigter *et al.*, 1982). Calibrations of the IRTs are best made in controlled situations where the ambient temperature around the instrument can be maintained relatively constant and the target temperature varied from 0 to 50 °C (Hatfield, 1990).

Blad and Rosenberg (1976) used an aluminum plate as a source of black body radiation. They immersed it in a water bath and raised the temperature of the water bath gradually from 0 to 50 °C. They found calibration expressions developed by best fitting data with linear and quadratic expressions.

Generally IRTs can be calibrated using the following two methods: the black body calibrator and the water cone calibrator.

2.3.2.1 *Black body calibrator*

Accurate calibration requires rigorous control of the sensor body temperature in addition to control of the target black body temperature (Bugbee *et al.*, 1999). A calibration device that independently controlled the sensor and target temperatures was built following the design described by Kalma *et al.* (1988). The calibration unit consists of a separate sensor block and a conical black body. The sensor block accommodates up to four sensors simultaneously. The black body cone was 90 mm long with a 38 mm diameter. The cone shape increases the effective emissivity of the black body approximately by the ratio of the surface area of the cone to the surface area of the opening (Kalma *et al.*, 1988). The two housings are separated thermally with 6 mm thick insulating material and nylon bolts. The sensors were inserted into cylindrical holes in the sensor block facing the black body. The temperature of the sensor body was measured by averaging thermocouples placed beside each of the sensors inside the sensor holes. The temperature uniformity of the sensor block was within ± 0.02 °C. Similarly, the black body temperature was measured by averaging for thermocouples placed in 1 mm holes drilled in the top, sides, bottom of the conical housing (Bugbee *et al.*, 1999).

2.3.2.2 *Water cone calibrator*

Water has an emissivity of 0.96, so a water cone calibrator is used to verify the black body calibration of the IRTs (Bugbee *et al.*, 1999; Savage, 2001b). This calibrator consists of a 2 to 5 litre beaker filled with water and placed on a magnetic stirring hot plate. The water is stirred with a large stirring bar to increase the effective emissivity of the water. The water temperature is measured by a number of thermocouples spread out throughout the beaker. IRT sensors are positioned just above the centre of the water cone facing downward. The water temperature is altered by changing the set point of the thermostat on the hot plate. This arrangement is a simple, low cost method compared to the more complex black body calibrator.

2.4 FACTORS AFFECTING CANOPY TEMPERATURE MEASUREMENTS

2.4.1 Instrumentation factors affecting canopy temperature measurements

Most hand-held IRTs are powered by rechargeable batteries. It is essential that these batteries be regularly and fully recharged to ensure accurate readings. IRTs can go off calibration. Calibration should be checked periodically by comparing the IRT output with that of a target black body varying in temperature under ambient temperature conditions covering the range expected when the instrument is used in the field (Nielsen *et al.*, 1992a). Location of the air temperature and water vapour pressure deficit measuring instrumentation can also affect canopy temperature measurements. IRTs have varying fields of view that can affect the area of the canopy viewed. The spot size should be calculated based on the IRT field of view, view angle, and distance from target (O'Toole and Real, 1984).

The one problem with an IRT is that it senses the combination of the temperature of sunlit leaves and shaded leaves as well as the temperature of plant parts deep in the canopy (Savage *et al.*, 1997a) and soil temperature (Jones, 1999). It includes measures of the surface temperature of leaves that may not be actively transpiring (Savage, 2002a). detailed anisotropy of thermal infrared exitance above and within a relatively closed fully irrigated sunflower canopy. They found azimuthal variation in thermal infrared exitance above canopies was weakly (statistically) related to solar position. However they stated that estimating canopy surface temperature from below the canopy results in large errors (1.5 to 8 °C) and is not recommended, because the closed canopy of their fully irrigated sunflower crop was relatively homogeneous. The measured anisotropy represents a minimal case relative to the spatial and physiological heterogeneity of many natural plant communities (Paw U *et al.*, 1989).

2.4.2 Environmental factors affecting canopy temperature measurements

O'Toole and Hatfield (1983) found that canopy temperature measured with an IRT declined with increasing wind speed. This occurs in response to the decline in aerodynamic resistance to sensible heat transfer that occurs with increasing wind speed.

An additional environmental factor to be aware of when using infrared thermometry is the solar irradiance level. Solar irradiance influences the radiative heat load on the plant canopy (Nielsen *et al.*, 1992a), as does the azimuth angle (Paw U *et al.*, 1989).

2.4.3 Plant factors affecting canopy temperature measurements

Solar irradiance by its influence on the radiative heat load of the plant is an important factor affecting measured canopy temperature. But even when incoming solar irradiance levels are high and nearly constant, there is still variability in the measured canopy temperature due to the differing radiative heat load between sunlit and shaded leaves (Nielsen *et al.*, 1992a). Shaded leaves can be much cooler than sunlit leaves, resulting in canopy to air temperature differential ($T_c - T_a$) values much lower than predicted by the non-water-stressed baseline equation. If the objective is to measure the maximum water stress on the plant, then measurements of mostly sunlit leaves are preferable since these leaves are more likely to experience water stress sooner and to a greater degree than shaded leaves (Nielsen *et al.*, 1992a). However, a measurement of mostly sunlit leaves is difficult. Paw U *et al.* (1989) measured higher leaf temperatures and higher thermal infrared exitances in the azimuthal direction opposite to the sun. They said this supports the hypothesis that preferential viewing of sunlit canopy relative to shaded parts produces higher readings. A view with the sun behind the infrared thermometer sees mostly sunlit, warm leaves while a view facing the sun may see more shaded and, cool leaves of maize canopy (Campbell and Norman, 1990).

CHAPTER 3

CROP WATER STRESS INDICES

3.1 INTRODUCTION

There are many ways to quantify plant water stress. One commonly used method is to use crop water stress index (CWSI). This is a measure of the relative transpiration rate occurring from a plant at the time of measurement using a measure of plant temperature and the water vapour pressure deficit which is a measurement of the dryness of the air (Sammis, 1996). Initially, a stress-degree-day value computed as canopy (T_c) minus air (T_a) temperature or (T_c - T_a) measured at midday and accumulated during the growing season was related to yield (Jackson *et al.*, 1977; Walker and Hatfield, 1979). This was followed by an empirical derivation of the CWSI by Idso *et al.* (1981) and a derivation based on energy balance principles by Jackson *et al.* (1981).

In the concept of CWSI there is a theoretical upper and lower limit for (T_c - T_a) at any given water vapour pressure deficit (Wanjura *et al.*, 1990). Wanjura *et al.* (1984) reported that CWSI appears to be crop specific and independent of environmental variability, except for cloud cover. A measure of canopy temperatures is related to the ratio of actual evapotranspiration (ET_a) to potential evapotranspiration (ET_p) using the water vapour pressure deficit and air temperature values in the procedure of Idso *et al.* (1981). In the energy balance procedure of Jackson *et al.* (1981), the CWSI is shown to be theoretically analogous to [1 - (ET_a)/ (ET_p)]. The CWSI is an improved description of plant stress condition over the stress-degree-day parameter, since CWSI is related to plant water potential and available soil water (Idso, 1982).

3.2 DETERMINATION OF CROP WATER STRESS INDEX

3.2.1 Empirical method

Idso *et al.* (1981) defined CWSI as

$$CWSI = \frac{(T_c - T_a) - (T_c - T_a)_{LL}}{(T_c - T_a)_{UL} - (T_c - T_a)_{LL}} \qquad 3.1$$

where $(T_c - T_a)$ is the actual measured canopy to air temperature differential (°C), $(T_c - T_a)_{LL}$ is the lower limit of canopy to air temperature differential (°C), and $(T_c - T_a)_{UL}$ is the upper limit of canopy to air temperature differential (°C).

The actual canopy temperature (T_c) is obtained from measurements made with an infrared thermometer. The lower limit of canopy to air temperature differential $(T_c - T_a)_{LL}$ is the non-water-stressed baseline which is equal to a + b* VPD (°C), where VPD is the water vapour pressure deficit (kPa), a is intercept of the non-water-stressed baseline (°C), and b is the slope of the non-water-stressed baseline (°C kPa^{-1}). Measurements of T_a and VPD have been obtained in several ways, including use of a psychrometer to get dry and wet bulb temperature, or other air temperature and humidity measuring devices.

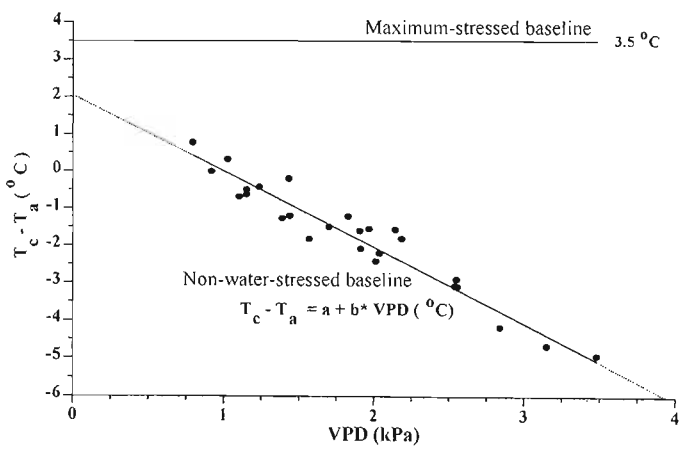

Fig. 3.1 Crop water stress index calculation based on the Idso method of relating $(T_c - T_a)$ and water vapour pressure deficit (Hatfield, 1990)

The value of CWSI can range from 0 (no stress) to 1 (maximum stress). Jackson *et al.* (1981) described this is "aesthetically pleasing", since scientists studying plant water relations often consider the ratio ET_a/ ET_p, which similarly ranges from 1 (ample water) to 0 (no available water).

The non-water-stressed baseline equation shows the dependency of $T_c - T_a$ on VPD (Fig. 3.1). As VPD increases due to either increasing air temperature or declining atmospheric water vapour pressure, the crop temperature becomes cooler relative to the air temperature. The non-water-stressed baseline equation can be determined empirically for well-watered crops from simultaneous measurements of T_c, T_a and VPD (Nielsen *et al.*, 1992b). Non-water-stressed baselines appear to be crop specific, and reported relationships for different crops are shown in Table 3.1 (Idso, 1982; Nielsen, 1990). Development of a non-water-stressed baseline at a single location is often limited by the VPD range that occurs, thereby limiting the baseline's transferability to other locations (Idso, 1982; Stockle and Dugas, 1992; Nielsen *et al.*, 1992b; Jones, 1999).

The value $(T_c - T_a)_{UL}$ in Eq. 3.1 and Fig. 3.1 is the value that occurs when no transpiration is occurring in the plant such that the radiant and convective heat exchange terms dominate in the energy balance of the canopy. Idso *et al.* (1981) showed that $(T_c - T_a)_{UL}$ is a function of air temperature, but variation of $(T_c - T_a)_{UL}$ was small within the limits of typical midday temperatures during the crop-growing season.

The use of this method has been criticized because of its inability to account for changes in canopy temperature due to solar irradiance and wind speed (Jackson *et al.*, 1988). O'Toole and Hatfield (1983) compared the empirically-estimated upper limit with measured values on severely water stressed crops and found that the poor agreement between measurements and estimates was mostly explained by fluctuations in wind speed. Furthermore, none of these authors tried to explain the problem of auto-self-correlation that exists between $T_c - T_a$ and VPD (Savage, 2001b).

Table 3.1 Results of linear regression analysis $T_c - T_a$ *vs* VPD (Idso, 1982)

Common Name	Scientific Name	Conditions	n	I	b	r	Syx	SI	Sb
Alfalfa	*Medigo sativa* L.	Sunlit	229	0.51	-2.92	0.953	0.65	0.11	0.041
Barley	*Hordeum vulgaris* L.	Sunlit pre-heading	34	2.01	-2.25	0.971	0.17	0.22	0.098
		Sunlit post-heading	72	1.72	-1.23	0.86	0.40	0.24	0.087
Bean	*Phaseolus vulgaris* L.	Sunlit	265	2.91	-2.36	0.978	0.72	0.11	0.031
		Shaded	65	-1.57	-2.11	0.973	0.39	0.17	0.064
Beet	*Beta vulgaris* L.	Sunlit	54	5.16	-2.3	0.982	0.46	0.16	0.060
Chard	Beta vulgaris L.(Cicla)	Sunlit	69	2.46	-1.88	0.955	0.58	0.17	0.071
Corn	*Zea Mays* L.	Sunlit	97	3.11	-1.97	0.985	0.32	0.1	0.035
Cotton	*Gossipuim hirsutum* L.	Sunlit	181	1.49	-2.09	0.971	0.38	0.13	0.038
Cowpea	*Vignia catjang Walp*	Sunlit	60	1.32	-1.84	0.991	0.34	0.14	0.034
Cucumber	*Cucumis sativus* L.	Sunlit	109	4.88	-2.52	0.962	0.82	0.23	0.069
		Shaded	59	-1.28	-2.14	0.982	0.57	0.19	0.054
Fig tree	*Ficus carica* L.	Sunlit	119	4.22	-1.77	0.924	0.66	0.21	0.068
Guyate	*Parthenium argentatum*	Sunlit	62	1.87	-1.75	0.928	0.89	0.31	0.094
Kohlrabi	*Brassica oleracea*	Sunlit	70	2.01	-2.17	0.979	0.46	0.13	0.054
Lettuce leaf	*Lactuca scariola* L.	Sunlit	89	4.18	-2.96	0.993	0.63	0.03	0.021
Pea	*Posmum sativum* L.	Sunlit	85	2.74	-2.13	0.951	0.54	0.17	0.076
Potato	*Solanum tuberasum* L.	Sunlit	26	1.17	-1.83	0.922	0.67	0.45	0.157
Pumpkin	*Cucurbita Pepo* L.	Sunlit	76	0.95	-1.93	0.978	0.46	0.22	0.048
		Shaded	89	-1.32	-2.1	0.985	0.47	0.14	0.039
Rutabaga	*Brassica napo brassica*	Sulit	91	3.75	-2.66	0.988	0.54	0.14	0.044
	Ruta baga A.P.DC	Shaded	53	-0.50	-2.51	0.913	0.86	0.37	0.157
Soybean	*Glicina max L.Merr.*	Sunlit	125	1.44	-1.34	0.897	0.83	0.18	0.060
Squash, hubbard	*Cucurbita Pepo* L.	Sunlit	90	6.91	-3.09	0.983	0.8	0.22	0.062
		Shaded	11	2.12	-2.83	0.993	0.65	0.44	0.113
Squash, zuchini	*Cucurbita Pepo* L.	Sunlit	87	2.00	-1.88	0.935	0.38	0.17	0.036
Sugar beet	*Beta vulgaris* L.	Sunlit	47	2.50	-1.92	0.898	0.78	0.40	0.140
Tomato	*Lycopersicum suculentum M.*	Sunlit	103	2.86	-1.96	0.936	0.64	0.13	0.033
Turnip	*Brassica rapa* L.	Sunlit	129	1.94	-2.26	0.979	0.63	0.14	0.042
Water lily	*Nuphar lateum Sibth. & Sm.*	Sunlit	36	8.99	-1.93	0.866	0.65	0.86	0.192
		Shaded	Not applicable to curvilinear relationship						
Wheat, produra	*Triticum durum Desf*	Sunlit pre-heading	161	3.33	-3.25	0.947	0.63	0.15	0.87
		Sunlit post-heading	56	2.88	-2.11	0.939	0.53	0.28	0.105

n = number of data points, I = Intercept, b = slope, r = correlation coefficient, S_{yx} = standard error estimate of Y on X S_I = standard error of the regression coefficient I, and S_b = standard error of the regression coefficient of b, for the linear equaton $Y = I + bX$, with temperature expressed in °C and water vapour pressure in kPa.

3.2.2 Theoretical approach

As defined by Jackson *et al.* (1981) the theoretical development of the crop water stress index is based on the energy balance at a crop surface, i.e.,

$$Rn = G + H + \lambda E \qquad 3.2$$

where R_n the net irradiance (W m^{-2}), G is the heat flux density into the surface (W m^{-2}), H is the sensible heat flux density (W m^{-2}) into the air above the surface, and λE is the latent heat flux (W m^{-2}). The terms H and λE in Eq. 3.2 can be expressed as,

$$H = \rho Cp(Tc - Ta)/ra \qquad 3.3$$

and,

$$\lambda E = \rho Cp(ec^{*} - ea)/[\gamma(ra + rc)] \qquad 3.4$$

where ρ is the density of air (kg m^{-3}), C_p the specific heat capacity of air (J kg^{-1} $^{o}C^{-1}$), T_c the canopy temperature (^{o}C), T_a the air temperature (^{o}C), e_c^{*} the saturated water vapour pressure of the air (Pa) at T_c, e_a the water vapour pressure of the air (Pa), γ the psychrometric constant (Pa $^{o}C^{-1}$), r_a the aerodynamic resistance (s m^{-1}), and r_c the canopy resistance (s m^{-1}).

Eqs 3.3 and 3.4 are based on several assumptions. One is that aerodynamic resistance (r_a) adequately represents the resistance to turbulent transport of heat (r_{ah}), water vapour (r_{av}), and momentum (r_{am}). As cited by Jackson *et al.* (1988), Thom (1972) noted that this is not theoretically correct because transport processes of scalars (i.e., heat, water vapour, carbon dioxide, etc.) differ from momentum transfer for vegetated surfaces. Pressure drag augments the transfer of momentum relative to scalar quantities and therefore r_a is less than either r_{ah} or r_{av} (Jackson *et al.*, 1988).

A second assumption is that the source of latent and sensible heat is primarily from the vegetation. That is, the underlying surface (soil) does not contribute significantly to H and λE values measured above the canopy. Both of these assumptions, although theoretically not valid, will cause only small errors for full canopy, non-stressed conditions because most of the incoming radiation is absorbed, reflected or emitted by the vegetation (Jackson *et al.*, 1988). The errors can be reduced somewhat by considering that G is about 0.1 R_n for full canopies and writing $R_n - G = 0.9R_n = I_c R_n$, Eq. 3.2 becomes $I_c R_n = H + \lambda E$, where I_c is radiation interception coefficient of the canopy. Combining this expression with Eqs 3.3 and 3.4 and defining Δ as the slope of the saturated water vapour pressure temperature relation curve, i.e.,

$$\Delta = (e_c^* - e_a^*)/(T_c - T_a) \qquad 3.5$$

the following equation is obtained:

$$T_c - T_a = \frac{r_a I_c R_n}{\rho Cp} * \frac{\gamma(1 + r_c / r_a)}{\Delta + \gamma(1 + r_c / r_a)} - \frac{(e_a * - e_a)}{\Delta + \gamma(1 + r_c / r_a)}, \qquad 3.6$$

Eq. 3.6 relates the difference between canopy and air temperature to the water vapour pressure deficit of the air $(e_a * - e_a)$, the net irradiance, and the aerodynamic and crop resistances (Jackson *et al.*, 1988).

The upper limit of $T_c - T_a$ can be found by allowing the canopy resistance r_c to increase without bound. As $r_c \rightarrow \infty$, Eq. 3.6 reduces to

$$(Tc - Ta)_{UL} = raIcuRn / \rho Cp \,, \qquad 3.7$$

the case for a non-transpiring crop.

The lower limit, found by setting $r_c = 0$ in Eq. 3.6, is

$$(T_c - T_a)_{LL} = \frac{r_a I_{cl} R_n}{\rho C p} * \frac{\gamma}{\Delta + \gamma} - \frac{e_a * - e_a}{\Delta + \gamma}, \qquad 3.8$$

which is the case for a wet canopy acting as a free water surface. Choudhury *et al.* (1986) noted that aerodynamic resistances in Eqs 3.7 and 3.8 are assumed to be identical, although this assumption is not strictly valid (Jackson *et al.*, 1988).

Theoretically, Eqs 3.7 and 3.8 form the bounds for all canopy-air temperature differences. However, the temperature difference for most well-watered crops will be greater than the lower limit because most crops exhibit some resistance to water flow, even when water is non-limiting. For these crops, the lower limit should be modified by replacing γ in Eq. 3.8 with $\gamma^* = \gamma\ (1+ r_{cp}/ r_a)$ where r_{cp} is the canopy resistance at potential transpiration (Jackson *et al.*, 1988).

A crop water stress index can be defined as

$$CWSI = \frac{(T_c - T_a) - (T_c - T_a)_{LL}}{(T_c - T_a)_{UL} - (T_c - T_a)_{LL}} \qquad 3.9$$

where $(T_c - T_a)$ is the measured temperature difference between the canopy surface and air.

The main problem facing the application of this method is that it requires large uniform fields and local meteorological data and that the complexity of the method precludes a thorough field test (Qiu *et al.*, 1999).

3.3 AERODYNAMIC AND CANOPY RESISTANCES

The first and critical step in the derivation of the Penman-Monteith equation is to reduce the three dimensional crop to a one-dimensional "big leaf" where all of the net irradiance is absorbed and from where water vapour and heat escapes from the canopy (Alves *et al.*, 1996). Since this "big leaf" is not saturated, it is also necessary to consider that there is another surface, at the same temperature, that is saturated and from where water vapour flux originates. So, while heat flux is commanded by a single resistance, the aerodynamic resistance to heat transfer (r_{aH}), water vapour flux encounters two resistances in series, the surface resistance and the aerodynamic resistance to water vapour transfer ($r_s + r_{aV}$). It is usually assumed that $r_{aH} = r_{aV} = r_a$ (Alves *et al.*, 1996).

Aerodynamic resistances can be determined given the values of roughness length (z_o) and zero plane displacement height (d), that depend mainly on crop height, soil cover, leaf area and structure of the canopy (Massman, 1987). The flux of momentum, invariant with height, is maintained between height Z (m), height $d + z_o$ by the potential difference U (wind speed) against a resistance (Jalali-Farahani *et al.*, 1994). This is the aerodynamic resistance to momentum transfer and can be written as (Monteith and Unsworth, 1990):

$$r_a = \frac{(\ln \frac{Z-d}{z_o})^2}{k^2 U} * [1 - \frac{ng(Z-d)(T_c - T_a)}{TU^2}] \qquad 3.10$$

where r_a is the stability-corrected aerodynamic resistance (s m^{-1}), U is wind speed (m s^{-1}) at a height Z (m), d is the zero plane displacement height (m), z_o is the surface roughness length (m), k is von Karman's constant (0.41), g is the acceleration due to gravity (m s^{-2}), T is the average absolute temperature of canopy or air, and n is an empirical constant; the bracketed multiplier contains the correction for stability. Typically, n = 5 for crops and grasses (Hatfield, 1985).

Plant canopy response to environmental conditions is a balance of several energy exchanges, and it has long been recognized that in the canopy there are resistances to water flow from the root, stems, petioles and leaves. However, it has been difficult to

obtain *in situ* canopy resistance measurements, which could be applied to transpiration studies (Hatfield, 1985). The Penman-Monteith equation can be used to determine canopy resistance (Malek *et al.*, 1991; Lindroth, 1993)

$$r_c = r_a/\gamma^* \{[(\Delta(R_n - G) + \rho_{air}Cp_{air}\,\delta e\,/r_a) / \lambda E] - \gamma - \Delta\} \qquad 3.11$$

where λE can be measured using a lysimeter or eddy correlation techniques (Malek *et al.*, 1991). Since, a large fraction of the total radiation available to a canopy is absorbed by the top half of the canopy (Alves *et al.*, 1996), canopy resistance of a crop can be estimated:

$$r_c = r_l / (0.5\,LAI) \qquad 3.12$$

where r_l is the resistance of a full illuminated leaf (Alves *et al.*, 1996).

Canopy resistance for a well-watered crop will not be zero as is the case for a free water surface (Van Bavel and Ehler, 1968), but will exihibit a particular resistance at potential evapotranspiration (r_{cp}) (Jackson *et al.*, 1981). Thus the lower limit of $T_c - T_a$ can be defined by substituting r_{cp} for r_c in Eq. 3.6.

$$(T_c - T_a)_p = \frac{r_a(R_n - G)}{\rho Cp} * \frac{\gamma(1 + r_{cp}/r_a)}{\Delta + \gamma(1 + r_{cp}/r_a)} - \frac{(e_a^* - e_a)}{\Delta + \gamma(1 + r_{cp}/r_a)} \qquad 3.13$$

O'Toole and Real (1986) and Jalali-Farahani *et al.* (1994) described $(T_c - T_a)_p$ as a linear single variable approximation of the Penman-Monteith equation (Eq. 3.11) when all the terms except VPD are held constant. The linear relationship can be expressed as: $(T_c - T_a)_p = a + b^*$ VPD, where a and b are the intercept and slope respectively. By rearranging Eq. 3.11, a and b can be represented:

$$a = \frac{ra(Rn - G)}{\rho Cp} * \frac{\gamma(1 + rcp/ra)}{\Delta + \gamma(1 + rcp/ra)} \qquad 3.14$$

$$b = -\frac{1}{\Delta + \gamma(1 + r_{cp}/r_a)} \qquad 3.15$$

From Eqs 3.14 and 3.15 r_a and r_c for potential ET conditions can be estimated as:

$$r_{ap} = \frac{a\rho Cp}{(R_n - G)(1 + b\Delta)} \qquad 3.16$$

$$r_{cp} = -r_a \frac{1 + b(\Delta + \gamma)}{b\gamma} \qquad 3.17$$

The r_{cp} and r_{ap} resistances are the theoretical canopy and aerodynamic resistances under potential ET conditions.

3.4 APPLICATION OF THE CROP WATER STRESS INDEX

Infrared thermometry has been used as a research tool to measure plant temperature and quantify water stress for over two decades. Several temperature indices have been proposed in the literature: the SDD, which is the canopy-air temperature difference measured post midday near the time of maximum heating; the TSD, which is the difference in canopy temperatures between a stressed crop and non-stressed (well-watered) reference crop; and the CTV, which is the range of temperatures encountered when measuring a plot during a particular measurement period (Jackson, 1982). The CWSI normalizes crop canopy minus air temperature measurements made with an IRT to water vapour pressure deficit, reducing variability in water stress measurements due to environmental variability (Nielsen *et al.*, 1992b). CWSI, while quantifying water stress, does not indicate the amount of water required to refill the root zone to field capacity (Human *et al.*, 1991). This information would have to come from soil water measurements and/or evapotranspiration estimates from equations, such as the modified Penman equations (Nielsen, 1990).

Successful use of CWSI in monitoring water stress and scheduling irrigations requires identification of the category of productivity response to water stress that exists for a particular crop. Each crop has a unique productivity response to water stress.

Consequently, the relationship of CWSI values to crop productivity also varies from crop to crop. Nielsen *et al.* (1992b) identified four general yield qualities versus CWSI relationships to be described below.

3.4.1 Crops extremely sensitive to water stress

Crops in this category cannot be scheduled for irrigation based on changes in CWSI readings, since any water stress that can be detected by a change in CWSI can reduce economic yield. Potatoes (*Solanum tuberosum* L.) are an example of this category of crop. Even though CWSI cannot be used to schedule irrigations for crops in this very sensitive category, CWSI can be used to monitor fields for uniformity of irrigation application or to detect disease problems by looking for hot spots (Nielsen *et al.*, 1992b).

3.4.2 Crops that tolerate mild water stress

Crops in this category can very effectively have irrigations scheduled by CWSI because no significant economic loss is incurred by allowing the plant to experience a mild water stress during the time between stress detection with IRT and application of irrigation. Crops in this category include wheat (*Triticum aestivum* L.), maize (*Zea mays* L.), and cotton. CWSI is allowed to rise between 0.2 and 0.3 index units (on a scale of 0 = no stress, 1 = maximum stress) (Nielsen *et al.*, 1992b).

3.4.3 Crops that tolerate moderate water stress

CWSI can be allowed to rise to moderate levels (0.5 index units) before irrigations are applied. Sugar beet (*Beta vulgaris* L. subsp *vulgaris*) is an example of this category of crop (Nielsen *et al.*, 1992b).

3.4.4 Crops that benefit from severe water stress

Crops in this category actually have improved yield under severe water stress, and CWSI can be used effectively to monitor and control the severity and timing of water stress. Seed alfalfa (*Medicago sativa* L.) is an example of this category of crops. Under

high levels of CWSI, it appears that insect pollinator activity is increased, vegetative growth is restricted producing a more open canopy, and flower production is enhanced. In situations such as alfalfa seed production, it is critical that once extreme stress levels have been reached, that stress be removed with irrigation. CWSI provides an effective means of cycling water stress between high and low levels to promote seed production (Nielsen *et al.*, 1992b).

The definition and determination of CWSI using the empirical and theoretical methods is reviewed. The non-water-stressed baseline used to compute CWSI has been described, and the use of CWSI to quantify water stress in relation to plant productivity discussed. A great deal of research has been conducted over the past three decades relating CWSI and plant temperatures to water stress and plant productivity for many crops. However, it appears to be there is lack of research on CWSI for cereal rye and annual ryegrass reported in the literature. The main aims of this study are to determine the CWSI of cereal rye and annual ryegrass using both the empirical and theoretical methods and to investigate their use for irrigation scheduling (Chapter 6) and to determine the non-water-stressed baselines (Chapter 7).

CHAPTER 4

GENERAL MATERIALS AND METHODS

4.1 SITE AND PLANT DESCRIPTION

The research was conducted at Cedara, located at latitude 29°32' S, longitude 30°17' E, Cedara, in KwaZulu-Natal, South Africa. The site is at an elevation of 1076 m above sea level, and has an approximate slope of 6 % in the N-S direction. The average minimum air temperature cited for the coldest month, July, was –1.9 ° C and the average maximum air temperature for the hottest month January was 33.1 ° C. The main rainy season is October to March with little rainfall during April to September with average monthly rainfall below 100 mm (meteorological data supplied by the Agricultural Research Council, Institute of Soil, Climate and Water, Pretoria). The site has Hutton type of soil according to the binomial classification of soils for South Africa (MacVicar *et al.*, 1977). A summary of the soil characteristics according to USDA taxonomic soil classification for upper and lower slopes of the research site is shown in Table 4.1.

The experiment was conducted on cereal rye (*Secale cereale* L.) from 22nd July to 26th September 2002 when the crop completely covered the soil. The experiment was also conducted on annual (Italian) ryegrass (*Lolium multiflorum* Lam.) from October 8 to December 4, 2002.

Cereal rye is grown in cool temperate zones at high altitudes. It is the most winter hardy of all small cereal grains. Cereal rye is an erect annual grass with flat blades and dense spikes; habit resembles that of wheat, but it is usually taller and the spikes longer and more slender. Cereal rye is a tufted annual 1 to 1.5 m tall, blue green, blades 12 mm broad, long pointed, spike slender, 70 to 150 mm long. It grows best with ample soil water, but in general it does better in low rainfall regions than do legumes, and it can out-yield other cereals on droughty, sandy, infertile soils. Its extensive root system enables it to be the most drought tolerant cereal crop, and its maturation date can alter based on soil water availability. In summary, cereal rye is one of the best crops where fertility is low and winter temperatures are extreme (http://www.sarep.ucdavis.edu, Internet 2002).

Table 4.1 Summary of the soil characteristics

Location	Soil depth	Clay	Silt	Sand	Texture	Particle density	Bulk density	OC	Ca	Mg	Na	K	Fe	SAR	CEC	pH	EC
	(mm)	(%)	(%)	(%)	--	(kg m^{-3})	(kg m^{-3})	(%)	(mol m^{-3})	(mol m^{-3})	(mol m^{-3})	(mol m^{-3})	(mol m^{-3})	_	_	(KCl)	(μS m^{-1})
Upper slope	100	25.80	44.55	29.65	Loam	2520	1294	3.1	0.83	0.60	1.01	0.07	0.14	0.85	2.51	4.49	4.36
	200	30.04	40.06	29.90	Clay loam	2510	1300	2.8	0.58	0.40	0.50	0.06	0.12	0.51	1.55	4.45	2.64
	300	29.30	41.50	29.20	Clay loam	2540	1393	2.8	0.60	0.31	0.57	0.04	0.07	0.59	1.51	4.50	2.58
	400	45.57	28.48	25.95	Clay	2580	1370	1.9	0.52	0.23	0.48	0.06	0.11	0.55	1.30	4.47	2.16
	600	46.71	20.44	32.85	Clay	2600	1315	-	0.49	0.25	0.64	0.03	0.02	0.74	1.41	4.76	2.35
	1000	48.35	21.15	30.50	Clay	2640	1210	-	0.38	0.36	0.86	0.03	0.01	1.00	1.63	4.65	2.62
Lower slope	100	32.20	32.20	35.60	Clay loam	2510	1433	2.3	1.49	1.09	1.48	0.19	0.03	0.92	4.26	4.93	7.58
	200	34.97	34.98	30.05	Clay loam	2590	1391	2.6	0.90	0.61	1.02	0.09	0.11	0.83	2.62	4.56	4.51
	300	34.55	34.55	30.90	Clay loam	2590	1313	1.9	0.82	0.44	0.48	0.08	0.04	0.42	1.82	4.8	3.38
	400	40.68	25.42	33.90	Clay	2500	1411	1.2	0.70	0.34	0.60	0.03	0.03	0.59	1.67	5.32	2.97
	600	38.03	30.42	31.55	Clay loam	2700	1369	-	0.21	0.13	0.45	0.02	0.03	0.77	0.81	5.04	1.24
	1000	47.51	27.94	24.55	Clay	2790	1420	-	0.10	0.13	0.67	0.03	0.03	1.41	0.93	4.40	1.23

OC: Organic carbon CEC: Cation exchange capacity

SAR: Sodium adsorption ratio EC: Electrical conductivity

Annual or Italian ryegrass grows mostly at lower elevations, and is best adapted in coastal areas with long seasons of cool, moist weather. Plants are yellowish-green at the base, with glossy leaves up to 0.31 m length. Annual ryegrass is bunch grass, and it germinates in cooler soils than most other cover crops and pasture seeds. It tolerates temporary floods, and does better than small grains on wet soils, but performs best on well-drained land. In general ryegrass is adapted to irrigated farming, and can grow on sandy soils if they are well fertilized, but do better on heavier clay or silty soils with adequate drainage (http://www.sarep.ucdavis.edu, Internet 2002).

4.2 INSTRUMENTATION OVERVIEW

Two Apogee and one Everest infrared thermometers were used to measure canopy temperature. The IRTs were placed at 2 meters above the soil surface facing south (Fig. 4.1). Water vapour pressure deficit (VPD), relative humidity, and air temperature were measured using Vaisala CS500 relative humidity and air temperature sensor 1.5 m above the soil surface. The sensor was placed in a six-plate radiation shield. Wind speed and direction were measured at 2 m using a 2-D wind propeller anemometer; one propeller facing north and the second facing east. Solar irradiance data was collected using a CM3 Kipp and Zonen pyranometer placed at a height of 2.5 m above the soil surface.

Net irradiance data was collected using two net radiometers, which were placed 5 m away from the automatic weather station to minimize shading. The sensors were placed 1.5 m above the soil surface at the ends of the supporting arms about 1 m apart. Soil heat flux density was measured using two sensors buried at a depth of 80 mm, with one of the sensors placed below the net radiometers and the second 5 m away. Soil water content was monitored using ML1 ThetaProbe buried 80 mm below the soil surface.

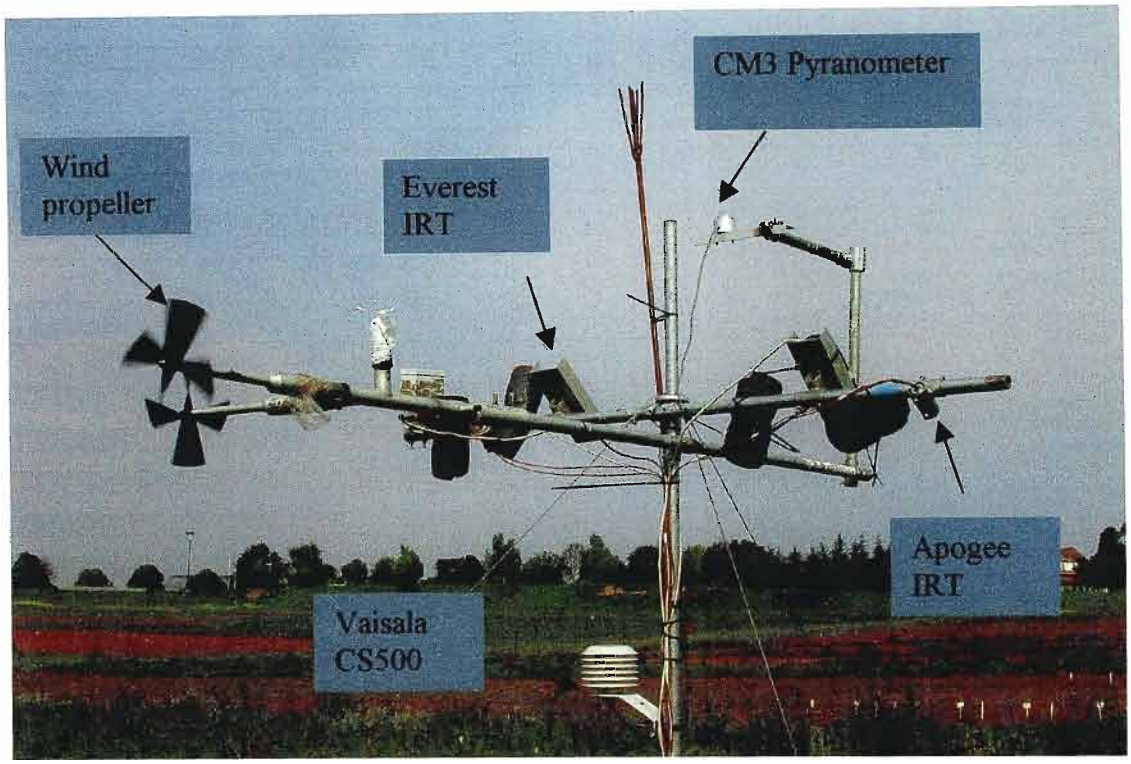

Fig. 4.1 Automatic weather station with most of the sensors at 2 m above the soil surface (Photo MJ Savage)

All sensors were connected to a Campbell Scientific Inc. CR7X datalogger using differential voltage measurements. An execution interval of 60 s was used for all sensors and every 15 minutes the datalogger converted an average of the input storage values to final storage. Once a week the data was transferred to computer using a storage module. Personal computers were used to analyse the data, which was stored in usable form on a hard disk.

4.3 INSTRUMENT DETAILS

4.3.1 Infrared thermometers

Two self-powered high precision Apogee infrared (Model IRTS-S, Apogee Instruments Inc., Logan UT, USA)[1], type K thermocouple sensors and an Everest infrared thermometer were used to measure canopy temperatures. The Apogee IRTs have dimensions of 60 mm long by 23 mm diameter with an accuracy of ± 1° C when sensor body and target are at the same temperature. The sensors have a silicon lens that detects wave lengths between 6 and 14 μm, and operate at an optimum temperature range of 0 °C to 50 °C. The relative energy received by the IRT detector depends on the sensor field of view (FOV). The FOV is 45 ° half angle, 90 ° full angle for 90 % target. The sensors were placed at 1.5 m above the canopy and this is referred to as a 1.5:1 FOV (at 1.5 meters from the sensor the FOV is 1 m diameter circle) (Internet: http://www.apogee-inst, 2001).

The Everest IRT (Model 4000ALCS, Everest Interscience Inc., Fullerton, CA, USA)[1] is a small, light, self contained, non-contact infrared temperature transducer with spectral pass band of 8 to 14 μm. It requires 5 V to 20 V DC power supply. The sensor has ± 0.5 °C accuracy, and emissivity of 0.100 to 0.999 settable *via* RS-232C port. Factory set emissivity of 0.98 was used in this experiment (Operating manual of model 4000A infrared temperature transducer). It operates at temperatures of –10 °C to 50 °C, up to 90% R.H. According to Savage (1995), the spot size can be calculated as:

$$\text{spot size (mm)} = (0.069841 * d) + 33.02$$

where d (mm) is the perpendicular distance between IRT and the surface. The sensor was placed perpendicularly at 1.5 m above the surface of the canopy; the spot size was calculated to be 137.78 mm.

[1] Mention of a commercial company in this thesis does not imply an endorsement

4.3.2 Vaisala CS500 Air temperature and relative humidity probe

The temperature and relative humidity probe (Model CS500, serial number R-1240093, Campbell Scientific, Logan, UT, USA)[1] has dimensions of 68 mm length by 12 mm diameter. The sensor contains a Platinum Resistance Temperature detector (PRT) and a Vaisala INTERCAP ® capacitive relative humidity sensor. It has a 12 mm filter which is made of 0.2 µm Teflon membrane. The sensor has less than 2 mA power consumption, and requires 7 to 28 V DC power supply. The temperature sensor operates at temperature ranges of – 40 °C to + 60 °C, and has temperature output signal range of 0.0 to 1.0 V DC. The relative humidity sensor operates at relative humidity measurement range of 0 to 100 % non- condensing and has relative humidity output signal range of 0.0 to 1.0 V DC.

The CS500 is usually housed inside a 6-plate solar radiation shield when used in the field. The sensor was placed at a height of 1.5 m above the soil surface in a 6-plate radiation shield (Fig.4.2.) on a CM6/CM10 Tripod mast. The radiation shield was checked monthly to make sure that it is free from debris. The filter surrounding the sensor was also checked for contaminants and cleaned.

Fig. 4.2 Vaisala CS500 relative humidity and air temperature probe inside a 6-plate radiation shield (Photo MJ Savage)

4.3.3 Propeller Anemometer

A three dimensional propeller anemometer (Model 08234, Weather Tronic, West Sacramento, CA, USA)[1] was used to measure wind speed and wind direction. Two dimensional wind speed measurement (Fig. 4.1) was obtained by removing the propeller in the vertical direction (W-axis). The propeller anemometer is a sensitive precision component wind speed instrument fitted with a structural foam polystyrene propeller moulded in the form of a true helicoid. The propellers have a very linear response for winds above 1 m s^{-1}. Increased slippage occurs down to the threshold speed of 0.2 m s^{-1}. The propeller drives a miniature direct current tachometer, which produces an analog output voltage proportional to wind speed. All voltages were measured every 60 seconds. The instrument measures both forward and reverse wind flow and the tachometer produces corresponding positive and negative voltages.

The propeller responds to only the component of wind in the axis of that instrument. The response closely follows the cosine law. When the wind is 90° to the axis, the propeller will stop all together. Caution should be exercised when handling and working around the instruments as the propellers are fragile and can break with impact (Savage, 2002a).

The propeller anemometer mounts on the Model 20701 Mast Adapter or the Model 20703 UVW mast adapter. The mast adapter was mounted on an iron pipe at a height of 2 m above the soil surface with anemometer serial number 160 (U) facing north and anemometer serial number 163 (V) facing east. Wind speed was calculated as a square root of the sum of the squares of the wind speeds in th U and V directions. Wind direction was calculated as ARCTAN (U/V) using the datalogger program instruction (P66).

4.3.4 Net radiometer

The net radiometers used (Fritschen-type, model Q*7.1, REBS, Seatle, WA, USA)[1] have a spectral response between 0.25 and 60 μm and a time constant of 30 s. The sensors have a high output 60-junction thermopile with a nominal resistance of 4 ohms, which generates a millivolt signal proportional to net irradiance. The thermopile is mounted in a glass reinforced plastic with a built-in level. The black paint absorbs the internally reflected radiation.

In order to avoid shading, the two sensors were installed with their heads facing north and the support arms facing south. They were horizontally mounted using a spirit level with the down domes facing downwards and the upper facing upward. The instruments were mounted at 1.5 m height above the soil surface (Fig. 4.3) to allow the sensor to sense the emitted long wave from the soil and crop surface, and the reflected solar irradiance from the surface. The net radiometer domes were cleaned every 14 days using distilled water and a camel hairbrush. The silica gel was replaced when its colour changed from blue to pink. If the radiometer domes have a "milky white" appearance, they should be replaced and the sensors should be recalibrated at least twice a year (Savage, 2002a).

Fig. 4.3 Two net radiometers placed at 1.5 m above the soil surface facing north about 5 m apart from the weather station (Photo MJ Savage)

4.3.5 CM3 Pyranometer

The pyranometer used (Kipp and Zonen, model CM3, serial number 014716, Delft, Holland)[1] consists of a thermopile sensor, housing, a glass dome, and a cable. The thermopile is coated with a black absorbent coating. The paint absorbs the radiation, and converts it to heat. The resulting heat flow causes a temperature difference across the thermopile. The thermopile generates a voltage output. The thermopile and the resistor determine most electrical specifications. Spectral specifications are determined by the absorber paint and the dome. The thermopile is encapsulated in the housing in such a way that its field of view is 180 degrees, and that its angular characteristics fulfil the cosine response. The nominal output resistance of the pyranometer is 125 ohms. This implies that the input impedance of the readout equipment should be at least 12.5 ohms, to give an error of less than 1 %. The cable can be extended without problems to a length of 100 m provided that the cable resistance remains within 0.1 % of the impedance of the readout equipment. The CM3 has spectral sensitivity error of within 5 % (350 to 1500 nm).

The sensor was mounted on a level, horizontal surface at a height of 2.5 m above the soil surface to avoid shade (Fig. 4.4.), with the dome facing upward. The dome was cleaned every 30 days using distilled water and a camel hairbrush.

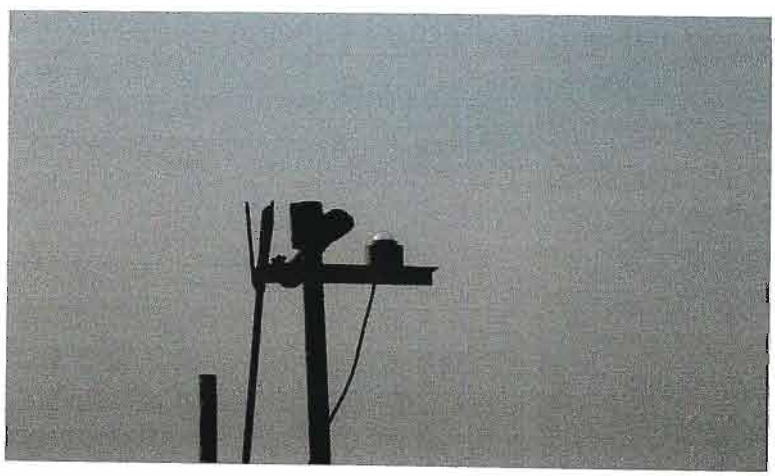

Fig. 4.4 CM3 pyranometer mounted on a horizontal plane surface. (Photo MJ Savage)

4.3.6 Soil heat flux plates and soil thermocouples

Two soil heat flux plates (Middleton Instruments, Model CN3, Australia)[1] were buried at a depth of 80 mm. Four thermocouples connected in parallel were used to average the heat stored in the soil layer above the plates, two at a depth of 20 mm and the other two at 60 mm. A diagrammatic representation of installation of the soil heat flux plates and soil thermocouples for determination of soil heat flux density is shown in Fig. 4.5. A small spade was used to cut the soil in vertical and horizontal positions; the soil was then replaced carefully after installing the sensors to ensure good contact between the sensors and the soil.

The soil heat flux, G, was calculated using a spreadsheet (Savage, 2002b) as the sum of the measured soil heat flux using a heat flux plate (G_p) and that stored in the layer above the soil heat flux plate (G_{stored}) as:

$$G = G_p + G_{stored} \quad 4.1$$

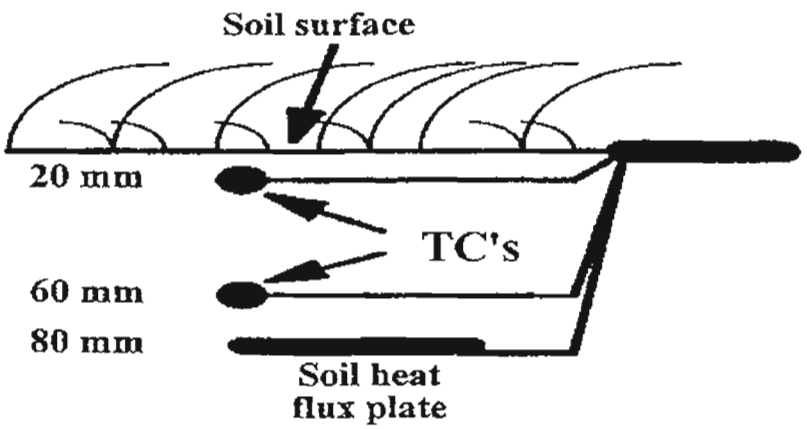

Fig. 4.5 Diagrammatic representation of the placement of soil heat flux plate and thermocouples for the measurement of soil heat flux density (Savage *et al.*, 1997).

The stored heat varies with changes in soil temperature (dT_{soil}) during a time interval, the soil bulk density (ρ_{bsoil}), the depth of the layer (Δz), the specific heat capacity of the soil (C_{Ps}) and water (C_{Pw}), and the soil ($\rho_{bsoil}/ \rho_{soil}$) and water ($\theta_{va}$) fraction in the soil system (ρ_{soil} refers to solid soil particle density). All the parameters were related by Hillel (1982) as follows:

$$G_{stored} = \rho_{bsoil}\, \Delta z\, dT_{soil}[(\rho_{bsoil}/ \rho_{soil})\, C_{Ps} + \theta_v\, C_{Pw}] \qquad 4.2$$

where Δt is the time (s) for soil temperature to change by the amount dT_{soil}. Particle density (ρ_{bsoil}) of 2650 kgm^{-3} was assumed to be constant for mineral soil and a constant value of 2000 J kg^{-1} K^{-1} and 4190 J kg^{-1} K^{-1} was used for specific heat capacity of the dry soil and water, respectively (Hillel, 1982).

4.3.7 ThetaProbe

An ML1 ThetaProbe (Delta-T Devices, Cambridge, UK)[1] was used to measure soil water content at a depth of 80 mm. The sensor rod has dimensions of 26.5 mm diameter, 60 mm length, and 3 mm rod diameter. The sensor requires 12 V power supply, and has a stabilization time of 10 seconds from the time the power is switched on. The ThetaProbe (Delta-T Devices, 1995) is a frequency domain reflectometry (FDR) sensor that depends on the frequency shift or ratio between the oscillator voltage and that reflected by rods installed in soil. The ratio of the two voltages is dependent essentially on the apparent dielectric constant of the soil, which is determined by the soil water content. A fifth order polynomial of the sensor analog output voltage V (in volts), can be used to estimate the square root of the dielectric constant of the soil as:

$$\sqrt{\varepsilon} = 1 + 6.19V - 9.72V^2 + 24.35V^3 - 30.84V^4 + 14.73V^5 \qquad 4.3$$

The soil water content θ_v (m^3 m^{-3}) is calculated from the square root of the apparent dielectric constant by using soil calibration constants a_0 and a_1:

$$\theta_v = (\sqrt{\varepsilon} - a_0) / a_1 \qquad 4.4$$

where $a_0 = \sqrt{\varepsilon_0}$ is the square root of the apparent dielectric constant obtained using the ThetaProbe voltage measured in an air-dry soil. The term $a_1 = \sqrt{\varepsilon_w}$ is the difference between the square root of the dielectric constant of saturated soil (Eq. 4.3 for the corresponding voltage) and dry soil divided by the soil water content of saturation:

$$a_1 = (\sqrt{\varepsilon} - \sqrt{\varepsilon_0}) / \theta_{vs} \qquad 4.5$$

Factory values for a_1 and a_0 of 8.4 and 1.6 for mineral and 7.8 and 1.3 for organic soils are used, respectively. The ML1 ThetaProbe is fast, precise, automated, non-destructive measurement technique. However, dielectric-based techniques are influenced by factors that affect the dielectric constant of soil components other than water, such as clay, organic matter, bulk density and soil temperature has been reported by Topp *et al.* (1980).

4.4 DATALOGGER AND POWER SUPPLY

The datalogger used was a Campbell Scientific Inc., CR7X unit, powered for field use by a 12 V car battery with internal lead acid battery packs as backup. The CR7X design represents a modular approach, combining precision measurement with processing and control capability. The control module includes a 16-pad keyboard and 8-digit LCD display. Programs are entered *via* this keyboard, which instruct the control functions, process data acquired from the input/output (I/O) module and store data in final storage. The control module has a serial interface, which provides for communication with up to 4 I/O modules and with peripheral interface on the panel. In addition to the keyboard card, CPU, and serial interface card, there is space for two additional cards for memory or interface expansion. The number of analog input and output channels, pulses and ports in a CR7X datalogger varies according to the users needs because the datalogger contains 7-card slots (Fig. 4.6), which can accommodate and combine input and output cards. The programs used in the field for measurements and calibrations of instruments and the schematic wiring of the sensors to the logger are given (Appendix 4.1, 4.2, 4.3).

The analog input cards are used for single ended and differential voltage measurements, with 0.04 % accuracy. The pulse card contains 4 pulse counters, switch closure, high frequency pulse and low-level AC programmable modes. The digital control output card

has high and low output voltages, and 400 ohms output resistance. Analog output card contains 8 switched and 2 continuous analog outputs with voltage ranges of ± 5 V and ± 2 V at 25 mA and 50 mA output current respectively.

The CR7X datalogger requires 9.6 V to 15 V power supply, and has a typical current drain of 3.5 to 6 mA (quiescent), 16 mA during processing, and 100 mA during analog measurements. A pair of 12 V batteries was connected in parallel to power the CR7X datalogger and another pair was also used to power the sensors. The batteries were replaced every seven days by charged batteries although the parallel connection of batteries provided longer lifetime for the batteries. A control switch box was connected to the pair of batteries, to power the sensors just prior to measurements to minimize the current drain. To protect the datalogger and the sensors from lightning, the ground of the datalogger and the common ground of the batteries was earth grounded using a lightning rod. The batteries were placed inside a metal enclosure (Fig. 4.6) and the datalogger was covered using a plastic container to prevent it from heating and rain.

Fig. 4.6 The CR7X datalogger (right) and metal enclosure (left) for the batteries. On top of the enclosure is the datalogger storage module (Photo MJ Savage)

4.5 DATA COLLECTION, HANDLING AND PROCESSING

The datalogger was programmed to take measurements at an execution interval of 60 seconds, which was converted to final storage locations every 15 minutes. The experimental data was downloaded from the datalogger to SM 192 storage module weekly. The data was then imported as PRN files into an Excel spreadsheet, which was used to manually perform the various computations. The PC208 Datalogger Support Software (SPLIT) was used to convert the 15 minutes data to average hourly and daily data. The data was checked for errors by plotting graphs of each measured variable for outliers. The calculation of fluxes of sensible and latent heat densities, canopy to air temperature differential, crop water stress index required several steps of processing in Excel spreadsheet. The data was analysed with Excel and PlotIT for Windows Version 3.2. Statistical analysis included regression analysis of the calculated and measured variables, with confidence limits and standard error estimates.

CHAPTER 5

SENSOR CALIBRATION AND THE INTEGRITY OF WEATHER DATA

5.1 INTRODUCTION

Science is the search for truth, which is largely equated with the accumulation of data. The aim of science is to find the 'laws of nature', everything the scientist measures is data, and every piece of data is potentially important. Relevant data about the area of research need to be collected and collated, which form one of the key foundations of the decision about whether or not to proceed with using the data. Therefore the data must be checked before it is transformed in some way in order to extract meaning from it.

Allen (1996) in a discussion on data analysis and application, were of the opinion that "no data are better than bad data." This statement applies primarily to measurements of evapotranspiration that are used to determine crop coefficients, however it also applies to weather data. When one has no data, one can look to regional weather data summaries for information that might be useful to represent conditions within the local area. However, bad data meaning biased, or faulty, or non-representative data collected locally, can cause more economic and hydrologic problems (Allen, 1996).

In this chapter the calibration of infrared thermometers, Vaisala CS500 air temperature and relative humidity sensor, and thermocouples is discussed in relation to the accuracy in measuring the respective variables. The integrity and quality of the measured weather data were analysed using graphical plots to display outliers.

5.2 MATERIALS AND METHODS

5.2.1 Infrared thermometers and thermocouples

Calibration of the sensors was conducted at the University of Natal, Agrometeorology laboratory. A water cone calibrator was used to calibrate two Apogee infrared thermometers (Model IRTS-S, with serial numbers 1144 and 1147) and an Everest infrared thermometer (Model 4000ALCS) following the method used by Fuchs and Tanner (1966), Berliner *et al.* (1984) and Bugbee *et al.* (1999). This calibrator consisted of a 4-litre beaker filled with water and placed on a magnetic stirring hot plate. The sensors were placed on a stand 100 mm above the water surface facing downward as shown in Fig 5.1.

Fig. 5.1 A magnetic stirrer is used to create a whorl of water. The IRT measures the surface temperature of the water and a thermocouple the water temperature (Savage *et al.*, 2000)

The sensors were connected to a Campbell Scientific 21X datalogger, which was programmed to take differential voltage measurements. The data logger scanned the sensors every 10 seconds and averaged the data every 1 minute. The water was rapidly stirred with a stirring bar to increase the effective emissivity of water. The water temperature was measured using a type E thermocouple that was immersed 10 mm below the surface of the water. Water temperature was altered by changing the set point of the thermostat on the hot plate up to 45 °C. Ice was added to lower the temperature of the water up to 0 °C. A magnifying glass was used to mercury thermometer temperature to within 0.2 °C.

The calibration of the thermocouples was done using the same materials used to calibrate the infrared thermometers together with a mercury thermometer. The thermocouples were connected to the 21X datalogger to take differential voltage measurement. Water temperature was altered using the set point of the thermostat. Water temperature was measured using the mercury thermometer and the thermocouples at the same time.

5.2.2 Vaisala CS500 air temperature and relative humidity sensor

The air temperature sensor was calibrated using the same method used to calibrate the thermocouples. The sensor was covered using a plastic cap and was wrapped using packaging tape to prevent leakage of water and condensation (Savage, 2002a). The temperature of the water was increased from 0 to 45 °C by heating the plate. Ice was added to lower the temperature. Water temperature was measured using a calibrated thermocouple averager as a standard and the Vaisala air temperature sensor simultaneously.

The relative humidity sensor was calibrated using a Li-Cor Inc. (Lincoln, USA) LI-610 dew point generator as the standard (Savage, 2002c). The apparatus generates an air stream with a known dew point temperature. The sensors were placed in a plastic tube with a connecting tube to the LI-610 (Fig. 5.2) and an outlet at the other end. The tubing was insulated to reduce the influence of temperature changes.

The command input of the LI-610 was connected to the continuous voltage of 0 mV (equivalent to setting the LI 610 to generate an air stream with an initial dew point, T_{dp610}, 0 °C). A separate copper-constantan thermocouple was used to measure the temperature of the air stream. The measurement of the temperature of the air stream and the set air stream dew point allows the water vapour pressure and relative humidity to be calculated. All temperatures and relative humidities and dew point of the air stream were measured every one second and averaged for each 5 minute period. Only the last two 5 minute averages prior to a dew point change were used to generate calibration relationships.

Fig. 5.2 The LI-610 portable dew point generator (Savage, 2002c)

5.2.3 Radiation measurements

The sensor used for measuring solar irradiance was Kipp and Zonen solarimeter (Model CM3, serial number 014716). The CM3 pyranometer had previously been calibrated against a CM11 solarimeter standard (Kipp and Zonen). The sensor was horizontally mounted on a level surface at 2.5 m height above the soil surface. Net radiometers (Model Q*7.1, REBS, Seattle, WA, USA) with serial numbers Q94330 and Q96178 were used to measure net irradiance. These sensors had recently been factory calibrated. In order to avoid shade, the sensors were installed with their heads facing north and the support arms facing south. They were horizontally mounted using a spirit level at 1.5 m height above the soil surface.

5.2.4 Soil heat flux measurements

Two soil heat flux plates (Middleton Instruments, Model CN3, Australia) were buried at a depth of 80 mm. Four thermocouples connected in parallel were used to measure the average temperature in the soil layer above the plates. The soil heat flux density G was calculated using a spreadsheet (Savage, 2002b) as the sum of the measured soil heat flux using a heat flux plate (G_p) and that stored in the layer above the soil heat flux plate (G_{stored}) calculated from the thermocouples as:

$$G = G_p + G_{stored} \qquad 5.1$$

5.2.5 Wind speed measurement

A three-dimensional propeller anemometer (Model-08234, Weather Tronic, West Sacramento, CA, USA) was used to measure wind speed. The propellers have a linear response for winds above 1 m s^{-1}. Two-dimensional wind speed measurement was obtained by removing the propeller in the vertical direction (W-axis). Anemometer serial number 160 (U) was installed facing north and anemometer serial number 163 (V) was installed facing east to measure wind speed at a height of 2 m above the soil surface. Wind speed was calculated as the square root of the sum of squares of the wind speeds from U and V directions.

5.3 RESULTS AND DISCUSSION

5.3.1 Calibration of sensors

5.3.1.1 *Infrared thermometers*

The calibration relationships for both Apogee IRTs and the Everest IRT were statistically different from the type E thermocouple reference sensor (Table 5.1). Although the relationships were highly linearly significant (Fig. 5.3, 5.4, 5.5), the slopes and intercepts need to be corrected since the slopes were statistically less than 1 and the intercepts were different from 0 (Table 5.1) for the Apogee IRTs and the Everest IRT at 99% levels of significance. The r^2 value exceeded 0.9974 for the two Apogee IRTs and the Everest IRT.

For Apogee IRT no. 1, T_{REF} - T_{IRT} decreased to –2.5 °C for T_{REF} < 5 °C (Fig. 5.3) compared to -3 °C for Apogee IRT no. 2 (Fig. 5.4) and –2 °C for the Everest IRT (Fig. 5.5). A plot of $T_{REF} - T_{IRT}$ *vs* T_{REF} was parabolic (Fig. 5.3 and 5.4). Both the Apogee and Everest IRTs require calibration for T_{IRT} < 15 °C and > 35 °C.

Table 5.1 Statistical parameters associated with the calibration of Apogee and Everest infrared thermometers

IRT number	n	Slope	Intercept	S_{yx}	Confidence interval (99%)	
					Slope	Intercept
Apogee IRT-1	653	0.9550	0.9618	0.3549	0.9502, 0.9599	0.8556, 1.0681
Apogee IRT-2	1363	0.9697	1.6187	0.2130	0.9664, 0.9730	1.5520, 1.6854
Everest IRT	653	0.9189	1.6861	0.2010	0.9161, 0.9216	1.6260, 1.7463

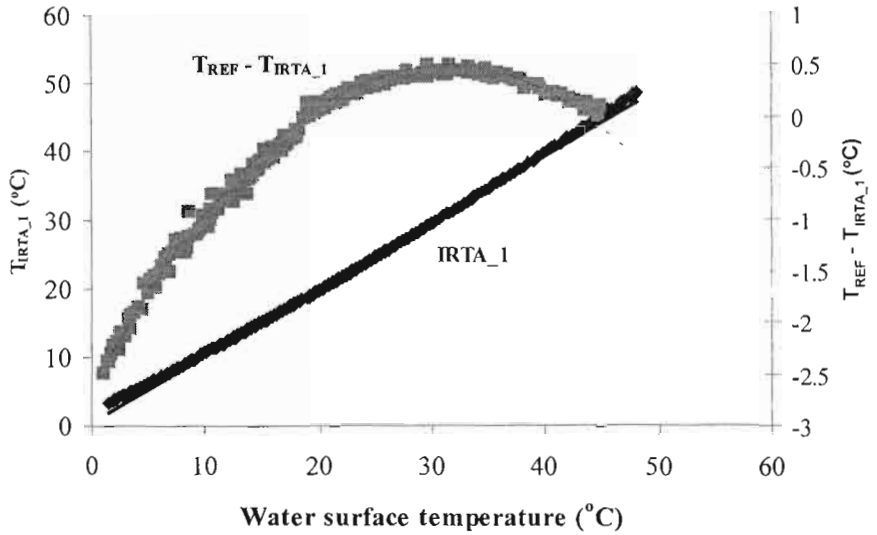

Fig. 5.3 Apogee IRTA_1 (no. 1) temperature (left hand y- axis, °C) and $T_{REF} - T_{IRTA\_1}$ (right hand y-axis) as a function of water surface temperature measured using four type E thermocouples

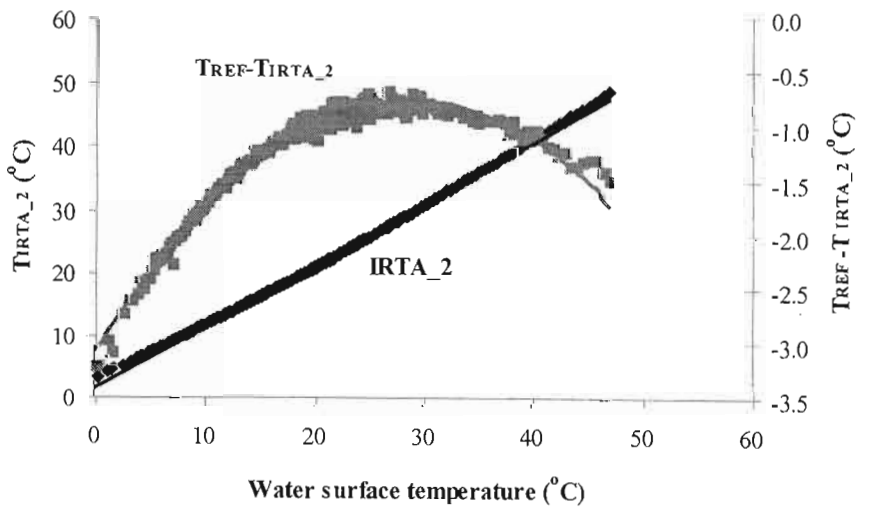

Fig. 5.4 Apogee IRTA_2 (no. 2) temperature (left hand y- axis, °C) and $T_{REF} - T_{IRTA\_2}$ (right hand y-axis) as a function of water surface temperature

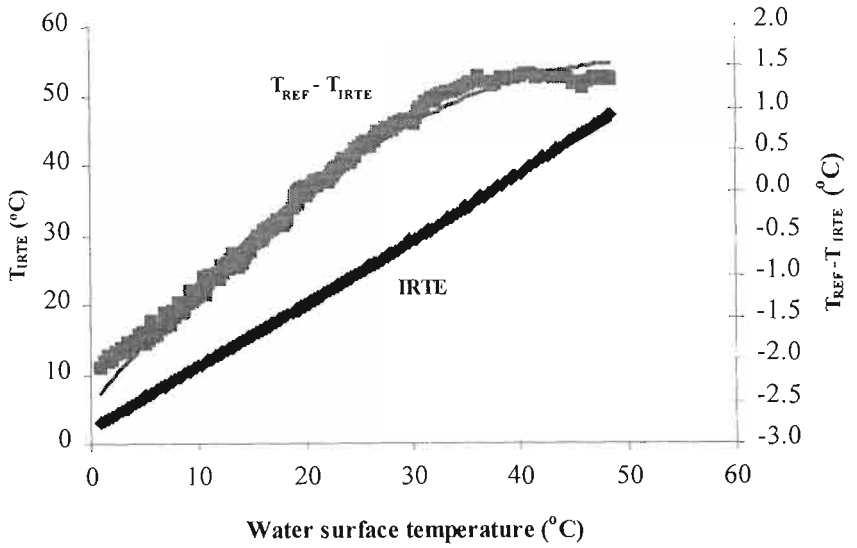

Fig. 5.5 Everest IRT temperature (left hand y- axis, °C) and $T_{REF} - T_{IRTE}$ (right hand y-axis) as a function of water surface temperature

5.3. 1.2 *Thermocouples*

Temperatures of type-T thermocouples were plotted against standard mercury thermometer temperature (Fig. 5.6, 5.7). Calibration relationships for thermocouple no. 1 (TC-1) were statistically different from the standard reference temperature (Table 5.2). The slope and intercept were statistically different from 1 and 0 for thermocouple no. 1, but for thermocouple no. 2 (TC-2) the intercept is not statistically different from zero (Table 5.2). For greater accuracy a multiplier should be used for both thermocouples and offset only for thermocouple no. 1.

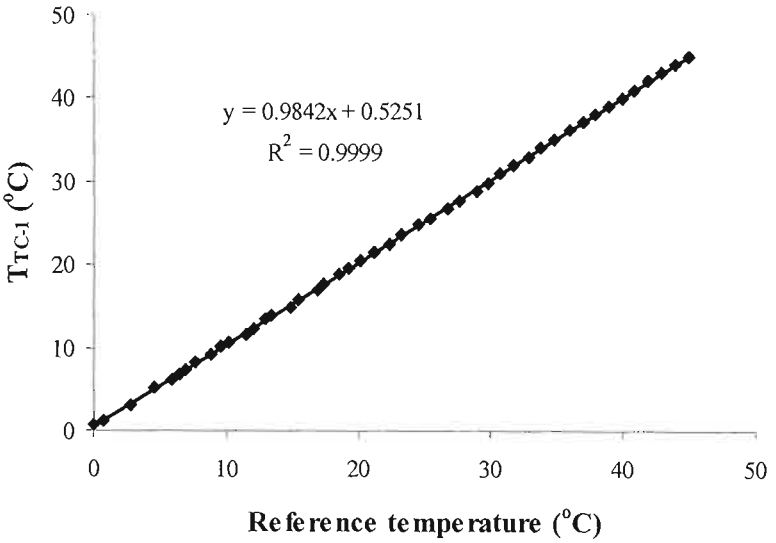

Fig. 5.6 Thermocouple no. 1 temperature *vs* reference temperature (mercury thermometer)

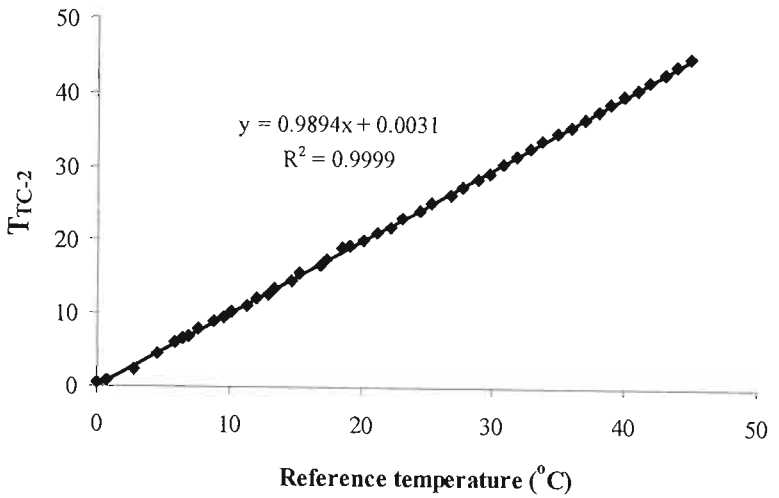

Fig. 5.7 Thermocouple no. 2 temperature *vs* reference temperature (mercury thermometer)

Table 5.2 Statistical parameters obtained from calibration of two type-T thermocouples

Thermocouple	n	Slope	Intercept (°C)	S_{yx}	Confidence interval (99%)	
					Slope	Intercept (°C)
TC-1	46	0.9842	0.5251	0.1118	0.9808, 0.9876	0.4365, 0.6136
TC-2	46	0.9868	0.0031	0.2734	0.9784, 0.9951	0.3930, 0.0403

5.3.1.3 *Vaisala air temperature and relative humidity sensor*

Vaisala CS500 relative humidity and air temperature sensor had linear calibration relationships for air temperature and relative humidity (Figs 5.8 and 5.9). The slope was statistically less than 1 at 99% levels of significance for the air temperature sensor (Table 5.3), but the offset was not significantly different from 0 °C. For the relative humidity (RH) sensor, both the slope and intercept were statistically different from 1 and 0 % respectively at 99% level of significance (Table 5.3). The systematic error was greater than the unsystematic error for the RH sensor (Fig. 5.9), which is an indication of the bias of the sensor from the 1:1 regression relationship.

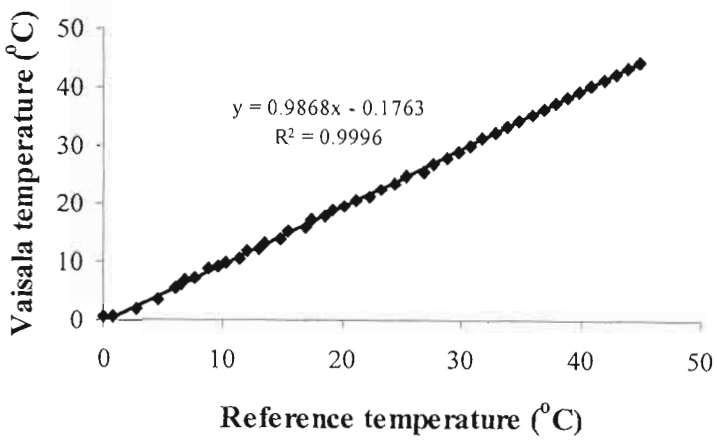

Fig. 5.8 Vaisala temperature (°C) *vs* mercury thermometer reference temperature (°C)

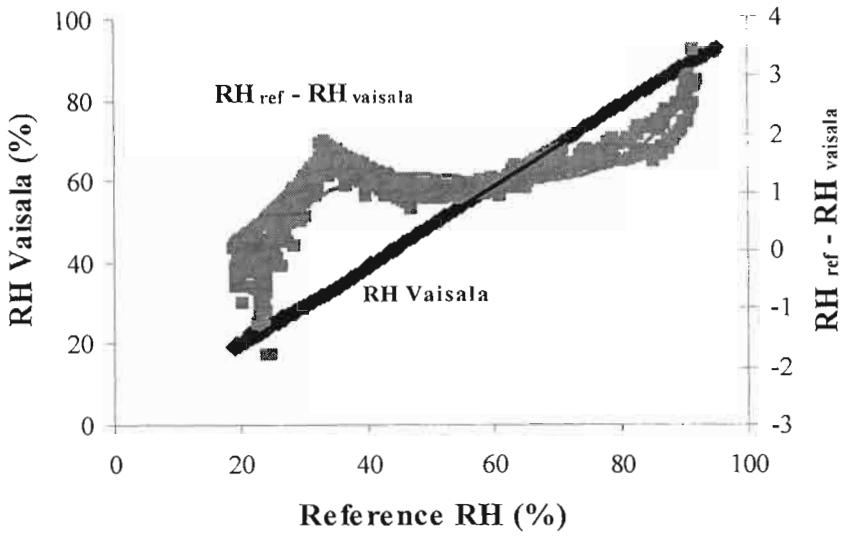

Fig. 5.9 Vaisala CS500 relative humidity (%) [left hand y-axis] and error (%) [right hand y-axis] *vs* reference relative humidity (LI-610)

Table 5.3 Statistical parameters associated with the calibration of Vaisala CS 500 air temperature and relative humidity sensor

Vaisala	n	Slope	Intercept (°C)	S_{yx}	Confidence interval (99%)	
					Slope	Intercept (°C)
Air temperature	46	0.9868	-0.1763	0.2734	0.9784, 0.9951	-0.3930, 0.0403
RH sensor	549	0.9738	0.2242	0.4736	0.9714, 0.9763	0.2137, 0.2346

5.3.2 Integrity of weather data

Assessments of weather data integrity and quality need to be conducted before data are utilized, and corrections to the data should be made to account for poor sensor calibration. Assessment of the integrity include computation of extreme outliers for weather data measurements, but do not generally provide means for assessing quality of data which fall within extreme ranges (Allen, 1996). The use of rejection criteria can also be used to test the integrity of data. For example, the computation of negative water vapour pressure deficit or relative humidity greater than 100% shows that either air or dew point temperature or both were measured inaccurately. On the other hand, the integrity of data can also be done by comparing measurements of the sensors used to measurements of standard sensors. A good comparison would justify use of the sensors used to collect data in this study.

5.3.2.1 *Radiation measurements*

Allen (1996) estimated the solar irradiance of clear sky (R_{so}) as the product between a clearness or transmission index (K_T) and extraterrestrial solar irradiance (R_a) as follows:

$$R_{so} = K_T R_a \qquad 5.2$$

Comparing the data with solar irradiance data from a different sensor can also be used for assessing the integrity of solar irradiance data. The pyranometer operation and accuracy was evaluated by plotting the hourly measurements of solar irradiance against another pyranometer, which was located at a distance of about 100 m from the measurement site (Fig. 5.10). The solar irradiance data measured using CM3 solarimeter was closely correlated to the data from the pyranometer. The deviation of the slope from 1 and intercept from zero was due to the use of different multipliers and offsets and calibration factors used for the CM3 and pyranometer were different.

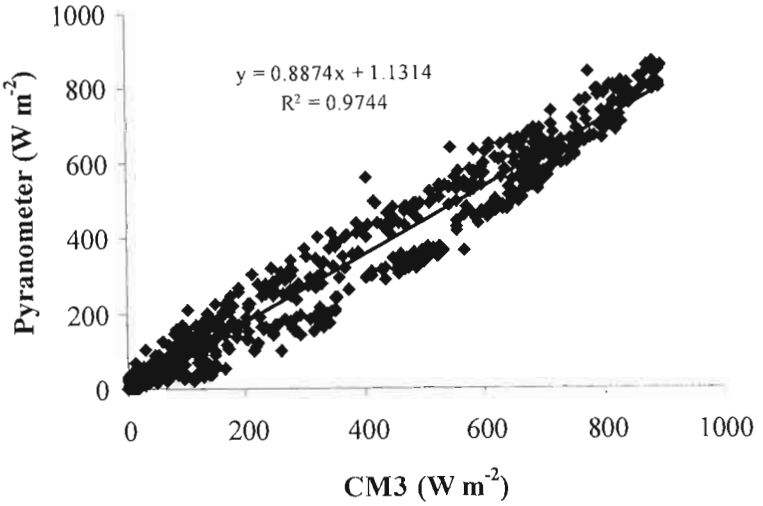

Fig. 5.10 Comparison of the measured hourly (CM3) solar irradiance (W m^{-2}) with Pyranometer solar irradiance (W m^{-2}) for day of year 204 to 268 (2002)

According to Allen (1996) equations for estimating hourly and daily average net irradiance (R_n) using solar irradiance measurements are accurate under most conditions. An equation by Monteith and Unsworth (1990) was used to estimate net irradiance (R_n):

$$R_n = a_s S_t + L_{ni} \qquad 5.3$$

where a_s is the absorptivity of the crop for solar irradiance, S_t is the incident solar irradiance, and L_{ni} is the atmospheric radiant emittance minus the crop emittance at air temperature. They showed that L_{ni} is closely approximated by f (S_t / S_o) * (0.0003 T_a - 0.107) in kWm^{-2}, where f (S_t / S_o) is cloudiness function and T_a is air temperature. The measured net irradiance was closely correlated to the estimated net irradiance (Fig. 5.11). Net irradiance was measured using two net radiometers of the same model. The comparison of the data from both sensors was not statistically different from one another.

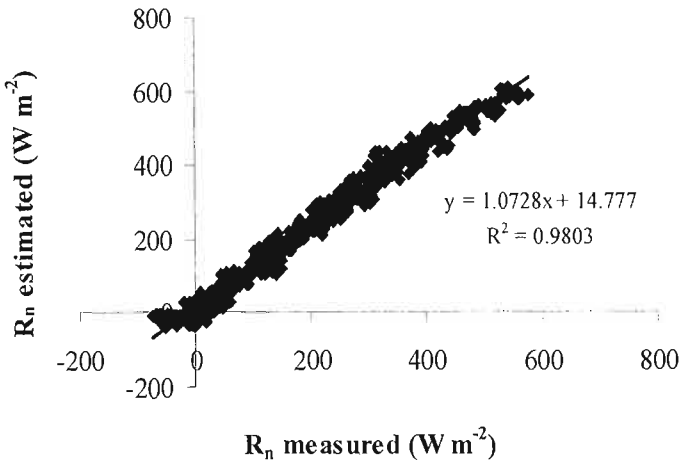

Fig. 5.11 Comparison between the hourly measured and the estimated net irradiance for day of year 204 to 268 (2002)

5.3.2.2 *Surface temperature*

The integrity of canopy surface temperature measurement was evaluated by plotting the 15 minutes average surface temperature of three IRTs against estimated surface temperature using Eq. 4.9 (Jackson *et al.*, 1988) as shown in Fig. 5.12.

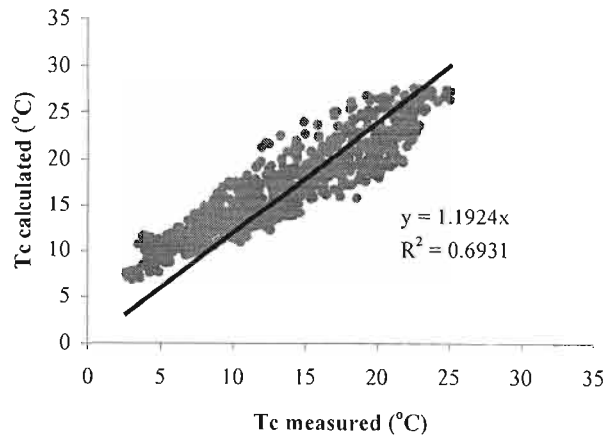

Fig. 5.12 Comparison between the hourly measured and estimated canopy surface temperature (T_c) for day of year 204 to 251 (2002)

The calculated surface temperature was overestimated for most of the measurement period except some data between 10 °C and 25 °C, which underestimated the calculated data (Fig. 5.12). This could be due to the calculations not adequately accounting for sensible heat advection, clouds, rain, irrigation or dew, which affect the measured surface temperature.

5.3.2.3 *Water vapour pressure and air temperature*

Water vapour pressure of air is difficult to measure accurately. Electronic relative humidity sensors are commonly plagued by hysteresis, non-linearity and calibration errors (Allen, 1996). Some of these errors are inherent in the sensor design, while other errors result from dust, moisture, insects, pollution and age.

The integrity of the water vapour pressure and air temperature data can be checked by transforming the water vapour pressure data to relative humidity or to vapour pressure deficit (Fig. 5.13). Hourly air temperature and relative humidity data were compared with another Vaisala CS500 sensor for day of year 204 to 268 (2002). The measurements of air temperature and relative humidity from the two Vaisala CS500 were closely related.

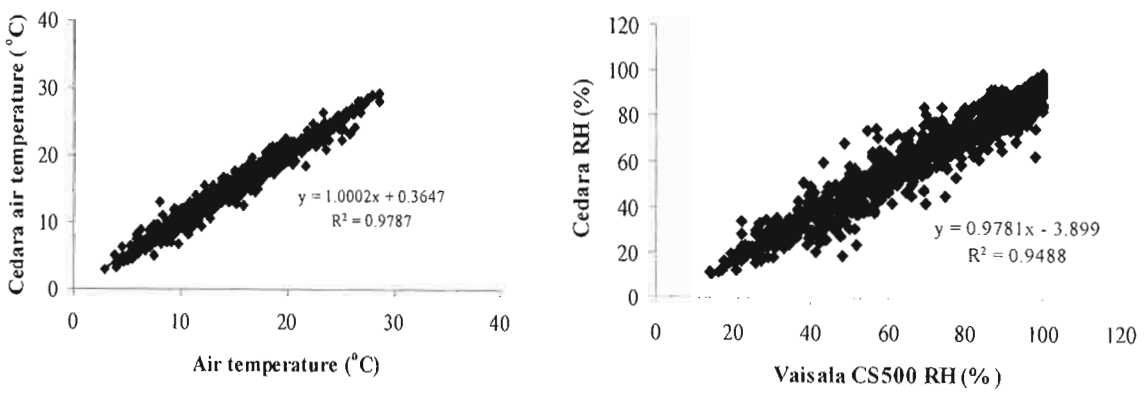

a b

Fig. 5.13a) Comparison of air temperature measurements of two Vaisala CS500 sensors at Cedara

b) Comparison of relative humidity measured using two Vaisala CS500 sensors at Cedara

The observed RH values were not greater than 100% and not less than 0%. No negative values of VPD were observed.

5.3.2.4 *Soil heat flux density*

A relationship proposed by Choudhury *et al.* (1987) for predicting soil heat flux density (G) under day light conditions is:

$$G = 0.4\, e^{-0.5LAI} R_n \qquad 5.3$$

where LAI = leaf area index; e = natural number; and G has the same units as R_n. This equation predicts $G = 0.1\ R_n$ for LAI = 2.8, which is typical for clipped grass, and for the nighttime G was found to be $0.5\ R_n$ (Allen, 1996).

Soil heat flux density was estimated as 10% of net irradiance during daytime and 50% during nighttime. The plot of the hourly estimated values *vs* the measured values for day of year 204 to 224 are shown in Fig. 5.14. The measured soil heat flux density was close to the estimated during the nighttime more than during the daytime.

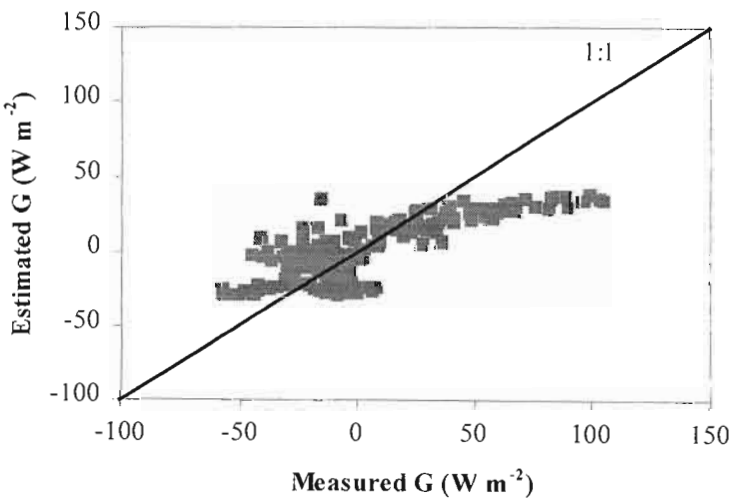

Fig. 5.14 Comparison between the estimated and measured ($G_p + G_{stored}$) soil heat flux density for an estimated LAI of 2.8

5.3.2.5 *Wind speed*

According to Allen (1996) the accuracy of wind speed measurements is difficult to assess unless duplicate instruments are used. One should always scan wind records for consistently low wind recordings. The presence of constant and consistent offsets in the data set indicates either the presence of exceptionally calm conditions or malfunctioning of the wind speed sensor (Allen, 1996).

The wind run measured using the weather Tronic wind propeller was compared with 3-cup anemometer (Model Schiltknecht 57227, Gossau, Switzerland) as shown in Fig. 5.15 for day of year 213 to 268 (2002). The wind speed measured using the wind propeller was closely related to the wind speed measured using three-cup anemometer. The deviation of the intercept from zero was due to the wind speed-starting threshold. The wind propeller measured down to the threshold speed of 0.2 m s^{-1} while the 3-cup anemometer (threshold speed of 0.5 m s^{-1}) recording 0.0 m s^{-1}. The wind run was the total distance that the wind had traveled during a day (24 hours) period of time.

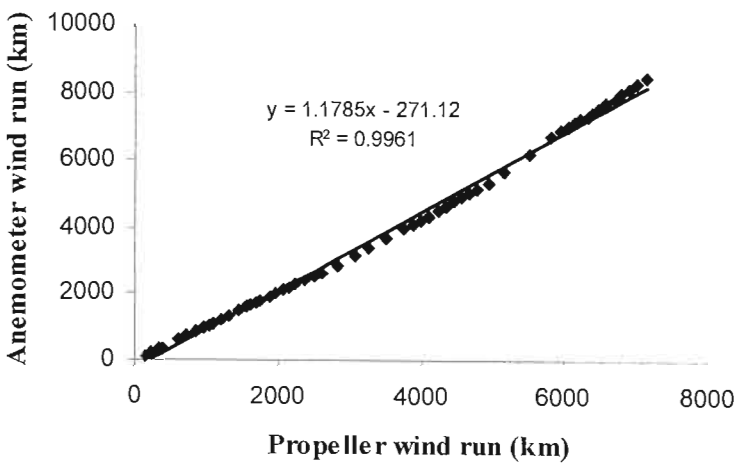

Fig. 5.15 Comparison of daily wind run measured using 2D-wind propeller and 3-cup anemometer for day of year 213 to 268 (2002)

5.5 CONCLUSIONS

The Everest and Apogee infrared thermometers require correction for surface temperatures less than 15 °C and greater than 35 °C. Although the calibration relationships were highly linearly significant the slopes and intercepts should be corrected for greater accuracy. Since the slope of the thermocouples and Vaisala CS500 air temperature sensor was statistically different from 1, multipliers were used to correct the readings. The relative humidity sensor needs to be calibrated for RH values less than 25 % and greater than 75 %. The integrity of weather data showed that solar irradiance, net irradiance, wind speed and vapour pressure deficit were measured accurately. Calculated soil heat flux density was underestimated. The calculated canopy temperature was overestimated for most of the experimental period compared to IRT-measured canopy temperature.

CHAPTER 6

DETERMINING THE CROP WATER STRESS INDEX USING THE EMPIRICAL AND THEORETICAL METHODS

6.1 INTRODUCTION

Canopy surface temperature measurement using infrared thermometers is a valuable tool for quantifying water stress and for irrigation scheduling. Several indices have been developed to time irrigation applications. One such index is the Crop Water Stress Index (CWSI), which normalizes plant minus air temperature measurements to atmospheric water vapour pressure deficit. Its use relies on two baselines, the non-water-stressed baseline, which represents the lower limit of temperature for a potentially transpiring plant, and the maximum-stressed baseline, which represents the upper limit of temperature that a non-transpiring crop would attain. Two forms of the index have been proposed, based on an empirical approach and a theoretical approach (Jackson *et al.*, 1988).

Idso *et al.* (1981) presented an empirical method for quantifying crop water stress by determining "non-water-stressed baselines" for crops. These baselines represent the lower limit of temperature that a particular crop canopy would attain if the plants were transpiring at their potential rate. In addition, estimation of the upper limit of temperature that a non-transpiring crop would attain is necessary (Jackson *et al.*, 1988). The non-water-stressed baseline equation is determined from simultaneous measurements of canopy temperature, air temperature, and atmospheric water vapour pressure deficit. The maximum-stressed baseline is a function of air temperature (Idso *et al.*, 1981) and occurs when there is no transpiration and the radiant and convective heat exchange terms dominate in the energy balance of the canopy (Nielsen *et al.*, 1992a). This empirical approach has received considerable attention because of its simplicity and the fact that one needs only to measure canopy temperature, air temperature, and the water vapour pressure deficit of the air (Hatfield, 1983a; Jackson *et al.*, 1988). It has also, however, received some criticism concerning its inability to account for canopy temperature changes due to solar irradiance (Jackson *et al.*, 1988) and wind speed (O'Toole and Hatfield, 1983a; Jackson *et al.*, 1988).

Jackson *et al.* (1981) presented a theoretical method for calculating the crop water stress index. The theory used an estimate of net irradiance and an aerodynamic resistance factor, in addition to the air temperature and water vapour pressure terms required by the empirical method as discussed briefly in Chapter 3. Although the theoretical approach specified how the upper and lower limits could be evaluated, the additional measurements of net irradiance and aerodynamic resistance, and perhaps some equations that appear more complex than they are, have resulted in this method not receiving the thorough field tests that the empirical method has undergone (Jackson *et al.*, 1988).

The objectives of this chapter are to determine:

i) the non-water-stressed baseline and maximum-stressed baseline for cereal rye and annual ryegrass

ii) the crop water stress index of cereal rye and annual ryegrass using the empirical and theoretical methods of Idso *et al.* (1981) and Jackson *et al.* (1981) respectively

iii) if the crop water stress index can be used to schedule irrigation in cereal rye and annual ryegrass to prevent water stress.

6.2 MATERIALS AND METHODS

The field experiment was conducted at Cedara (latitude 29°32' S, longitude 30°17' E, altitude 1076 m, KwaZulu-Natal, South Africa). Measurements were made on cereal rye (*Secale cereale* L.) from 22 July to 26 of September 2002 and on annual (Italian) ryegrass (*Lolium multiflorum* Lam.) from October 8 to December 4, 2002, when the respective canopies completely covered the soil. The crops were irrigated using overhead sprinklers during the night or early morning.

Two Apogee infrared (type K) thermocouple sensors (Model IRTS-S, Apogee Instruments, Logan, USA), and one Everest infrared thermometer (Model 4000ALCS, Everest Interscience Inc., Fullerton, CA, USA) were used to monitor canopy temperatures (45° angle) at a height of 2 m above the ground with the sensor facing south. This orientation increased the likelihood that the sensor faced sunlit leaves. Air temperature and relative humidity were measured at a height of 1.5 m above the ground using Vaisala CS500 air temperature and relative humidity probe (Model CS 500, serial number R-1240093). Wind speed and direction were measured at a height of 2 m using 2-D propeller anemometers (Model-08234, Weather Tronic, West Sacramento, CA, USA). Two net radiometers (Fritschen-type, model Q*7.1, REBS, Seatle, WA, USA) were installed at a height of 1.5 m above the ground to measure net irradiance. The net radiometers were mounted horizontally facing north to avoid shade on the sensor by supporting poles. Two soil heat flux plates (Middleton Instruments, model CN3, Australia) buried at 80 mm depth and four type T thermocouples (buried at 20 and 60 mm) were used to measure soil heat flux density. Soil water content was monitored at 80 mm depth using ML1 Theta Probe (Delta-T Devices, Cambridge, UK). Since the soil is mineral, from the soil analysis made (Table 4.1), soil water contents were calculated using the factory-supplied parameters for mineral soil.

Canopy temperature, air temperature, atmospheric water vapour pressure deficit (VPD), net irradiance, and aerodynamic resistance data between 12h00 and 14h00 were used to determine the crop water stress index. Only the data when the sky was clear and solar irradiance was greater than 230 W m^{-2} were used to calculate the non-water-stressed baseline equation and crop water stress index. Since the crops need to transpire at a

potential rate to determine the non-water-stressed baselines, only the data when the soil water content measurements greater than 0.35 $m^3 m^{-3}$ were used in the analysis.

6.3 RESULTS AND DISCUSSION

6.3.1 Actual, potential, and non-transpiring surface to air temperature differential

The non-water-stressed baseline (the potential surface to air temperature differential) was determined empirically by the regression line of the scatter diagram of $(T_c - T_a)_{LL}$ *vs* VPD as shown in Figs 6.1 and 6.2. Data were collected 1 to 2 days after irrigation or rainfall event and only the data between 12h00 and 14h00, when solar irradiance was greater than 230 W m^{-2} were used in these regressions. Average hourly values of $(T_c - T_a)_{LL}$ and VPD for the 3 hours were used to determine the non-water-stressed baseline equations. The slope, intercept, and r^2 values for cereal rye and annual ryegrass are shown Table 6.1 together with that reported (Idso, 1982) for wheat (*Triticum durum* D.) and for perennial ryegrass (*Lolium perenne* L.) reported by Jensen *et al.* (1990).

The maximum-stressed baseline (non-transpiring surface to air temperature differential) was determined using the following equation:

$$(T_c - T_a) = a + b * VPG \qquad 6.1$$

where the constants a and b are the intercept and slope of the non-water-stressed baseline equation respectively and *VPG* (kPa) is the difference between the saturation water vapour pressure evaluated at air temperature (T_a) and a temperature equal to T_a + a (Idso *et al.*, 1981).

Taking the upper limit of air temperature as 30 °C for Cedara during the experiment of cereal rye, a maximum-stressed baseline of 3.5 °C (Fig. 6.1) was estimated using Eq. 6.1. For annual rye grass, a maximum-stressed baseline of 6 °C (Fig. 6.2) was calculated using Eq. 3.7, with mean net irradiance of 400 W m^{-2} and aerodynamic resistance under stress conditions of 20 s m^{-1}. Jalali-Farahani *et al.* (1994) obtained an aerodynamic resistance value of 20 s m^{-1} from measurements of $T_c - T_a$ on severely water stressed Bermuda turf grass.

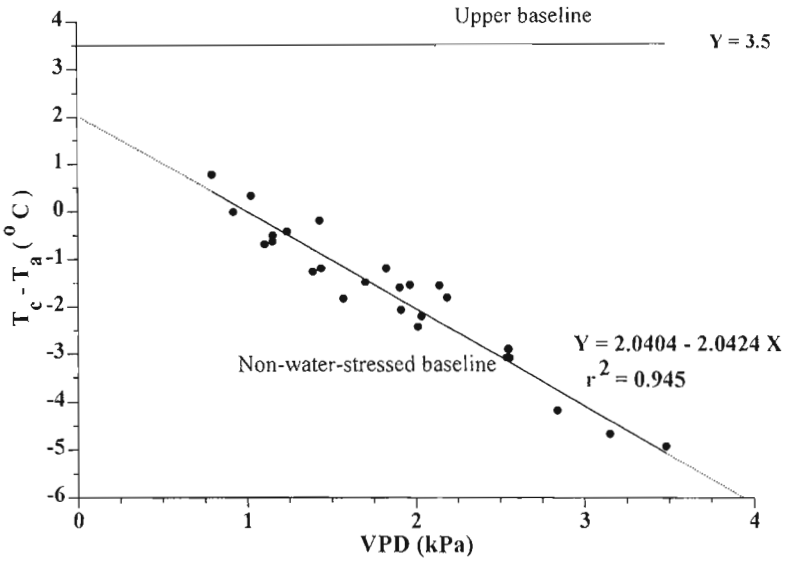

Fig. 6.1 The non-water-stressed baseline and maximum-stressed (upper) baseline for cereal rye based on the Idso (1982) method. Each point is an average of the 15-min measurements for a period of 2 h for which solar irradiance was greater than 230 W m^{-2}

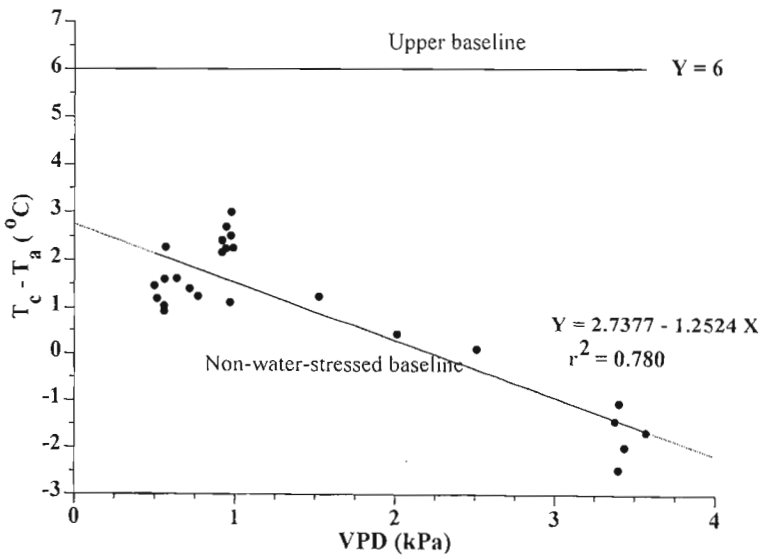

Fig. 6.2 The non-water-stressed baseline and maximum-stressed (upper) baseline for annual ryegrass based on the Idso (1982) method. Each point is an average of the 15-min measurements for a period of 2 h for which solar irradiance was greater than 230 W m^{-2}

Table 6.1 The regression of the potential canopy to air temperature differential (Y) *versus* atmospheric water vapour pressure deficit (X)

Common Name	Scientific Name	n	a	b	r^2	Authors
Cereal rye	*Secale cereale* L.	29	2.0404	-2.0424	0.945	experiment
Annual ryegrass	*Lolium multiflorum*	25	2.7377	-1.2524	0.780	experiment
Perennial ryegrass	*Lolium perenne* L.	90	3.0	-1.60	0.100	Jensen *et al.* (1990)
Wheat, produra	*Triticum durum* D.	56	2.88	-2.11	0.939	Idso (1982)

The correlation between the estimated actual ($T_c - T_a$) using Eq. 3.6 and measured actual ($T_c - T_a$) was relatively poor and statistically insignificant, with $r^2 < 0.3$ (Table 6.2) for both cereal rye and annual ryegrass. The estimated actual canopy to air temperature differential (hourly data) was compared with the measured actual canopy to air temperature differential for 5 days of the experiment as shown in Fig. 6.3 for cereal rye and Fig. 6.4 for annual ryegrass. The estimated actual ($T_c - T_a$) was overestimated for both cereal rye and annual ryegrass. This could be due to sensible heat advection and/or inaccurate values of aerodynamic resistances used in Eq. 3.6 that are estimated using empirical equations. The canopy to air temperature differentials were often negative at night and positive during the day, except for few days where the canopy to air temperature differentials were negative during the day due to the presence of advection. A negative daytime differential indicated that the sensible heat flux was directed toward the canopy and therefore the latent heat flux exceeded the net irradiance. Blad and Rosenberg (1974) also reported that strong advection increased latent heat to a point of using more than the available energy (R_n - G).

Table 6.2 The correlation between the estimated actual ($T_c - T_a$) using Eq. 3.6 and measured actual ($T_c - T_a$)

Common Name	Scientific Name	n	Slope	Intercept	r^2
Cereal rye	*Secale cereale* L.	1407	0.29	0.86	0.237
Annual ryegrass	*Lolium multiflorum*	912	0.36	0.77	0.192

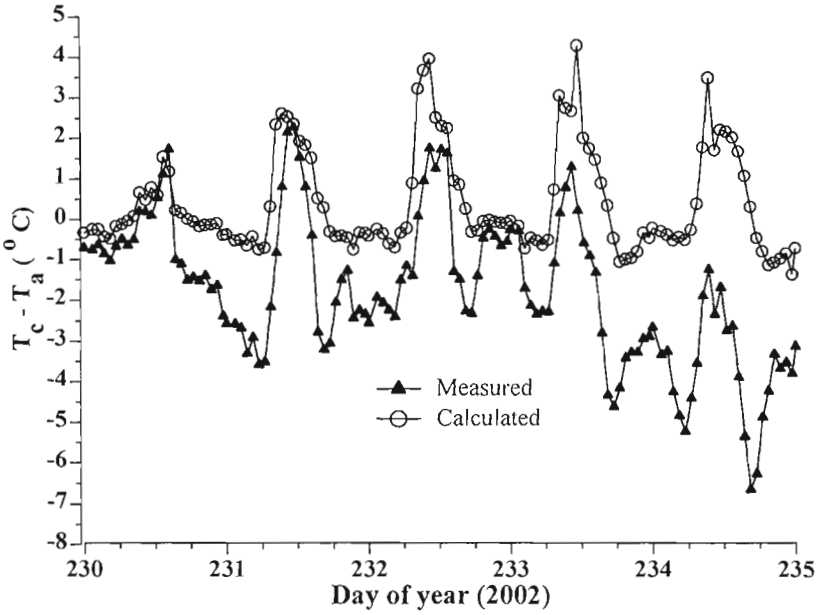

Fig. 6.3 Actual measured and estimated canopy to air temperature differential for cereal rye for hourly data

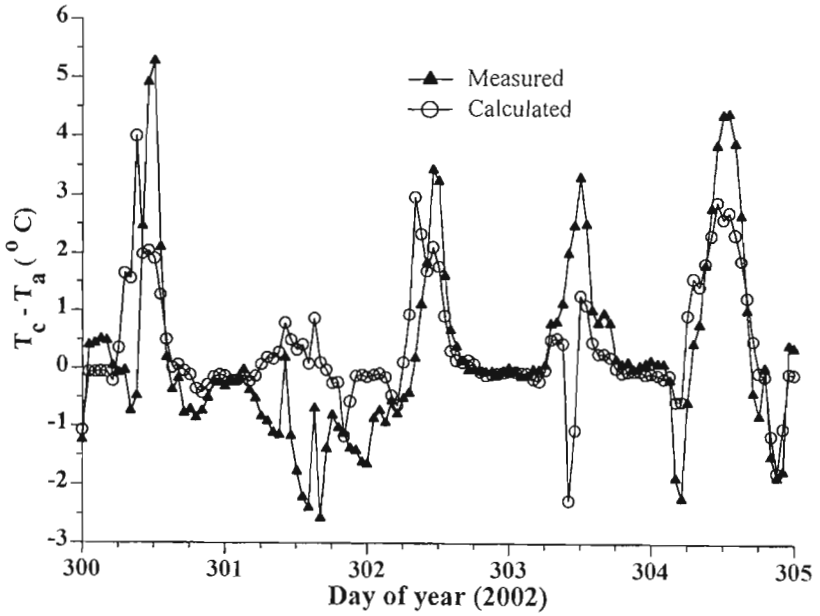

Fig. 6.4 Actual measured and estimated canopy to air temperature differential for annual ryegrass for hourly data

6.3.2 Crop Water Stress Index (CWSI)

The daily empirical $(CWSI)_E$ and theoretical $(CWSI)_T$ are plotted together in Fig. 6.5 for cereal rye and Fig. 6.6 for annual ryegrass for the average data collected between 12h00 and 14h00. The empirical CWSI was lower than the theoretical CWSI for most of the experimental days.

The empirical CWSI was calculated using Eq. 3.1 based on the measured actual canopy to air temperature ($T_c - T_a$) differential, the non-water-stressed baseline equation (Fig. 6.1 and 6.2), and the non-transpiring surface to air differential, which is 3.5 °C for cereal rye and 6.0 °C for annual ryegrass. The CWSI should be between 0 for well-watered crop and 1 for water-stressed crop. Negative values of CWSI were calculated for a few days for cereal rye and annual ryegrass (Fig. 6.5 and 6.6). This can be attributed to the scatter in the data used to construct the non-water-stressed baseline equations (Nielsen, 1990). Nielsen *et al.* (1992a) attributed these negative values of CWSI to low solar irradiance levels (clouds), wind speeds higher than that occurred during determination of the non-water-stressed baseline, and air temperatures cooler than the conditions that existed at the time of non-water-stressed baseline determination, resulting in an unusually cool canopy even in the presence of high solar irradiance.

The theoretical CWSI was calculated using Eq. 3.9 based on the estimated actual canopy to air temperature differential (Eq. 3.6), upper limit of $T_c - T_a$ (Eq. 3.7), and lower limit of $T_c - T_a$ (Eq. 3.8). Actual aerodynamic resistance (r_a) in Eq. 3.6 was calculated using a log-law version of Eq. 3.10. Aerodynamic resistance (10 s m^{-1}) of well-watered wheat (*Triticum aestivum* L.) was used for cereal rye (Jackson *et al.*, 1981). Well-watered Bermuda grass turf (*Cynodon dactylon* M.) aerodynamic resistance (13 s m^{-1}) was used for annual ryegrass in Eq. 3.8 to calculate the lower limit of $T_c - T_a$ (Jalali-Farahani *et al.*, 1994). The use of Eqs 3.16 and 3.17 yielded higher estimates of potential aerodynamic resistance (r_{ap}) and potential canopy resistance (r_{cp}), which resulted in erroneous estimates of canopy to air temperature differentials.

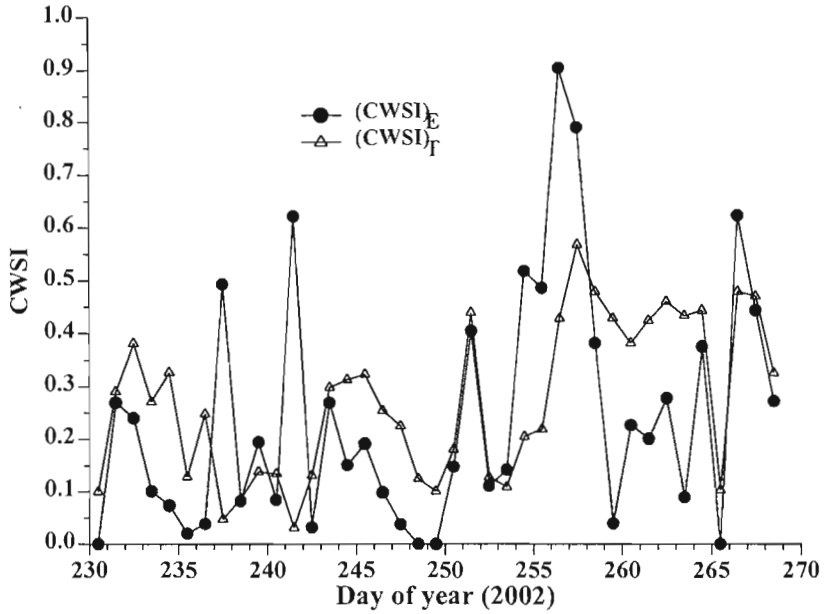

Fig. 6.5 The daily variation of empirical and theoretical CWSI for the average data collected between 12h00 and 14h00 for cereal rye

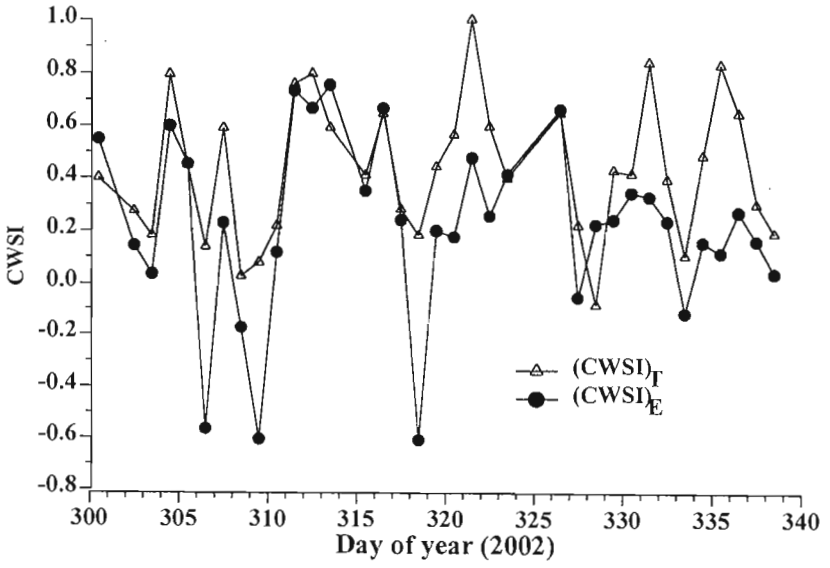

Fig. 6.6 The daily variation of empirical and theoretical CWSI for the average data collected between 12h00 and 14h00 for annual ryegrass

The psychrometric constant corrected for atmospheric pressure (γ), the slope of the saturation vapour pressure *vs* temperature relationship (Δ), density of air (ρ), and specific heat capacity of air (C_p) were calculated according to a report by Savage *et al.* (1997b).

6.3.3 Energy balance of the cereal rye and annual rye grass canopies

Micrometeorological methods for determining evapotranspiration are based on the surface energy balance. The energy balance of a crop surface can be given by

$$R_n + G + \lambda E + H + \mu P + J + A = 0 \qquad 6.2$$

where R_n is the net irradiance (W m^{-2}), G is the soil heat energy flux density (W m^{-2}), E is the water vapour flux density (kg s^{-1} m^{-2}), λ is the specific latent heat of vaporization (J kg^{-1}), H is the sensible heat energy flux density (W m^{-2}), μP is the energy flux density used in photosynthesis (W m^{-2}), μ is the quantum yield (J kg^{-1}), P is the carbon dioxide flux density (kg s^{-1} m^{-2}), J is the energy flux density stored in the crop (W m^{-2}), and A is advection energy flux density (W m^{-2}).

The amount of energy utilized in photosynthesis is very low and the energy stored in the crop (J) is usually neglected when considering crops of a short height. Thus neglecting these components and advection, the energy balance is expressed as

$$R_n + G + \lambda E + H = 0 \qquad 6.3$$

The sign convention is that energy towards the crop is positive and away from the crop canopy is negative (Stone *et al.*, 1974).

Crop evapotranspiration (ET_c) shown in Figs 6.7 and 6.8 was determined by the crop coefficient approach whereby the effect of the various weather conditions were incorporated into reference evapotranspiration (ET_o) and the crop characteristics into the K_c coefficient:

$$ET_c = K_c\, ET_o \qquad 6.4$$

Reference evapotranspiration was calculated using the FAO Penman-Monteith equation, which determines the evapotranspiration from a hypothetical grass reference surface using a spreadsheet by Savage (2002b). For normal irrigation planning and management purposes, average crop coefficients are relevant and more convenient than the K_c computed using a separate crop and soil coefficient (Allen *et al.*, 1998). Since the measurements were taken when the crops fully covered the soil, mid season $K_{c\ mid}$ value of wheat (1.15) for cereal rye and 1.05 for ryegrass with averaged cutting effects were used in the calculations (Allen *et al.*, 1998). For specific adjustment in climates where RH_{min} differs from 45 % or where U_2 is greater or smaller than 2 m s^{-1}, $K_{c\ mid}$ values should be adjusted according to

$$K_{c\ mid} = K_{c\ mid}(\text{Tab}) + [0.04\ (U_2 - 2) - 0.004\ (RH_{min} - 45)]\ (h / 3)^{0.3} \qquad 6.5$$

where $K_{c\ mid}$(Tab) was taken from Allen et al., (1998), Tab is table value, U_2 mean value for daily wind speed at 2 m height during the mid season growth stage (m s^{-1}), RH_{min} is mean value for daily minimum relative humidity during the mid season growth stage (%), and h mean plant height during the mid season growth stage (Allen *et al.*, 1998). Using U_2 = 1.5 m s^{-1}, RH_{min} = 20 %, and h = 0.5 m, adjusted $K_{c\ mid}$ values of 1.138 for cereal rye and 1.09 for annual ryegrass were calculated.

The sensible heat flux density (W m^{-2}) was calculated from the energy balance Eq. 6.3 as:

$$H = - R_n - G - \lambda E \qquad 6.6$$

As shown in Figs 6.7 and 6.8, R_n and G were measured values and H was calculated using Eq. 6.6, since the sensible heat flux density estimated using surface temperature techniques was overestimated and yielded very large errors in the energy balance equation. The latent heat flux density (W m^{-2}) was calculated as the product of the crop evapotranspiration rate (mm s^{-1} equivalent to 1kg m^{-2} s^{-1}) and the specific latent heat of vaporization (J kg^{-1}).

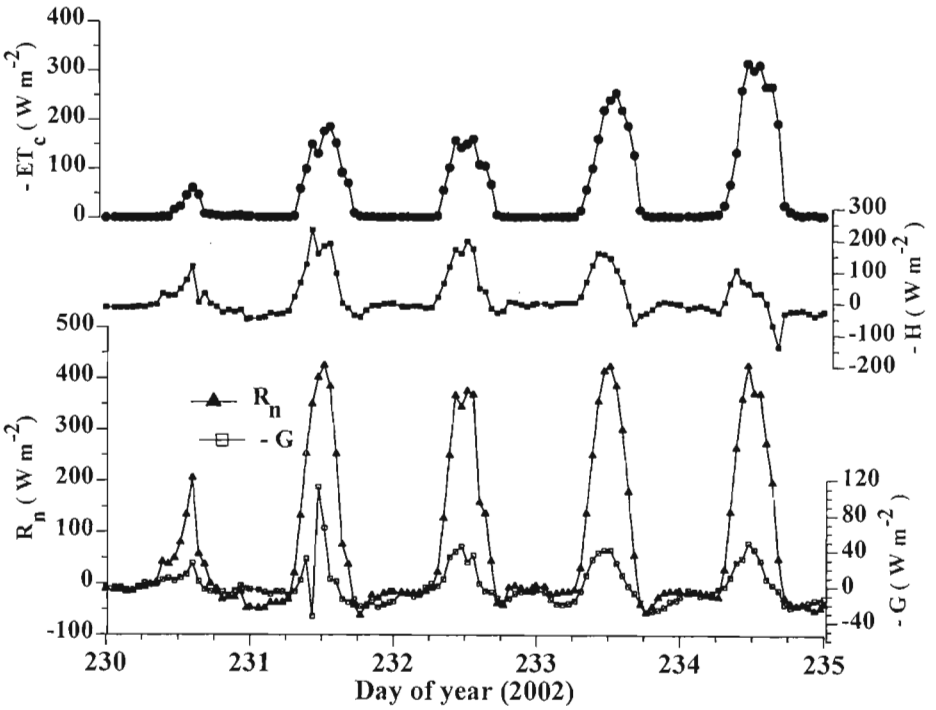

Fig. 6.7 Energy balance of the cereal rye canopy computed as (R_n + G = - λE - H)

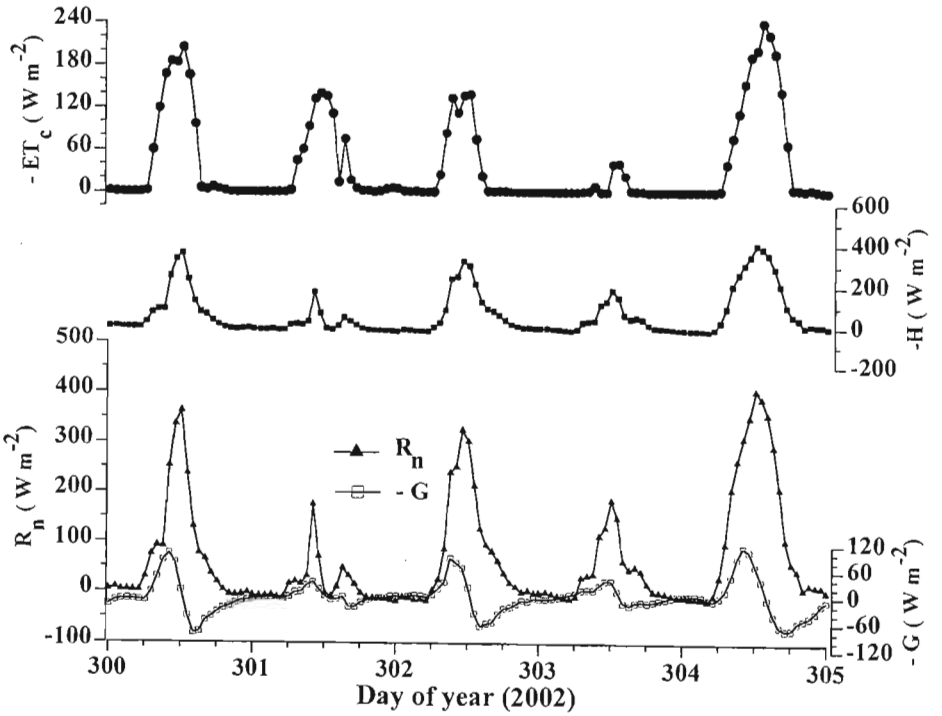

Fig. 6.8 Energy balance of the annual ryegrass canopy computed as (R_n + G = - λE - H)

6.3.4 Timing of irrigation using crop water stress index

The most common purpose of irrigation is to alleviate crop water stress by the timely application of water. Three major approaches to schedule irrigations are currently in use by growers: using the soil, the atmosphere, and the plants (Reginato, 1990; Wanjura *et al.*, 1992). The first two approaches are site specific, and many samples are required to characterize a field, requiring a considerable effort in time and labour. Therefore using the plant as an indicator of water needs is appropriate, since it integrates its total environment, soil and atmosphere (Reginato, 1990). The crop water stress index includes a direct, rapid, and non-destructive measurement of plant water stress. Crop water stress index is a normalized value where 0 and 1 represent completely non-stressed and completely stressed conditions, respectively.

The empirical and theoretical CWSI, the average soil water content for the top 100 mm rooting zone, and the recorded rainfall and irrigation are shown in Fig. 6.9 for cereal rye. The empirical and theoretical CWSI varied fairly reasonably with the amount of applied water and with the measured soil water content. The soil water content limits were determined using the laboratory method by using undisturbed soil samples. The field capacity and the refill point for the soil were 0.38 and 0.33 m^3 m^{-3} respectively. The refill point is the soil water content below which crop growth is measurably decreased. The CWSI value of 0.24 was found to correspond to the refill point soil water content for cereal rye by plotting CWSI against the soil water content. Wanjura *et al.* (1992) reported a CWSI of 0.1 to 0.2 corresponding to the refill point for cotton (*Gossypium hirsutum L.*). Jalali-Farahani *et al.* (1994) also found a refill CWSI of 0.16 for Bermuda grass (*Cynodon dactylon* M.) corresponding to actual canopy resistance of 125 s m^{-1}.

The cereal rye crop should be irrigated when the CWSI is above the CWSI = 0.24 equivalent to the refill point soil water content of the soil, to alleviate the water stress. As shown in Fig. 6.9 the crop was stressed from day of year 232 to 234, 251 to 258 and 266 to 268 (2002). The soil water content increased on day of year 248 (2002) as shown in Fig. 6.9. This could be due to unrecorded rainfall or irrigation.

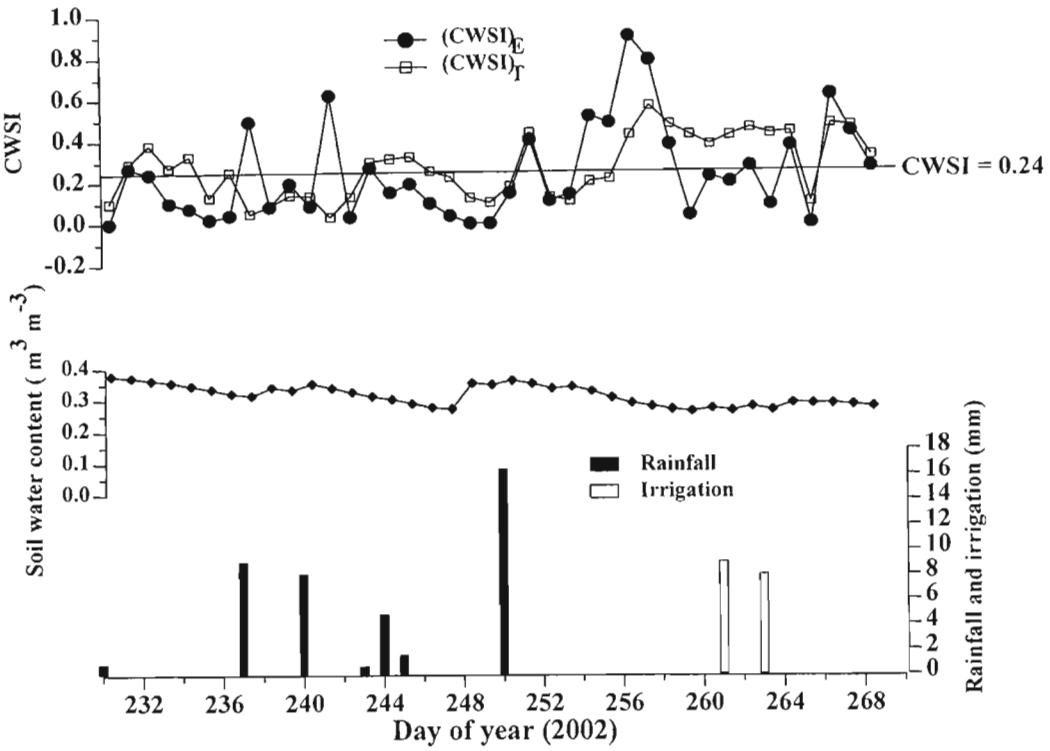

Fig. 6.9 The daily variation of CWSI, soil water content, and the recorded rainfall and irrigation for cereal rye

The CWSI was above 0.5 for day of year 256 to 258 when the soil water content was below 0.3 $m^3 m^{-3}$, but after the field was irrigated on day of year 261 the CWSI declined below 0.24 on day of year 263. Therefore irrigations needed to be initiated when the CWSI was between 0.2 and 0.24 to maintain the refill point soil water content and hence reduce the water stress.

The daily variation of the empirical and theoretical CWSI and soil water content for the top 100 mm rooting depth are shown (Fig. 6.10) for annual ryegrass. Data for the amount of irrigation water applied was not available; hence the amount of water applied was monitored by soil water content measurements. Both the empirical and theoretical CWSI varied with the measured soil water content. As the soil water content decreased the CWSI increased, which is an indication of plant water stress and *vice versa*. The field capacity and refill point for the soil were 0.38 and 0.33 $m^3 m^{-3}$ respectively. The CWSI value of 0.29 was found to correspond to the refill point soil water content by plotting CWSI against soil water content.

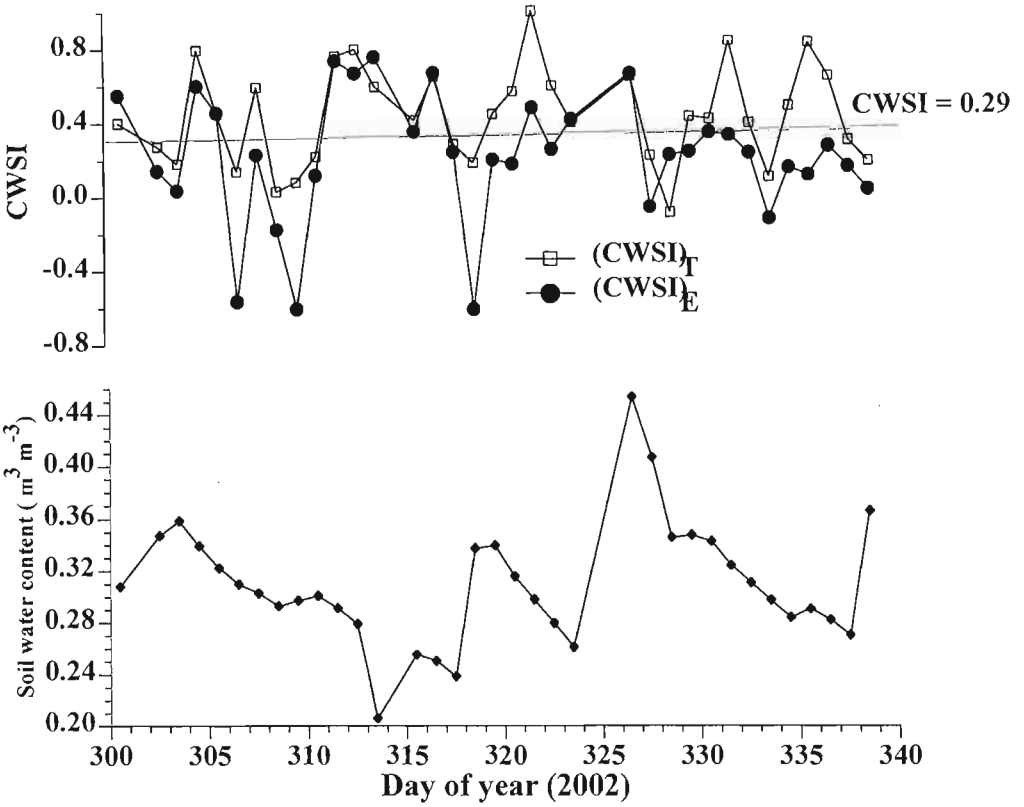

Fig. 6.10 The daily variation of CWSI and soil water content for annual ryegrass

Therefore the crop should be irrigated when the CWSI is above the threshold CWSI of 0.29 to alleviate the water stress. Howell *et al.* (1999) found CWSI value of 0.3 to 0.4 for corn as a conservative timing parameter to avoid excess irrigation.

The CWSI increased to 0.8 when the crop was stressed and the soil water content was 0.21 m^3 m^{-3} on day of year 313. However, after irrigation was applied on day of year 314 the CWSI decreased to 0.3. The crop was irrigated on day of year 325 after a long water stress, as a result the CWSI decreased to 0.3 and to around 0 on day of year 333 after an irrigation application.

6.4 CONCLUSIONS

The upper (stressed) and lower (non stressed) baselines were calculated to quantify and monitor crop water stress for cereal rye and annual ryegrass. The non-water-stressed baselines were described by the linear equations $T_c - T_a = 2.0404 - 2.0424 * \text{VPD}$ for cereal rye and $T_c - T_a = 2.7377 - 1.2524 * \text{VPD}$ for annual ryegrass. There are no previously determined baselines reported in the scientific literature for cereal rye and annual ryegrass that can be used for comparison with the non-water-stressed baselines developed from this study.

The CWSI technique offers some important advantages for quantifying plant stress between irrigations and monitoring yield potential. It is a rapid, direct, and non-destructive technique, which can be used to survey large fields in a short period of time. Variability of $(\text{CWSI})_E$ and $(\text{CWSI})_T$ values followed soil water content as expected. The CWSI values responded predictably to rainfall and irrigation. CWSI values of 0.24 and 0.29 were found from this study for cereal rye and annual ryegrass, which can be used for timing irrigations to alleviate water stress and avoid excess irrigations.

CHAPTER 7

THE USE OF NON-WATER-STRESSED BASELINES FOR IRRIGATION SCHEDULING

7.1 INTRODUCTION

One of the main decisions that are made in irrigation water management is the timing of irrigations. Several methods exist, plant, soil or atmosphere based, that may be time consuming or that may rely on expensive equipment. The use of canopy temperature measurements for irrigation scheduling became practical with the development of inexpensive infrared thermometers that are able to measure emitted thermal radiation (Stockle and Dugas, 1992). Infrared thermometers are used to detect crop water stress, and several indices have been proposed as an aid to irrigation scheduling. The CWSI method is the most often currently used, and can be determined empirically or theoretically as discussed briefly in Chapter 3.

The CWSI method relies on two baselines: the non-water-stressed baseline, that represents a fully watered crop and the maximum stressed baseline, which corresponds to a non-transpiring crop (Idso *et al.*, 1981). The non-water-stressed baseline can also be used alone whenever the aim of the irrigator is to obtain maximum yields (Alves and Pereira, 2000). The non-water-stressed baseline can be calculated using Eq. 3.6, which needs the computation of aerodynamic resistance (r_a) and canopy resistance (r_c). Aerodynamic resistance can be computed using Eq. 3.10 from the top of the canopy to the reference level. However, it is not possible to proceed further, as the knowledge of canopy resistance and the values it can assume for a given climatic situation and throughout the day is still scarce. T_o is the temperature at the surface level of the canopy, of which radiometric temperature T_s measured using an infrared thermometer may not be a good approximation. So the baseline still has to be determined experimentally. However, as discussed in Chapter 3, the empirical method has two drawbacks: 1) baselines cannot be transposed to other locations 2) baselines are only valid for clear sky conditions.

As cited by Alves and Pereira (2000), Wanjura and Upchurch (1996) stated that the wet bulb temperature (T_w), calculated from the air temperature and atmospheric water vapour pressure at a height of 2 m above ground, is the lower temperature limit for an evaporating surface. Wanjura and Upchurch (1996) estimated that a canopy is likely to cool only to about 2 °C above the ambient wet bulb temperature. They attributed this difference to the different geometry of plant leaves when compared to that of an aspirated wet bulb thermometer. However, these authors failed to realise that the air at the surface level, being the source of vapour flux is more humid than the air at the reference height (2 m), which actually leads to a smaller wet bulb depression (Alves *et al.*, 2000). Also as sensible heat flux density (H) is usually negative during the day, the following flux equation is used:

$$H = -\rho c_p \frac{T_o - T_a}{r_a} \qquad 7.1$$

where ρ is air density (kg m^{-3}), C_p is specific heat capacity at constant pressure (J kg^{-1} $°C^{-1}$), T_o is the temperature at the surface level of the canopy (°C), T_a is air temperature at the reference level (°C), and r_a is aerodynamic resistance to the sensible heat flow between the surface and the reference level (s m^{-1}). This shows that $T_o > T_a$, therefore a higher T_w at the surface level of the canopy is to be expected (Alves and Pereira, 2000).

The latent heat flux density (λE) is given by:

$$\lambda E = - (\rho_a c_p / \gamma) * (e_o - e_z) / r_a \qquad 7.2$$

where e_o (kPa) is the water vapour pressure at the canopy surface level, e_z (kPa) is the water vapour pressure at reference height (z), and r_a is aerodynamic resistance to the latent heat flow between the surface and the reference level (s m^{-1}). By similarity $r_{ah} = r_{av} = r_{am}$, where h, v, and m are the sensible, latent and momentum fluxes respectively.

This study was then performed to evaluate whether the infrared surface temperature, T_s, is a good representation of a wet bulb temperature ($T_s = T_w$) and hence to propose a procedure for the calculation of surface temperature that can be used for irrigation scheduling aiming at maximum yields.

7.2 MATERIALS AND METHODS

The field experiment was conducted at Cedara, located at latitude 29°32' S, longitude 30°17' E, and altitude 1076 m, KwaZulu-Natal, South Africa. Measurements were made on cereal rye (*Secale cereale* L.) from 22 July to 26 of September 2002 and on annual (Italian) ryegrass (*Lolium multiflorum* Lam.) from October 8 to December 4, 2002, when the crops completely covered the soil. The crops were irrigated using overhead sprinklers during the night or early morning.

Two Apogee infrared (type K) thermocouple sensors (Model IRTS-S, Apogee Instruments Inc. Logan, USA), and one Everest infrared thermometer (Model 4000ALCS, Everest Interscience Inc., Fullerton, CA, USA) were used to monitor canopy temperatures at a height of 2 m above the ground with the sensor facing south. Air temperature and relative humidity were measured at a standard height of 1.5 m above the ground using Vaisala CS500 air temperature and relative humidity probe (Model CS500, serial number R-1240093). Wet bulb temperature was calculated from air temperature and actual vapour pressure using a Fortran program wet bulb calculator (Savage, 2002c). The program iteratively uses a wet bulb temperature and the specified dry bulb temperature to calculate the atmospheric water vapour pressure and compares this value with the actual water vapour pressure. The process continues until the two water vapour pressures are equal to within 0.0001 kPa. Alternatively, with reduced accuracy the wet bulb temperature (T_w) may be calculated from the approximation $T_w \approx T_a - \delta e /(\Delta + \gamma)$ where δe is the VPD and Δ is the slope of the saturation water vapour pressure *vs* temperature relationship. Wind speed and direction were measured at a height of 2 m using 2-D propeller anemometers (Model-08234, Weather Tronic, West Sacramento, CA, USA). Two net radiometers (Fritschen-type, model Q*7.1, REBS, Seatle, WA, USA) were installed at a height of 1.5 m above the ground to measure net irradiance. The net radiometers were mounted horizontally facing north to avoid shade on the sensor by supporting poles. Two soil heat flux plates (Middleton Instruments, model CN3, Australia) buried at a depth of 80 mm and four type T thermocouples (buried at 20 mm and 60 mm) were used to measure soil heat flux density. Soil water content at a depth of 80 mm was monitored using ML1 ThetaProbe (Delta-T Devices, Cambridge, UK).

All the instruments were calibrated and checked before the field trial, and were installed on a 2.5 m stand in the center of the fields taking into consideration the effect of fetch. Only the 15-min data recorded during the periods for which the net irradiance was positive were used for the calculation of the surface temperature (T_s). Aerodynamic resistance was calculated according to Eq. 3.10, with h = 0.95, d = 0.64 m and z_o = 0.1 m. Since the crops need to be irrigated daily to maintain field capacity, only the data when the soil water content measurements greater than 0.35 m^3 m^{-3} were used in the analysis.

7.3 THE RADIOMETRIC SURFACE TEMPERATURE AS A WET BULB TEMPERATURE

Flux calculations involve measurements of temperature and water vapour at various positions of the soil-plant-atmosphere continuum. The convention is that the subscript o, is used to indicate surface measurements, subscript z, for measurement at a height z at $z = z_1$, and $z = z_2$, subscript a is used for atmospheric measurement, and subscript w for wet bulb measurements (Table 7.1). The subscript s, saturation water vapour pressure in e_s (T), and also indicates canopy surface temperature in T_s.

Table 7.1 Definition of symbols used in flux measurements

Symbol	Position	Meaning
e_a	reference height	actual water vapour pressure
e_o	surface of the canopy	water vapour pressure at the surface level
e_z	height z above soil surface	water vapour pressure
e_s	reference height	saturation water vapour pressure
$e_s(T)$	reference height	saturation water vapour pressure at temperature T
T	reference height	air (dry bulb) temperature
T_a	reference height	air (dry bulb) temperature
T_c	reference height	canopy temperature
T_z	height z	air (dry bulb) temperature
T_1	height 1	air (dry bulb) temperature
T_2	height 2	air (dry bulb) temperature
T_o	surface of the canopy	canopy temperature
T_s	at the canopy	IRT surface canopy temperature
T_w	reference height	wet bulb temperature
T_{w1}	height 1	wet bulb temperature at height 1above soil surface
T_{w2}	height 2	wet bulb temperature at height 2 above soil surface

Monteith and Unsworth (1990) described wet bulb temperature with two distinct connotations: the thermodynamic wet bulb temperature, which is a theoretical abstraction; and the temperature of a thermometer covered with a wet sleeve, which, at best, is a close approximation to the thermodynamic wet bulb temperature. In an adiabatic system within which the sum of sensible and latent heat remains constant, the initial state of the air can be specified by its temperature T, water vapour pressure e and total atmospheric pressure P. Water will evaporate and, both e and P will increase provided that e is smaller than or equal to $e_s(T)$, the saturation vapour pressure at air temperature T. The process of cooling continues until the air becomes saturated at a temperature T_w which, by definition is, the thermodynamic wet bulb temperature (Monteith and Unsworth, 1990).

From the saturation pressure curve (Fig. 7.1), $\Delta \approx [e_s(T) - e_s(T_w)]/ (T - T_w)$ and $-\gamma = [e - e_s(T_w)]/ (T - T_w)$, where T is dry bulb (air) temperature (°C), T_w is wet bulb temperature at the surface level (°C), e is actual vapour pressure at a reference height (Pa) and $e_s(T)$ is saturated vapour pressure (Pa) at temperature T. Hence, eliminating $e_s(T_w)$ from these two equations yields:

$$e \approx e_s(T) - (\Delta + \gamma)(T - T_w) \qquad 7.3$$

Therefore the change of actual water vapour pressure between two heights (h_1 and h_2), given the definition of Δ, will be:

$$e_1 - e_2 = (\Delta + \gamma)(T_{w1} - T_{w2}) - \gamma (T_1 - T_2) \qquad 7.4$$

Applying Eq. 7.4 to determine the water vapour pressure difference between the canopy surface (subscript o), with T_s and T_o, respectively, as the wet bulb temperature and the dry bulb temperature at surface level, and the reference height (subscript z), where measurements of T_w and T_a are made, gives:

$$e_o - e_z = (\Delta + \gamma)(T_s - T_w) - \gamma (T_o - T_a) \qquad 7.5$$

where e_o and T_o are the water vapour pressure and dry bulb temperature at the canopy surface respectively, T_s is the wet bulb temperature at the canopy surface, and T_w is the wet bulb temperature at the reference height, which is 2 m in this study.

Substituting sensible (Eq. 7.1) and latent (Eq. 7.2) heat flux density into the energy balance equation

$$R_n + G = -\lambda E - H \qquad 7.6$$

And solving for $T_s - T_w$ one obtains:

$$T_s - T_w = \frac{\gamma}{\gamma + \Delta} \frac{r_a}{\rho_a Cp} (R_n + G) \qquad 7.7$$

where Δ is calculated at temperature $(T_a + T_w)/2$. Eq. 7.7 can be considered as a new definition of the non-water-stressed baseline. If the calculated canopy surface temperature T_s, using $T_s = T_w + [\gamma / (\Delta + \gamma)] * (r_a/\rho Cp) * (R_n + G)$, compares with the measured canopy temperature T_s, then for the fully irrigated conditions, the surface temperature may be regarded as a surface wet bulb temperature.

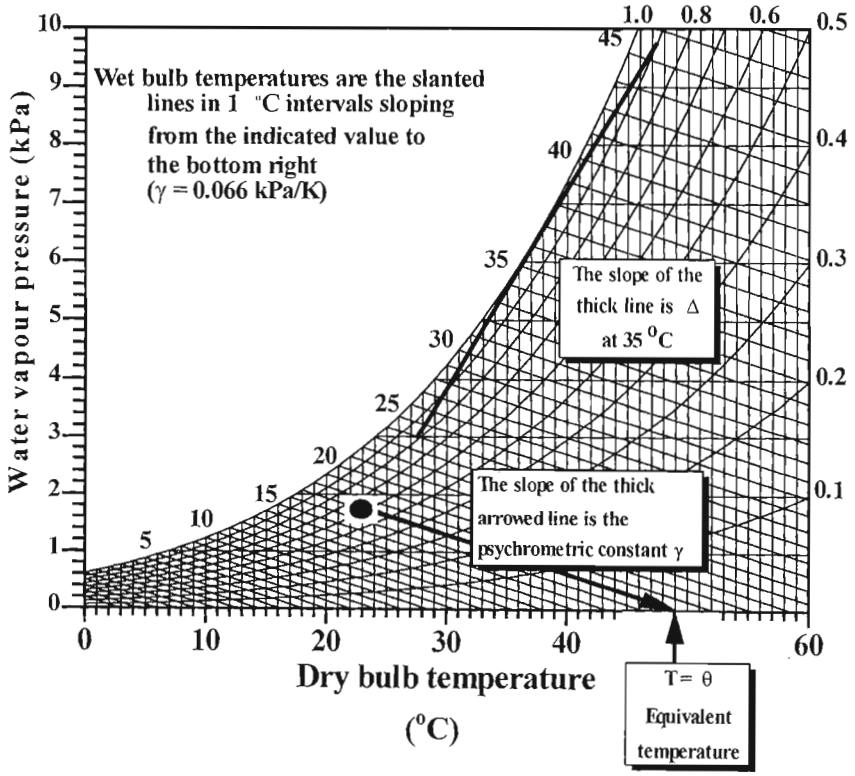

Fig. 7.1 The psychrometric chart (taken from Savage, 2000)

7.4 RESULTS AND DISCUSSION

The weather parameters for cereal rye recorded during the experiment and belonging to the set of data retained for analysis are plotted in Fig. 7.2. The value of net irradiance (R_n) varied from - 40 W m^{-2} to 400 W m^{-2}. The maximum value of air temperature (T_a) recorded during this 3 days period was 24 °C and minimum 2 °C. Maximum water vapour pressure deficit (VPD) recorded was 2.4 kPa. The maximum values of R_n, VPD, T_a, and G were recorded between 12h00 and 13h00 each day and this shows consistency of the data. Aerodynamic resistance varied from 10 s m^{-1} up to 30 s m^{-1} for most of the time except for very low wind speeds where r_a was 100 s m^{-1}.

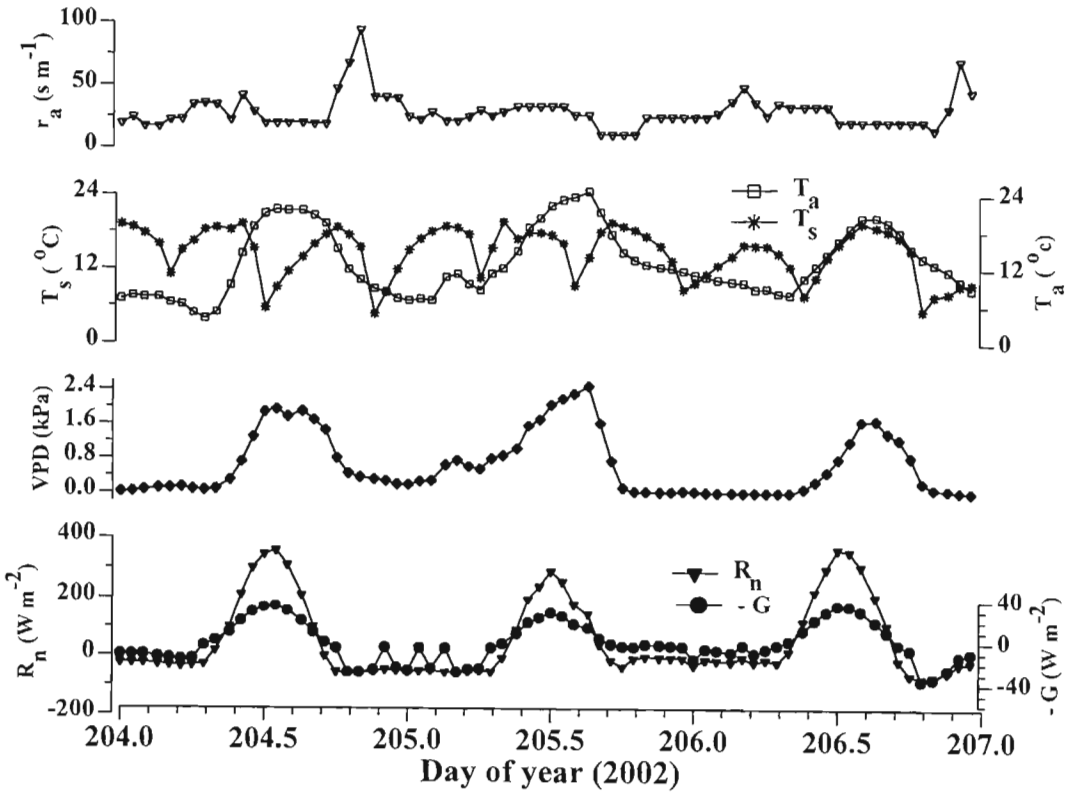

Fig. 7.2 Hourly micrometeorological data recorded at Cedara, for cereal rye that was used for further analysis

The weather parameters recorded on annual (Italian) ryegrass and belonging to the set of data kept for further analysis are plotted in Fig. 7.3. The maximum value of R_n recorded was 800 W m^{-2}, which is almost double that recorded for cereal rye. Maximum value of 32 °C was recorded for air temperature and infrared surface temperature during these 3 days. The aerodynamic resistance was almost in the same range as the r_a recorded on cereal rye. Maximum values of R_n, T_a, T_s, G, and VPD were recorded between 12h00 and 13h00 and the values were greater than the values recorded on cereal rye, typical of a summer day for this site.

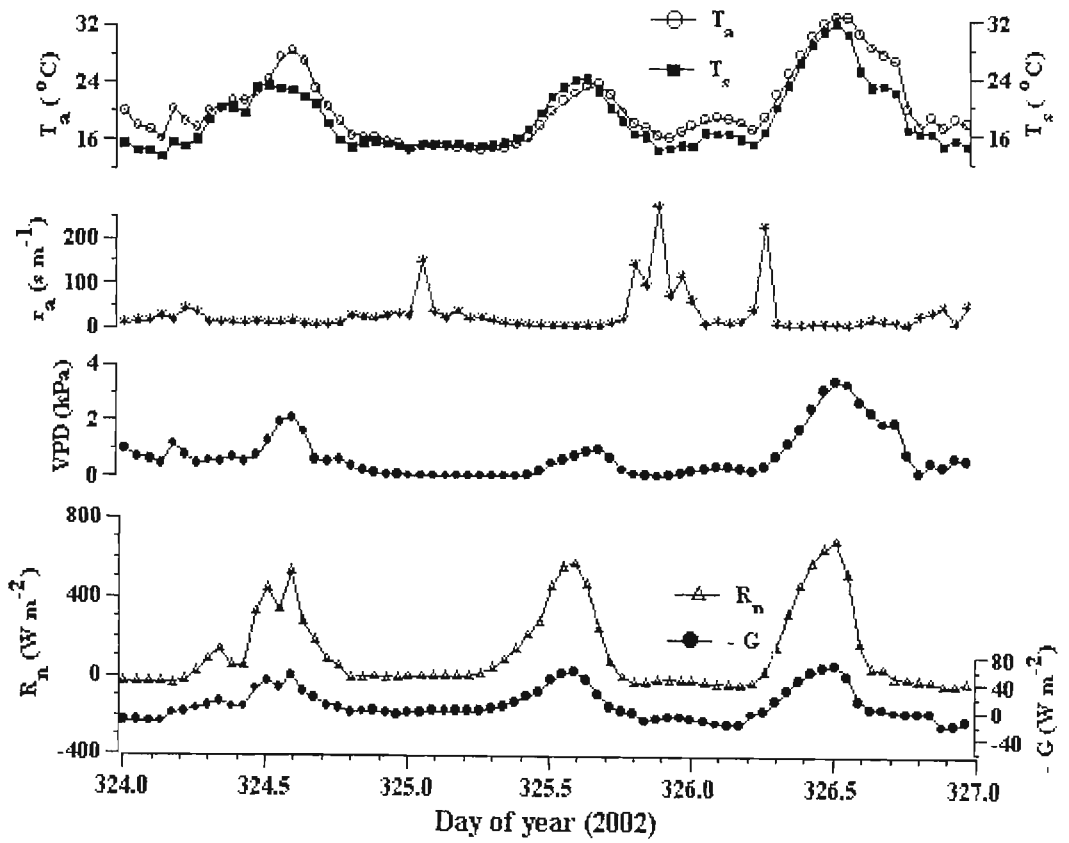

Fig. 7.3 Hourly micrometeorological data recorded at Cedara for annual ryegrass belonging to the data set kept for further analysis

The measured values of infrared (surface) temperature T_s obtained in the experiments were compared with those calculated using Eq. 7.7 and are plotted in Fig. 7.4 for cereal rye and Fig. 7.5 for annual ryegrass. Several statistical parameters are also presented in Table 7.1 for both cereal rye and annual ryegrass. The slopes and intercepts are not statistically different from the measured values for both cereal rye and annual ryegrass at the 95 % level of statistical confidence. This indicates that the agreement is good, thus supporting the validity of the approach. Alves and Pereira (2000) found the same results on an iceberg lettuce crop (*Lactuca sativa* S.) with r^2 = 0.920, slope 0.93, and intercept 1.37 °C. They attributed the small differences between the two values due to either the fact that G was not measured (giving an error in the $R_n + G$ term and thus in T_s calculated) or to errors in the measured values themselves, as the sun height and azimuth of the measurements, which are known to influence the infrared measurements (Choudhury , 1986).

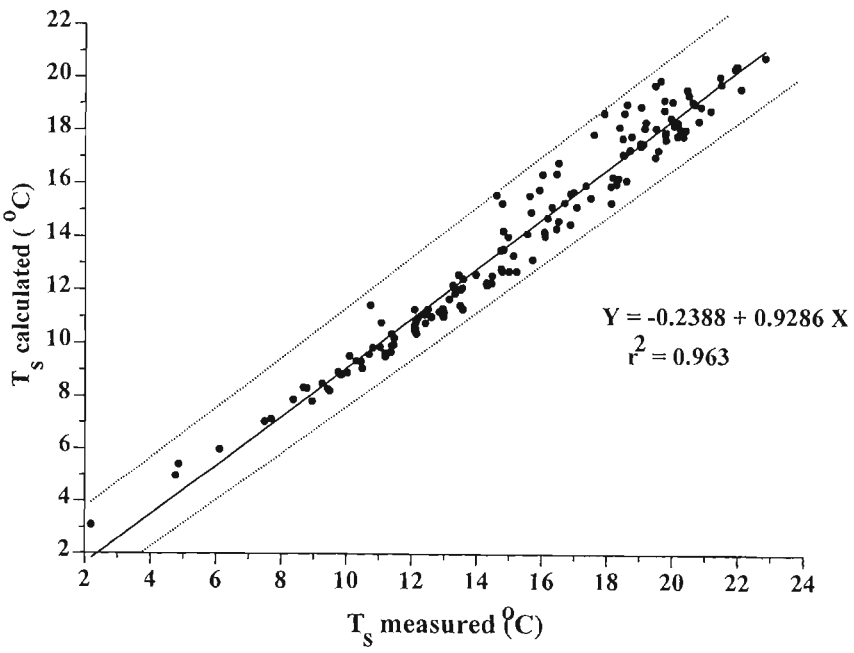

Fig. 7.4 Comparison between the measured values of infrared surface temperature (T_s measured) and the computed values using Eq. 7.7 (T_s calculated) for cereal rye. Each point represents hourly data from day of year 204 to 260 (2002) for $R_n > 0$ W m^{-2}

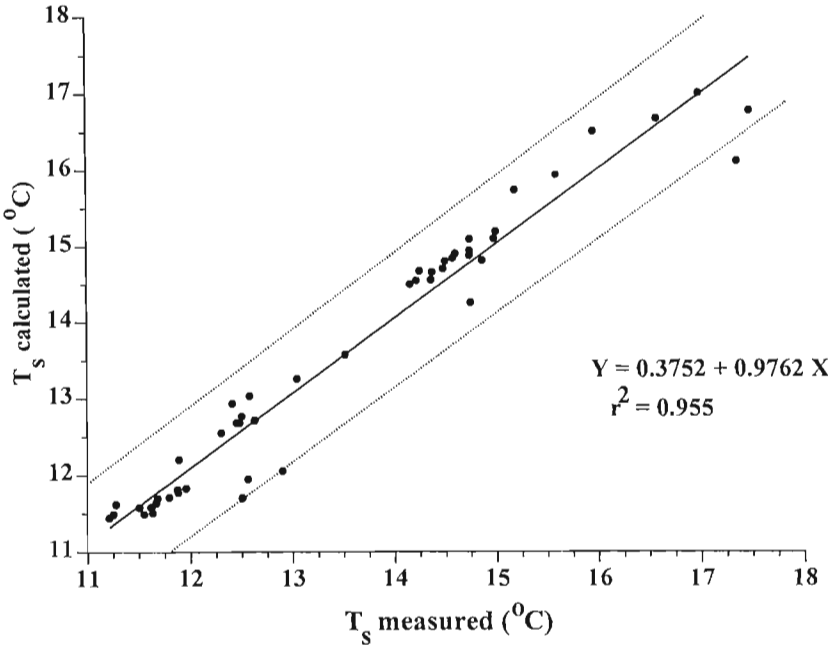

Fig. 7.5 Comparison between the measured values of infrared surface temperature (T_s measured) and the computed values using Eq. 7.7 (T_s calculated) for annual ryegrass. Each point represents hourly data from day of year 300 to 333 (2002) for $R_n > 0$ W m^{-2}

Table 7.2 Statistical parameters associated with the comparison of hourly measured and calculated infrared surface temperature (T_s)

Statistical parameters	Cereal rye	Annual ryegrass
n	150	50
Slope	0.9286	0.9762
Intercept (° C)	-0.2388	0.3752
Sy.x (° C)	0.7629	0.3727
SEslope (° C)	0.0150	0.0306
Upper 95 % for slope	0.9582	1.0377
Lower 95 % for slope	0.8990	0.9148
SEintercept	0.2358	0.4160
Upper 95 % for intercept (° C)	0.2272	1.2116
Lower 95 % for intercept (° C)	-0.7049	-0.4612
% Unsystematic MSE	33.7881	96.6456
% Systematic MSE	66.2119	3.3544

The calculated canopy surface temperature T_s is not statistically different from the measured canopy surface temperature using infrared thermometers for both cereal rye and annual ryegrass. Therefore the infrared surface temperature of fully transpiring crops can be regarded as a wet bulb temperature and Eq. 7.7 can be used to calculate T_s values for non-water-stressed conditions. This equation has the advantage over Eq. 3.6 in that it does not require any knowledge of r_c since the crop is well irrigated. It also has a more flexible use than the experimentally derived non-water-stressed baseline in that measurements can be made under any climatic condition. Previous observations to derive or to validate a baseline are not necessary (Alves and Pereira, 2000).

The values of $R_n + G$ are plotted against $T_s - T_w$, (Tw is the wet bulb temperature (°C)), in Fig. 7.6 for cereal rye and in Fig. 7.7 for annual ryegrass. It can be seen from Fig. 7.6 and 7.7 that $T_s - T_w$ is linear with respect to $R_n + G$, with slope $\frac{\gamma}{\Delta + \gamma} \frac{r_a}{\rho_a C_p}$. The relationship is crop specific since crop height h and the aerodynamic parameters d and z_o affect the calculations of the aerodynamic resistance (r_a). Alves and Pereira (2000) plotted $(R_n - G) / u_z$ against $T_s - T_w$, for lettuce crop and they found a linear relationship (Fig. 7.8) with different values of wind speed. They have used the opposite sign convention, where soil heat flux density (G) is negative during the day.

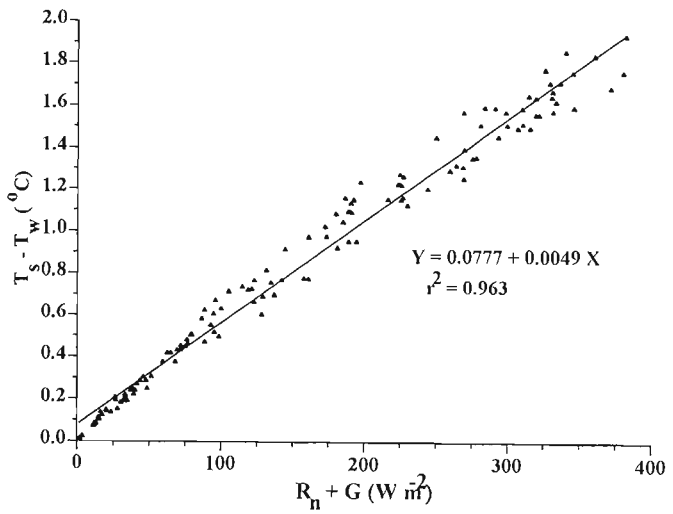

Fig. 7.6 Graphical representation of hourly data of ($T_s - T_w$) *vs* ($R_n + G$) for cereal rye from day of year 204 to 260 (2002)

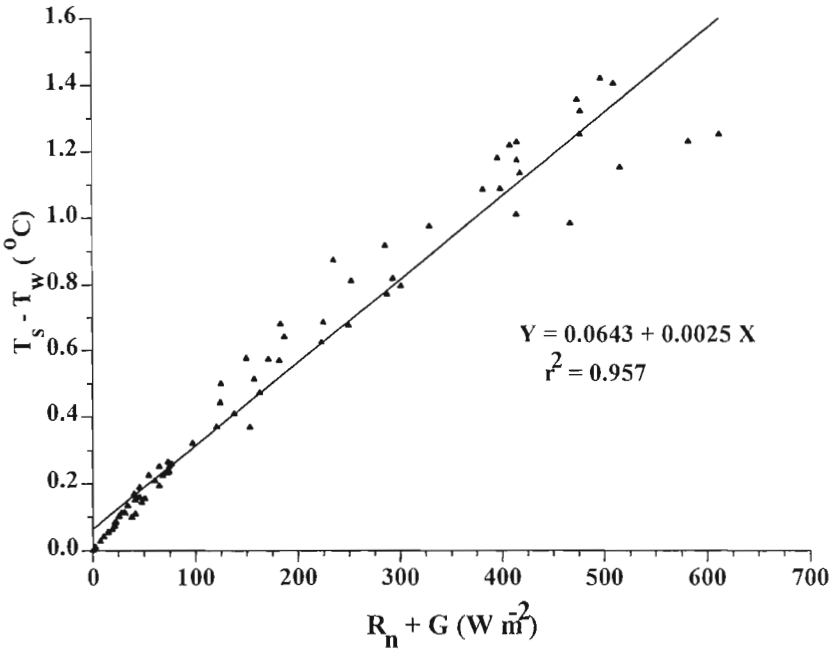

Fig. 7.7 Graphical representation of hourly data of ($T_s - T_w$) *vs* ($R_n + G$) for annual ryegrass from day of year 300 to 333 (2002)

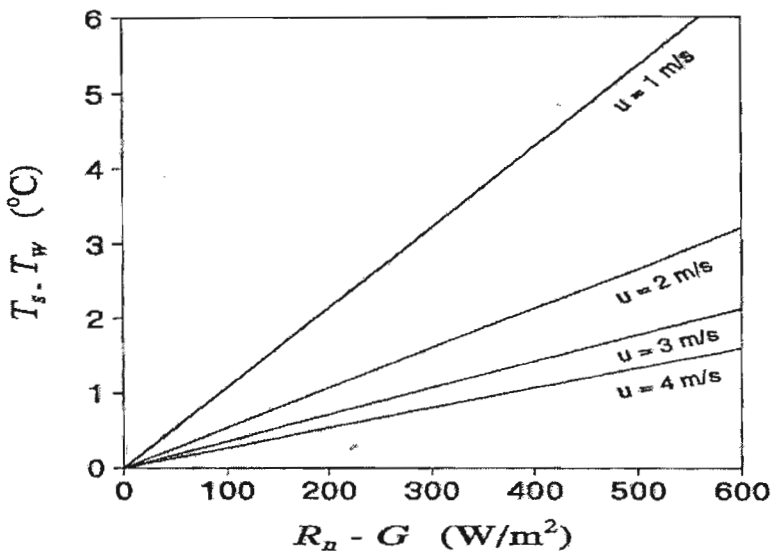

Fig. 7.8 Graphical representation of baselines for lettuce crop based on Eq. 7.7, considering a fixed, average value of Δ (Alves and Pereira, 2000). U is wind speed (m s^{-1})

In Fig. 7.8, Alves and Pereira (2000), used an average value of Δ to show that $T_s - T_w$ values could widely vary, from zero, when there is no energy input to the crop ($R_n + G = 0$), the crop being then in equilibrium with the air mass above it, to infinity, when low wind speeds hinder heat fluxes and cause the crop to decouple from the surrounding atmosphere.

For irrigation scheduling, the use of Eq. 7.7 is similar to the empirical baseline of Idso *et al.* (1981). The value of T_s obtained using this equation has to be used to calculate $(T_s - T_a)_{\text{potential}}$ since it corresponds to a non-water-stressed crop. To obtain maximum yield the measured surface temperature must not be higher than the computed value. If the difference between the measured and the calculated value of T_s is significant, the crop must be irrigated in order to alleviate water stress.

7.5 CONCLUSIONS

The calculated canopy surface temperature T_s is not statistically different from the measured canopy surface temperature using infrared thermometers for both cereal rye and annual ryegrass. Therefore, the infrared surface temperature of fully irrigated cereal rye and annual ryegrass can be regarded as a surface wet bulb temperature. The value of infrared surface temperature can be computed from measured or estimated values of net irradiance, soil heat flux density, aerodynamic resistance and air temperature. The non-water-stressed baseline is a useful concept that can effectively guide the irrigator to obtain maximum yields and to schedule irrigation. Surface temperature can be used to monitor the crop at any time of the day even on cloudy days, which may greatly ease the task of the irrigator.

CHAPTER 8

CONCLUSIONS AND RECOMMENDATIONS FOR FUTURE RESEARCH

8.1 CONCLUSIONS

8.1.1 Introduction

A proper irrigation water management system requires an accurate, simple, automated, non-destructive method to schedule irrigation. Utilization of infrared thermometry to assess plant water stress provides a rapid, non-destructive, reliable estimate of plant water status which would be amenable to larger scale applications and would overcome some of the sampling problems associated with point measurements. Several indices have been developed to schedule irrigation. A useful index is the crop water stress index (CWSI), which normalizes canopy to air temperature differential measurements to water vapour pressure deficit. Therefore an accurate measurement of canopy to air temperature differential is crucial for the determination of CWSI. General discussion and conclusions on the calibration of sensors and the integrity of weather data, determination of the CWSI, and the use of non-water-stressed baselines for irrigation scheduling are presented in this chapter.

8.1.2 Sensor calibration and the integrity of weather data

Accurate measurements of canopy temperature, air temperature, VPD, net irradiance, wind speed and other weather variables are very important for the determination of non-water-stressed baseline and CWSI. Calibration of infrared thermometers, Vaisala CS500 air temperature and relative humidity sensor and thermocouples were performed, and the reliability of the measured weather data analysed.

The Everest and Apogee infrared thermometers require correction for temperatures less than 15 ^{o}C and greater than 35 ^{o}C. Although the calibration relationships were highly linearly significant, the slopes and intercepts should be corrected for greater accuracy.

Since the calibration slope for the thermocouples and Vaisala CS500 air temperature sensor were statistically different from 1, multipliers were used to correct the measurements. The relative humidity sensor needs to be calibrated for RH values less than 25 % and greater than 75 %. The integrity of weather data showed that solar irradiance, net irradiance, wind speed and water vapour pressure deficit were measured accurately. Calculated soil heat flux was underestimated compared to measurements. The calculated surface temperature was underestimated for most of the experimental period compared to measured canopy temperature.

8.1.3 Determination of the crop water stress index

The CWSI technique offers some important advantages for quantifying plant stress between irrigations and monitoring yield potential. It is a rapid, direct, and non-destructive technique, which can be used to survey large fields in a short period of time. The CWSI was determined using the empirical and theoretical methods, and an investigation was made to determine if the CWSI could be used to schedule irrigations in cereal rye and annual rye grass. Both the empirical and theoretical methods require an estimate or measurement of the canopy to air temperature differential, the non-water-stressed baseline, and the non-transpiring canopy to air temperature differential.

The upper (stressed) and lower (non-stressed) baselines were calculated to quantify and monitor crop water stress for cereal rye and annual ryegrass. The non-water-stressed baselines developed in this study can be described by the linear equations $T_c - T_a = 2.0404 - 2.0424 * VPD$ for cereal rye and $T_c - T_a = 2.7377 - 1.2524 * VPD$ for annual ryegrass. There are no baselines previously reported in the literature for both cereal rye and annual ryegrass that can be used for comparison with the non-water-stressed baselines developed from this study.

The theoretical CWSI was greater than the empirical CWSI for most of the experimental days. Variability of empirical $(CWSI)_E$ and theoretical $(CWSI)_T$ values followed soil water content as expected. The CWSI values responded predictably to rainfall and irrigation. The CWSI values of 0.2 to 0.3, corresponding to the refill point of the soil, were found for cereal rye and annual ryegrass from this study, which can be used for timing irrigations to alleviate water stress and avoid excess irrigations.

8.1.4 The use of non-water-stressed baselines for irrigation scheduling

The CWSI method relies on two baselines: the non-water-stressed baseline and the maximum stressed baseline. The non-water-stressed baseline can also be used alone if the aim of the irrigator is to obtain maximum yields (Alves and Pereira, 2000). However the non-water-stressed baseline determined using the empirical method cannot be used for other locations and is only valid for clear sky conditions. The non-water-stressed baseline determined using the theoretical method requires computation of aerodynamic resistance and canopy resistances, as the knowledge of canopy resistance and the values it can assume throughout the day are scarce. The baseline was then determined using a new method by Alves and Pereira (2000), which overcomes these problems. This method evaluated the infrared surface temperature as a wet bulb temperature (Fig. 7.4) for cereal rye and (Fig. 7.5) for annual ryegrass.

From this study, it is concluded that the infrared measured surface temperature of fully irrigated cereal rye and annual ryegrass can be regarded as a surface wet bulb temperature. The value of infrared surface temperature can be computed from measured or estimated values of net irradiance, soil heat flux density, aerodynamic resistance and air temperature. The non-water-stressed baseline is a useful concept that can effectively guide the irrigator to obtain maximum yields and to schedule irrigation. Surface temperature can be used to monitor the crop at any time of the day even on cloudy days, which may greatly ease the task of the irrigator.

8.2 RECOMMENDATIONS FOR FUTURE RESEARCH

Further research on the determination of the non-water-stressed baseline using the empirical method should be conducted since there are no previously reported non-water stressed baselines for cereal rye and annual ryegrass. The theoretical method was based on the assumption that aerodynamic resistance (r_a) adequately represents the resistance to turbulent transport of heat (r_{ah}), water vapour (r_{av}), and momentum. This is not theoretically correct because transport processes of scalars differ from momentum transfer for vegetated surfaces (Thom, 1972). The lower limit of canopy to air temperature differential was calculated by setting the canopy resistance (r_c) to zero, the

case for a wet canopy acting as a free water surface. However the canopy resistance to water flow is not zero for most well watered crops, since they exhibit some resistance to water flow. There is a need to perform more research on the canopy resistance and aerodynamic resistance for cereal rye and annual ryegrass.

Furthermore, studies need to be conducted on the determination of sensible and latent heat flux density using the surface temperature method. This method is simple and could be used for regional monitoring of evapotranspiration, therefore further research should focus on estimating the sensible and latent heat advection, which could be the cause for the overestimation of evaporation.

REFERENCES

Allen RG (1996) Assessing integrity of weather data for reference evaporation estimation. J Irrig Drain Eng ASCE 122: 97-106

Allen RG, Pereira LS, Raes D, Smith M (1998) Crop evapotranspiration – Guidelines for computing crop water requirements – *FAO irrigation and drainage paper* 56. http://www.fao.org/docrep/x049E/X0490e07.htm

Alves I, Fontes JC, Pereira LS (2000) Evapotranspiration estimation from infrared surface temperature. II: The surface temperature as a wet bulb temperature. Amer Soc Agric Eng 43: 599-602

Alves I, Pereira LS (2000) Non-water-stressed baselines for irrigation scheduling with infrared thermometers: A new approach. Irrig Sci 19: 101-106

Alves I, Pereira LS, Perrier A, Pereira LS (1996) Aerodynamic resistances of complete cover crops: How good is the "Big leaf"? Evapotranspiration and irrigation scheduling international conference. (Nov 3-7). ASCE/IA/ICID, San Antonio, Texas, USA.

Apogee Instruments Inc (2001) Standard infrared thermocouple transducer specifications: Model IRTS-S. [Online] [1p] Available at. http://www.apogee-inst.com/irtspects.htm # IRTS-S (accessed 13 Nov. 2001). Apogee Instruments, Inc, Logan, UT, USA.

Berliner P, Oosterhuis DM, Green GC (1984) Evaluation of the infrared thermometer as a crop water stress detector. Agric Forest Meteorol 31: 219-230

Blad BL, Rosenberg NJ (1974) Evapotranspiration by sub irrigated alfalfa and pasture in the East Central Great Plains. Agron J 66: 248-252

Blad BL, Rosenberg NJ (1976) Measurement of crop temperature by leaf thermocouple, infrared thermometry and remotely sensed thermal imagery. Agron J 68: 635-641

Bugbee B, Droter M, Monje O, Tanner B (1999) Evaluation and modification of commercial infrared tranducers for leaf temperature measurement. Adv Space Res 10: 1425-1434

Campbell GS, Norman JM (1990) Estimation of plant water status from canopy temperature: An analysis of the inverse problem. *Applications of Remote Sensing in Agriculture. Butterworths, London, England.* pp 255-271.

Choudhury BJ (1986) An analysis of infrared temperature observations over wheat and calculation of latent heat flux. Agric Forest Meteorol 37: 75-88

Choudhury BJ, Idso SB, Reginato RJ (1987) Analysis of an empirical model for soil heat flux under a growing wheat crop for estimating evaporation by an infrared temperature based energy balance equation. Agric Forest Meteorol 39: 283-297

Clawson KL, Blad BL (1982) Infrared thermometry for scheduling irrigation of corn. Agron J 74: 311-316

Curtis OF (1936) Leaf temperatures and the cooling of leaves by radiation. Plant Physiol 11: 343-364 (cited by Jackson, 1982).

Curtis OF (1938) Wallace and Clum, "Leaf temperatures": A critical analysis with additional data. Am J Bot 25: 761-771 (cited by Jackson, 1982).

Delta-T Devices (1995) ThetaProbe soil moisture sensor. Cambridge, England.

Ehlers JH (1915) The temperature of leaves of pinus in winter. Am J Bot 2: 32-70 (cited by Jackson, 1982).

Ehrler WL (1973) Cotton leaf temperatures as related to soil water depletion and meteorological factors. Agron J 65: 404-409

Ehrler WL, Idso SB, Jackson RD, Reginato RJ (1978) Wheat canopy temperature: Relation to water potential. Agron J 70: 251-256

Fuchs M, Tanner CB (1966) Infrared thermometry of vegetation. Agron J 58: 597-601

Hatfield JL (1983a) The utilization of thermal infrared radiation measurements from grain sorghum crops as a method of assessing their irrigation requirements. Irrig Sci 3: 259-268

Hatfield JL (1983b) Evapotranspiration obtained from remote sensing methods. Adv Irrig 2, 395-415

Hatfield JL (1985) Wheat canopy resistance determined by energy balance techniques. Agron J 77: 279-283

Hatfield JL (1990) Measuring plant stress with an infrared thermometer. HortScience 25(12): 1535-1537

Hillel D (1982) Introduction to Soil Physics. Academic Press, Orlando, USA.

Howell TA, Yazar A, Dusek DA, Copeland KS (1999) Evaluation of crop water stress index for LEPA irrigated corn. Irrig Sci 18: 171-180

Human JJ, de Bruyn LP, Pretorius JP (1991) Research on crop water stress as a key to increased water use efficiency. *Proceedings of the Southern African Irrigation Symposium. (4-6 June), Durban, South Africa.*

Idso SB (1982) Non-water-stressed baselines: A key to measuring and interpreting plant water stress. Agric Meteorol 27: 59-70

Idso SB, Jackson RD, Pinter PJ Jr., Reginato RJ, Hatfield JL (1981) Normalizing the stress-degree-day parameter for environmental variability. Agric Meteorol 24: 45- 55

Jackson RD (1982) Canopy temperature and crop water stress index. Adv Irrig 1: 43-85

Jackson RD, Idso SB, Pinter PJ Jr., Reginato RJ (1981) Canopy temperature as a stress indicator. Water Resour Res 17: 1133-1138

Jackson RD, Kustas WP, Choudhury BJ (1988) A re-examination of the crop water stress index. Irrig Sci 9: 309-317

Jackson RD, Reginato RJ, Idso SB (1977) Wheat canopy temperature: a practical tool for evaluating water requirements. Water Resour Res 13: 651-656

Jalali-Farahani HR, Slack DC, Kopec DM, Matthias AD, Brown PW (1994) Evaluation of resistances for Bermuda grass turf crop water stress index models. Agron J 75: 574-581

Jensen HE, Svendsen H, Jensen SE, Mogensen VO (1990) Canopy-air temperature of crops grown under different irrigation regimes in a temperate humid climate. Irrig Sci 11: 181-188

Jones HG (1999) Use of infrared thermometry for estimation of stomatal conductance as a possible aid to irrigation scheduling. Agric Forest Meteorol 95:139-149

Kalma JD, Alksnis H, Laughlin GP (1988) Calibration of small infrared surface temperature transducers. Agric Forest Meteorol 43: 83-98

Lindroth A (1993) Aerodynamic and canopy resistance of short-rotation forest in relation to leaf area index and climate. Boundary-Layer Meteorol 66: 265-279

MacVicar CN, de Villiers, Loxton RF, Vester E, Lambrechts JN, Merryweather FR, Le Roux J, Van Roogen TH, Harmse HJ Von M (1977) Soil classification. A binomial system for South Africa. *Sci Bull* 390, Dep of Agric Tech Services, Pretoria.

Malek E, Bingham GE, Mccurdy GD (1991) Continuous measurement of aerodynamic and alfalfa canopy resistances using the Bowen ratio-energy balance and Penman-Monteith methods. Boundary-Layer Meteorol 59: 189-194

Massman WJ (1987) A comparative study of some mathematical models of the mean wind structure and aerodynamic drag of plant canopies. Boundary-Layer Meteorol 40: 179-197

Monteith JL, Unsworth MH (1990) Principles of Environmental Physics. 2nd edition, Edward Arnold, England

Nielson DC (1990) Scheduling irrigations for soybeans with the crop water stress index. Field Crops Res 23:103-116

Nielson DC, Gardner BR, Shock CC (1992a) Infrared thermometry and the crop water stress index. 1. History, theory, and baselines. J Prod Agric 5: 462-466

Nielson DC, Gardner BR, Shock CC (1992b) Infrared thermometry and the crop water stress index. 2. Sampling procedures and interpretation. J Prod Agric 5: 466-475

Norman JM, Becker F (1995) Terminology in thermal infrared remote sensing of natural surfaces. Agric Forest Meteorol 77: 153-166

O'Toole JC, Hatfield JL (1983) Effect of wind on the crop water stress index derived by infrared thermometry. Agron J 75: 811-817

O'Toole JC, Real JG (1984) Canopy target dimensions for infrared thermometry. Agron J 76: 863-865

O'Toole JC, Real JG (1986) Estimation of aerodynamic resistances from canopy temperature. Agron J 78: 305-310

Patel NR, Mehta AN, Shekh AM (2001) Canopy temperature and water stress quantification in rainfed pigeonpea (*Cajanus cajan* (L.) Millsp.). Agric Forest Meteorol 109: 223-232

Paw U KT, Ustin SL, Zhang C-A (1989) Anisotropy of thermal infrared exitance in sunflower canopies. Agric Forest Meteorol 48: 45-58

Pinter PJ Jr, Fry KE, Guinn G, Mauney JR (1983) Infrared thermometry: A remote sensing technique for predicting yield in water-stressed cotton. Agric Water Manage 6: 385-395

PlotITW.V3.2 (1999) Scientific Programming Enterprise (SPE). Haslett, Michigan, USA

Qiu GY, Miyamoto K, Sase S, Okushima L (1999) Detection of crop transpiration and water stress by temperature-related approach under field and greenhouse conditions. [Online] [5p] Available at http://ss.jircas.affrc.go.jp/enpage/jarq/34-1/contents.htm (accessed 15 October 2001). Japan Agricultural Research Quarterly. Vol. 34 No. 1

Rameaux (1843) Des temperatures vegetales. (Cited by Jackson, 1982)

Reginato RJ (1990) Scheduling of irrigation for vegetable crops under field conditions. Acta Hort 278: 375-379

Sammis TW (1996) Crop water stress index. [Online] [3p] Available at http://weather.nmsu.edu/Teaching material/soil698/CWSI.htm (accessed 22 Dec. 2001)

Savage (1995) Unpublished. IRT information card for Campbell dataloggers. *SPAC Res. Unit, School of Applied Environmental Sci., Univ. Natal, Pietermaritzburg, South Africa.*

Savage MJ (1998) A spreadsheet for calculating statistical parameters for model evaluation. *SPAC Res. Unit, School of Applied Environmental Sci., Univ. Natal, Pietermaritzburg, South Africa.*

Savage MJ (2000) Unpublished Agrometeorology 210 course notes. *SPAC Res. Unit, School of Applied Environmental sci. Univ. Natal South Africa.*

Savage MJ (2001a) Unpublished Agrometeorology 210 course notes. Environmental Remote Sensing. *SPAC Res. Unit, School of Applied Environmental Sci., Univ. Natal, South Africa.*

Savage MJ (2001b) Personal communication.

Savage MJ (2002a) Personal communication.

Savage MJ (2002b) A spreadsheet for calculating hourly reference evaporation. *SPAC Res. Unit, School of Applied Environmental Sci., Univ. Natal, Pietermaritzburg, South Africa.*

Savage MJ (2002c) Recalibration procedure of capacitive relative humidity sensors improves sensor accuracy to within 1 % relative humidity. Annual Congress of the South African Society of Crop Science. Cedara, January 2002.

Savage MJ, Allan P, Lightbody KE (1997a) The temperature of mature macadamia canopies to intermittent overhead sprinkling. J. S. Afr. Soc. Hort. Sci 7: 74-78

Savage MJ, Everson CS, Metelerkamp BR (1997b) Evaporation measurement above vegetated surfaces using micrometeorological techniques. WRC Report No. 349/1/97, p248, ISBN No: 1868453634.

Savage MJ, Leclerc MY, Karipot A and Prabha TV (2000) Underestimation of eddy covariance sensible heat flux? 24th Agricultural and Forest Meteorology Conference, Davis, California, USA. P 46-47

Stigter CJ, Jiwaji NT, Makonda MM (1982) A calibration plate to determine the performance of infrared thermometers in field use. Agric Meteorol 26: 279-283

Stockle CO, Dugas WA (1992) Evaluating canopy temperature-based indices for irrigation scheduling. Irrig Sci 13: 31-37

Stone LR, Horton ML (1974) Estimating evaporation using canopy temperature. Agron J 66: 450-454

Tanner CB (1963) Plant temperature. Agron J 55: 210- 211

Thom AS (1972) Momentum, mass and heat exchange of vegetation. Quart J Roy Meteorol Soc 98: 124 (cited by Jackson, 1988).

Topp GC, Davis JL, Annan AP (1980) Electromagnetic determination of soil water content: Measurements in coaxial transmission lines. Water Resour Res 16:574-582

University of California, Sustainable Agriculture Research and Education Program (2002) Cover Crop Database [Online] Available at (http://www.sarep.ucdavis.edu) accessed 24 Nov, 2002

Van Bavel CH, Ehrler WL (1968) Water loss from a sorghum field and stomatal control. Agron J 60: 84-86

Walker GK, Hatfield JL (1979) A test of the stress-degree-day concept using multiple planting dates of red kidney beans. Agron J 71: 967-972

Wallace RH, Clum HH (1938) Leaf temperatures. Amer J Bot 25: 83-97

Wanjura DF, Hatfield JL, Upchurch DR (1990) Crop water stress index relationships with crop productivity. Irrig Sci 11: 93-99

Wanjura DF, Kelly CA, Wendt CW, Hatfield JL (1984) Canopy temperature and water stress of cotton crops with complete and partial ground cover. Irrig Sci 5: 37-46

Wanjura DF, Upchurch DR (1996) Time thresholds for canopy temperature-based irrigation. Evapotranspiration and irrigation scheduling. Proceedings of the International Conf. (San Antonio, Texas, 3-6 Nov), ASAE/AI/ICID, 295-303 (taken from Alves I, Pereira LS, 2000)

Wanjura DF, Upchurch DR, Mahan JR (1992) Automated irrigation based on threshold canopy temperature. Trans ASAE 35: 153-159

Wikipedia: The free encyclopedia (2003) Stefan-Boltzmann constant. [Online] [1p] Available at http://www.wikipedia.org/wiki/Stefan-Boltzmann_constant (modified 27 Jan. 2003; accessed 15 April 2003)

APPENDIX 4.1

CR7X Program and wiring of the sensors to the logger used for measurement in the field

```
;{CR7}
;IRTE1      C1: 1H BROWN/ORANGE, 1L BLACK,
+12V RED
;IRTE2      C1: 2H BROWN/ORANGE, 2L BLACK,
+12V RED
;APOGEE1    C1: 3H YELLOW, 3L RED(TARGET), 4H
YELLOW, 4L RED
;APOGEE2    C1: 5H YELLOW, 5L RED(TARGET), 6H
YELLOW, 6L RED
;INET1      C1: 7H RED/WHITE, 7L BLACK
;INET2      C1: 8H RED/WHITE, 8L BLACK
;CM3        C1: 9H RED, 9L BLUE/BLACK
;WIND SPEED C1: 10H WHITE, 10L BLUE (160), 11H
YELLOW, 11L GREEN (163V)
;FSOIL 1    C1: 12H Red 12L Black
;FSOIL 2    C1: 13H Red 13L Black
;THETA PROBE C2: 1H YELLOW, 1L GREEN, +12V
RED
;Tair       C2: 2H PURPLE
;RH         C2: 2L BROWN, G GREEN, +12V YELLOW
;TSOILAVERAGEC2: 3H BLUE, 3L RED
;RAIN       C1: PI RED G BLACK
;12 V CONTROL BOX
;YELLOW TO C1; BLACK TO G; RED TO 12
V;(CARD 2)
;RED TO SECOND 12 V; RED TO STRIP
CONNECTOR FOR SENSORS

;{CR7}
;
*Table 1 Program
 01: 60      Execution Interval (seconds)

1: Battery Voltage (P10)
 1: 1       Loc [ Vbattery  ]

2: Panel Temperature (P17)
 1: 1       In Card
 2: 2       Loc [ Panel_T   ]


3: Set Port(s) (P20)
 1: 1       Set High
 2: 2       Ex Card
 3: 1       Port Number

;The delay for the everst is at least 700 cs (800 for saftey)

4: Excitation with Delay (P22)
 1: 2       Ex Card
 2: 1       Ex Channel
 3: 0       Delay w/Ex (units = 0.01 sec)
 4: 800     Delay After Ex (units = 0.01 sec)
 5: 0       mV Excitation

;Everst IRTE1

5: Volt (Diff) (P2)
 1: 1       Reps
 2: 8       5000 mV Slow Range
 3: 1       In Card
 4: 1       DIFF Channel
 5: 3       Loc [ IRTE_1    ]
 6: .10883  Mult
 7: -1.8349 Offset

;Everst IRTE2

6: Volt (Diff) (P2)
 1: 1       Reps
 2: 8       5000 mV Slow Range
 3: 1       In Card
 4: 2       DIFF Channel
 5: 5       Loc [ IRTE_2    ]
 6: .11342  Mult
 7: -2.9449 Offset

7: Volt (Diff) (P2)
 1: 1       Reps
 2: 8       5000 mV Slow Range
 3: 2       In Card
 4: 1       DIFF Channel
 5: 23      Loc [ Theta_V   ]
 6: 0.001   Mult
 7: 0.0     Offset

;Purple Tair
8: Volt (SE) (P1)
 1: 1       Reps
 2: 8       5000 mV Slow Range
 3: 2       In Card
 4: 3       SE Channel
 5: 26      Loc [ Tair      ]
 6: .10134  Mult
 7: -40.356 Offset

;Brown RH
;Yellow 12V

9: Volt (SE) (P1)
 1: 1       Reps
 2: 8       5000 mV Slow Range
 3: 2       In Card
 4: 4       SE Channel
 5: 27      Loc [ RH        ]
 6: 0.1     Mult
 7: 0.0     Offset


10: Set Port(s) (P20)
 1: 0       Set Low
 2: 2       Ex Card
 3: 1       Port Number

11: Polynomial (P55)
 1: 1       Reps
 2: 3       X Loc [ IRTE_1    ]
 3: 4       F(X) Loc [ IRTE1_POL ]
 4: -2.9404 C0
 5: 0.1884  C1
```

```
6: -0.002  C2
7: 0       C3
8: 0       C4
9: 0       C5

12: Z=X+Y (P33)
1: 3       X Loc [ IRTE_1   ]
2: 4       Y Loc [ IRTE1_POL ]
3: 4       Z LOC [ IRTE1_POL ]

13: Polynomial (P55)
1: 1       Reps
2: 5       X Loc [ IRTE_2   ]
3: 6       F(X) Loc [ IRTE2_POL ]
4: -4.1032  C0
5: 0.2391   C1
6: -0.0023  C2
7: 0       C3
8: 0       C4
9: 0       C5

14: Z=X+Y (P33)
1: 5       X Loc [ IRTE_2   ]
2: 6       Y Loc [ IRTE2_POL ]
3: 6       Z LOC [ IRTE2_POL ]

;Apogee IRTA1

15: Thermocouple Temp (DIFF) (P14)
1: 1       Reps
2: 2       5000 æV Slow Range
3: 1       In Card
4: 3       DIFF Channel
5: 3       Type K (Chromel-Alumel)
6: 2       Ref Temp (Deg. C) Loc [ Panel_T  ]
7: 7       Loc [ IRTA_1   ]
8: 1047.1  Mult
9: -1.0071  Offset

16: Thermocouple Temp (DIFF) (P14)
1: 1       Reps
2: 2       5000 æV Slow Range
3: 1       In Card
4: 4       DIFF Channel
5: 3       Type K (Chromel-Alumel)
6: 2       Ref Temp (Deg. C) Loc [ Panel_T  ]
7: 8       Loc [ IRTA1_BOD ]
8: 1.0     Mult
9: 0.0     Offset

17: Z=X*F (P37)
1: 7       X Loc [ IRTA_1   ]
2: 0.001   F
3: 7       Z LOC [ IRTA_1   ]

18: Polynomial (P55)
1: 1       Reps
2: 7       X Loc [ IRTA_1   ]
3: 9       F(X) Loc [ IRTA1_POL ]
4: -3.0081  C0
5: 0.2261   C1
6: -0.0036  C2
7: 0       C3
8: 0       C4
9: 0       C5

19: Z=X+Y (P33)
1: 7       X Loc [ IRTA_1   ]
2: 9       Y Loc [ IRTA1_POL ]
3: 9       Z LOC [ IRTA1_POL ]

;Apogee IRTA_2

20: Thermocouple Temp (DIFF) (P14)
1: 1       Reps
2: 2       5000 æV Slow Range
3: 1       In Card
4: 5       DIFF Channel
5: 3       Type K (Chromel-Alumel)
6: 2       Ref Temp (Deg. C) Loc [ Panel_T  ]
7: 10      Loc [ IRTA_2   ]
8: 1031.3  Mult
9: -1.6693  Offset

21: Thermocouple Temp (DIFF) (P14)
1: 1       Reps
2: 2       5000 æV Slow Range
3: 1       In Card
4: 6       DIFF Channel
5: 3       Type K (Chromel-Alumel)
6: 2       Ref Temp (Deg. C) Loc [ Panel_T  ]
7: 11      Loc [ IRTA2_BOD ]
8: 1.0     Mult
9: 0.0     Offset

22: Z=X*F (P37)
1: 10      X Loc [ IRTA_2   ]
2: 0.001   F
3: 10      Z LOC [ IRTA_2   ]

23: Polynomial (P55)
1: 1       Reps
2: 10      X Loc [ IRTA_2   ]
3: 12      F(X) Loc [ IRTA2_POL ]
4: -3.4538  C0
5: 0.1847   C1
6: -0.0031  C2
7: 0       C3
8: 0       C4
9: 0       C5

24: Z=X+Y (P33)
1: 10      X Loc [ IRTA_2   ]
2: 12      Y Loc [ IRTA2_POL ]
3: 12      Z LOC [ IRTA2_POL ]

;Net radiometers
;Inet_1

25: Volt (Diff) (P2)
1: 1       Reps
2: 5       150 mV Slow Range
3: 1       In Card
4: 7       DIFF Channel
5: 13      Loc [ Inet_1   ]
6: 1       Mult
7: 0       Offset

26: If (X<=>F) (P89)
1: 13      X Loc [ Inet_1   ]
2: 3       >=
3: 0       F
4: 30      Then Do

27: Z=X*F (P37)
1: 13      X Loc [ Inet_1   ]
2: 9.43    F
3: 13      Z LOC [ Inet_1   ]

28: Else (P94)
```

```
29: Z=X*F (P37)
 1: 13     X Loc [ Inet_1   ]
 2: 11.83  F
 3: 13     Z LOC [ Inet_1   ]

30: End (P95)

;Inet_2

31: Volt (Diff) (P2)
 1: 1      Reps
 2: 5      150 mV Slow Range
 3: 1      In Card
 4: 8      DIFF Channel
 5: 14     Loc [ Inet_2   ]
 6: 1.0    Mult
 7: 0.0    Offset

32: If (X<=>F) (P89)
 1: 14     X Loc [ Inet_2   ]
 2: 3      >=
 3: 0      F
 4: 30     Then Do

33: Z=X*F (P37)
 1: 14     X Loc [ Inet_2   ]
 2: 9.38   F
 3: 14     Z LOC [ Inet_2   ]

34: Else (P94)

35: Z=X*F (P37)
 1: 14     X Loc [ Inet_2   ]
 2: 11.75  F
 3: 14     Z LOC [ Inet_2   ]

36: End (P95)

;CM3

37: Volt (Diff) (P2)
 1: 1      Reps
 2: 4      50 mV Slow Range
 3: 1      In Card
 4: 9      DIFF Channel
 5: 15     Loc [ Is       ]
 6: 50.226 Mult
 7: 0      Offset

;Wind speed
;Sensor 160 (north)

38: Volt (Diff) (P2)
 1: 2      Reps
 2: 6      500 mV Slow Range
 3: 1      In Card
 4: 10     DIFF Channel
 5: 16     Loc [ WindmV_1  ]
 6: 1.0    Mult
 7: 0.0    Offset

39: If (X<=>F) (P89)
 1: 16     X Loc [ WindmV_1  ]
 2: 4      <
 3: 59.29  F
 4: 30     Then Do

40: Z=X*F (P37)
 1: 16     X Loc [ WindmV_1  ]
 2: 0.0123 F
 3: 16     Z LOC [ WindmV_1  ]

41: Z=X+F (P34)
 1: 16     X Loc [ WindmV_1  ]
 2: 0.13   F
 3: 16     Z LOC [ WindmV_1  ]

42: Else (P94)

43: Z=X*F (P37)
 1: 16     X Loc [ WindmV_1  ]
 2: 0.0149 F
 3: 16     Z LOC [ WindmV_1  ]

44: Z=X+F (P34)
 1: 16     X Loc [ WindmV_1  ]
 2: 0.034  F
 3: 16     Z LOC [ WindmV_1  ]

45: End (P95)

;Sensor 163 (east)

46: If (X<=>F) (P89)
 1: 17     X Loc [ WindmV_2  ]
 2: 4      <
 3: 62.09  F
 4: 30     Then Do

47: Z=X*F (P37)
 1: 17     X Loc [ WindmV_2  ]
 2: 0.0125 F
 3: 17     Z LOC [ WindmV_2  ]

48: Z=X+F (P34)
 1: 17     X Loc [ WindmV_2  ]
 2: 0.13   F
 3: 17     Z LOC [ WindmV_2  ]

49: Else (P94)

50: Z=X*F (P37)
 1: 17     X Loc [ WindmV_2  ]
 2: 0.0145 F
 3: 17     Z LOC [ WindmV_2  ]

51: Z=X+F (P34)
 1: 17     X Loc [ WindmV_2  ]
 2: 0.023  F
 3: 17     Z LOC [ WindmV_2  ]

52: End (P95)

53: Z=X*Y (P36)
 1: 16     X Loc [ WindmV_1  ]
 2: 16     Y Loc [ WindmV_1  ]
 3: 18     Z LOC [ U        ]

54: Z=X*Y (P36)
 1: 17     X Loc [ WindmV_2  ]
 2: 17     Y Loc [ WindmV_2  ]
 3: 19     Z LOC [ Winddirec ]

55: Z=X+Y (P33)
 1: 18     X Loc [ U        ]
 2: 19     Y Loc [ Winddirec ]
 3: 18     Z LOC [ U        ]

56: Z=SQRT(X) (P39)
```

```
 1: 18     X Loc [ U       ]
 2: 18     Z LOC [ U       ]

57:  Z=ARCTAN(X/Y) (P66)
 1: 16     X Loc [ WindmV_1  ]
 2: 17     Y Loc [ WindmV_2  ]
 3: 19     Z LOC [ Winddirec ]

;Soil heat

58:  Volt (Diff) (P2)
 1: 1      Reps
 2: 3      15 mV Slow Range
 3: 1      In Card
 4: 12     DIFF Channel
 5: 20     Loc [ Fsoil_1   ]
 6: 47.6   Mult
 7: 0.0    Offset

59:  Volt (Diff) (P2)
 1: 1      Reps
 2: 3      15 mV Slow Range
 3: 1      In Card
 4: 13     DIFF Channel
 5: 21     Loc [ Fsoil_2   ]
 6: 46.3   Mult
 7: 0.0    Offset

60:  Thermocouple Temp (DIFF) (P14)
 1: 3      Reps
 2: 2      5000 æV Slow Range
 3: 2      In Card
 4: 3      DIFF Channel
 5: 1      Type T (Copper-Constantan)
 6: 2      Ref Temp (Deg. C) Loc [ Panel_T   ]
 7: 32     Loc [ Tsoilave1 ]
 8: 1.0161  Mult
 9: -0.5335  Offset

;Theta probe (ML1)

61:  Polynomial (P55)
 1: 1      Reps
 2: 23     X Loc [ Theta_V   ]
 3: 24     F(X) Loc [ Theta_m   ]
 4: 1.0    C0
 5: 6.19   C1
 6: -9.72  C2
 7: 24.35  C3
 8: -30.84  C4
 9: 14.73  C5


62:  Polynomial (P55)
 1: 1      Reps
 2: 23     X Loc [ Theta_V   ]
 3: 25     F(X) Loc [ Theta_o   ]
 4: 1      C0
 5: 6.19   C1
 6: -9.72  C2
 7: 24.35  C3
 8: -30.84  C4
 9: 14.73  C5

63:  Z=X+F (P34)
 1: 24     X Loc [ Theta_m   ]
 2: -1.6   F
 3: 24     Z LOC [ Theta_m   ]
;1/8.4 = 0.11905 for mineral soils

64:  Z=X*F (P37)
 1: 24     X Loc [ Theta_m   ]
 2: .11905  F
 3: 24     Z LOC [ Theta_m   ]


65:  Z=X+F (P34)
 1: 25     X Loc [ Theta_o   ]
 2: -1.3   F
 3: 25     Z LOC [ Theta_o   ]
;1/7.8 = 0.12987 for organic soils


66:  Z=X*F (P37)
 1: 25     X Loc [ Theta_o   ]
 2: .12987  F
 3: 25     Z LOC [ Theta_o   ]

;Vaisala RH and air_t

67:  If (X<=>F) (P89)
 1: 27     X Loc [ RH      ]
 2: 3      >=
 3: 100    F
 4: 30     Then Do

68:  If (X<=>F) (P89)
 1: 27     X Loc [ RH      ]
 2: 4      <
 3: 108    F
 4: 30     Then Do

69:  Z=F (P30)
 1: 100    F
 2: 27     Z LOC [ RH      ]

70:  End (P95)

71:  End (P95)

72:  Saturation Vapor Pressure (P56)
 1: 26     Temperature Loc [ Tair    ]
 2: 29     Loc [ es_kPa    ]

73:  Z=X*F (P37)
 1: 27     X Loc [ RH      ]
 2: 0.01   F
 3: 28     Z LOC [ RH001   ]

74:  Z=X*Y (P36)
 1: 28     X Loc [ RH001   ]
 2: 29     Y Loc [ es_kPa    ]
 3: 28     Z LOC [ RH001   ]

75:  Z=X-Y (P35)
 1: 29     X Loc [ es_kPa    ]
 2: 28     Y Loc [ RH001   ]
 3: 30     Z LOC [ vpd_kPa   ]

76:  Pulse (P3)
 1: 1      Reps
 2: 1      In Card
 3: 1      Pulse Input Channel
 4: 2      Switch Closure, All Counts
 5: 31     Loc [ Rain      ]
 6: 1.0    Mult
 7: 0.0    Offset

77:  If time is (P92)
 1: 0      Minutes into a
```

```
 2: 15     Minute Interval
 3: 10     Set Output Flag High

78: Set Active Storage Area (P80)
 1: 1      Final Storage
 2: 100    Array ID

79: Real Time (P77)
 1: 0220   Day,Hour/Minute (midnight = 2400)

80: Average (P71)
 1: 24     Reps
 2: 3      Loc [ IRTE_1    ]

81: Average (P71)
 1: 1      Reps
 2: 28     Loc [ RH001     ]

82: Average (P71)
 1: 1      Reps
 2: 30     Loc [ vpd_kPa   ]

83: Sample (P70)
 1: 1      Reps
 2: 27     Loc [ RH        ]

84: Totalize (P72)
 1: 1      Reps
 2: 31     Loc [ Rain      ]

85: Average (P71)
 1: 3      Reps
 2: 32     Loc [ Tsoilave1 ]

86: If time is (P92)
 1: 0      Minutes into a
 2: 1440   Minute Interval
 3: 10     Set Output Flag High

87: Set Active Storage Area (P80)
 1: 1      Final Storage
 2: 200    Array ID

88: Real Time (P77)
 1: 0220   Day,Hour/Minute (midnight = 2400)

89: Average (P71)
 1: 1      Reps
 2: 1      Loc [ Vbattery  ]


*Table 2 Program
 02: 60     Execution Interval (seconds)

1: Serial Out (P96)
 1: 30     Storage Module

*Table 3 Subroutines

End Program

-Input Locations-
1 Vbattery  1 1 1
2 Panel_T   1 5 1
3 IRTE_1    1 3 1
4 IRTE1_POL 1 2 2
5 IRTE_2    1 3 1
6 IRTE2_POL 1 2 2
7 IRTA_1    5 4 2
8 IRTA1_BOD 1 1 1
9 IRTA1_POL 1 2 2
10 IRTA_2   5 4 2
11 IRTA2_BOD 1 1 1
12 IRTA2_POL 1 2 2
13 Inet_1   1 4 3
14 Inet_2   1 4 3

15 Is       1 1 1
16 WindmV_1 5 9 5
17 WindmV_2 17 9 5
18 U        1 3 3
19 Winddirec 1 2 2
20 Fsoil_1  5 1 1
21 Fsoil_2  1 1 1
22 empity   1 1 0
23 Theta_V  1 3 1
24 Theta_m  1 3 3
25 Theta_o  1 3 3
26 Tair     1 2 1
27 RH       1 4 2
28 RH001    1 3 2
29 es_kPa   1 2 1
30 vpd_kPa  1 1 1
31 Rain     1 1 1
32 Tsoilave1 5 1 1
33 Tsoilave2 9 1 1
34 Tsoilave3 17 0 1
35 Tsoilave4 1 0 0
36 Tsoilav_5 1 0 0
37 Tsoilav_6 1 0 0
38 Tsoilav_7 1 0 0
39 Tsoilav_8 1 0 0
40 Tsoilav_9 1 0 0
41 Tsoila_10 1 0 0
-Program Security-
0
0000
0000
```

```
Program Trace Information File for:  CR710702.CSI
Date: 10/1/2002
Time: 12:06:05

T = Program Table Number
N = Sequential Program Instruction Location Number
Instruction = Instruction Number and Name

Inst ExTm = Individual Instruction Execution Time
Block ExTm = Cumulative Execution Time for program block,
        i.e., subroutine
Prog ExTm = Cumulative Total Program Execution Time


Output Flag High
                                                Inst  Block
Prog      Inst  Block   Prog
                                                ExTm   ExTm
ExTm      ExTm   ExTm   ExTm
T|N|Instruction                                 (msec) (msec)
(msec)    (msec) (msec) (msec)
----------------                                ------ ------ ----
--   ------ ------ ------
1|1|10 Battery Voltage                          22.6   22.6
22.6      22.6   22.6   22.6
1|2|17 Panel Temperature                        116.2  138.8
138.8     116.2  138.8  138.8
1|3|20 Set Port(s)                               2.9  141.7
141.7       2.9  141.7  141.7
1|4|22 Excitation with Delay                   8010.8 8152.5
8152.5   8010.8 8152.5 8152.5
1|5|2 Volt (Diff)                              97.4 8249.9
8249.9      97.4 8249.9 8249.9
1|6|2 Volt (Diff)                              97.4 8347.3
8347.3      97.4 8347.3 8347.3
1|7|2 Volt (Diff)                              97.4 8444.7
8444.7      97.4 8444.7 8444.7
1|8|1 Volt (SE)                                79.4 8524.1
8524.1      79.4 8524.1 8524.1
1|9|1 Volt (SE)                                79.4 8603.5
8603.5      79.4 8603.5 8603.5
1|10|20 Set Port(s)                             2.9 8606.4
8606.4       2.9 8606.4 8606.4
1|11|55 Polynomial                              4.0 8610.4
8610.4       4.0 8610.4 8610.4
1|12|33 Z=X+Y                                   1.1 8611.5
8611.5       1.1 8611.5 8611.5
1|13|55 Polynomial                              4.0 8615.5
8615.5       4.0 8615.5 8615.5
1|14|33 Z=X+Y                                   1.1 8616.6
8616.6       1.1 8616.6 8616.6
1|15|14 Thermocouple Temp (DIFF)              104.2 8720.8
8720.8     104.2 8720.8 8720.8
1|16|14 Thermocouple Temp (DIFF)              104.2 8825.0
8825.0     104.2 8825.0 8825.0
1|17|37 Z=X*F                                   0.9 8825.9
8825.9       0.9 8825.9 8825.9
1|18|55 Polynomial                              4.0 8829.9
8829.9       4.0 8829.9 8829.9
1|19|33 Z=X+Y                                   1.1 8831.0
8831.0       1.1 8831.0 8831.0
1|20|14 Thermocouple Temp (DIFF)              104.2 8935.2
8935.2     104.2 8935.2 8935.2
1|21|14 Thermocouple Temp (DIFF)              104.2 9039.4
9039.4     104.2 9039.4 9039.4
1|22|37 Z=X*F                                   0.9 9040.3
9040.3       0.9 9040.3 9040.3
1|23|55 Polynomial                              4.0 9044.3
9044.3       4.0 9044.3 9044.3
1|24|33 Z=X+Y                                   1.1 9045.4
9045.4       1.1 9045.4 9045.4
1|25|2 Volt (Diff)                             97.4 9142.8
9142.8      97.4 9142.8 9142.8
1|26|89 If (X<=>F)                              0.4 9143.2
9143.2       0.4 9143.2 9143.2
1|27|37 Z=X*F                                   0.9 9144.1
9144.1       0.9 9144.1 9144.1
1|28|94 Else                                    0.2 9144.3
9144.3       0.2 9144.3 9144.3
1|29|37 Z=X*F                                   0.9 9145.2
9145.2       0.9 9145.2 9145.2
1|30|95 End                                     0.2 9145.4
9145.4       0.2 9145.4 9145.4
1|31|2 Volt (Diff)                             97.4 9242.8
9242.8      97.4 9242.8 9242.8
1|32|89 If (X<=>F)                              0.4 9243.2
9243.2       0.4 9243.2 9243.2
1|33|37 Z=X*F                                   0.9 9244.1
9244.1       0.9 9244.1 9244.1
1|34|94 Else                                    0.2 9244.3
9244.3       0.2 9244.3 9244.3
1|35|37 Z=X*F                                   0.9 9245.2
9245.2       0.9 9245.2 9245.2
1|36|95 End                                     0.2 9245.4
9245.4       0.2 9245.4 9245.4
1|37|2 Volt (Diff)                             97.4 9342.8 9342.8
97.4 9342.8 9342.8
1|38|2 Volt (Diff)                            140.8 9483.6 9483.6
140.8 9483.6 9483.6
1|39|89 If (X<=>F)                              0.4 9484.0 9484.0
0.4 9484.0 9484.0
1|40|37 Z=X*F                                   0.9 9484.9 9484.9
0.9 9484.9 9484.9
1|41|34 Z=X+F                                   0.9 9485.8 9485.8
0.9 9485.8 9485.8
1|42|94 Else                                    0.2 9486.0 9486.0
0.2 9486.0 9486.0
1|43|37 Z=X*F                                   0.9 9486.9 9486.9
0.9 9486.9 9486.9
1|44|34 Z=X+F                                   0.9 9487.8 9487.8
0.9 9487.8 9487.8
1|45|95 End                                     0.2 9488.0 9488.0
0.2 9488.0 9488.0
1|46|89 If (X<=>F)                              0.4 9488.4 9488.4
0.4 9488.4 9488.4
1|47|37 Z=X*F                                   0.9 9489.3 9489.3
0.9 9489.3 9489.3
1|48|34 Z=X+F                                   0.9 9490.2 9490.2
0.9 9490.2 9490.2
1|49|94 Else                                    0.2 9490.4 9490.4
0.2 9490.4 9490.4
1|50|37 Z=X*F                                   0.9 9491.3 9491.3
0.9 9491.3 9491.3
1|51|34 Z=X+F                                   0.9 9492.2 9492.2
0.9 9492.2 9492.2
1|52|95 End                                     0.2 9492.4 9492.4
0.2 9492.4 9492.4
1|53|36 Z=X*Y                                   1.2 9493.6 9493.6
1.2 9493.6 9493.6
1|54|36 Z=X*Y                                   1.2 9494.8 9494.8
1.2 9494.8 9494.8
1|55|33 Z=X+Y                                   1.1 9495.9 9495.9
1.1 9495.9 9495.9
1|56|39 Z=SQRT(X)                              12.0 9507.9 9507.9
12.0 9507.9 9507.9
1|57|66 Z=ARCTAN(X/Y)                           6.7 9514.6 9514.6
6.7 9514.6 9514.6
1|58|2 Volt (Diff)                             97.4 9612.0 9612.0
97.4 9612.0 9612.0
1|59|2 Volt (Diff)                             97.4 9709.4 9709.4
97.4 9709.4 9709.4
1|60|14 Thermocouple Temp (DIFF)              190.6 9900.0 9900.0
190.6 9900.0 9900.0
1|61|55 Polynomial                              5.2 9905.2 9905.2
5.2 9905.2 9905.2
1|62|55 Polynomial                              5.2 9910.4 9910.4
5.2 9910.4 9910.4
1|63|34 Z=X+F                                   0.9 9911.3 9911.3
0.9 9911.3 9911.3
1|64|37 Z=X*F                                   0.9 9912.2 9912.2
0.9 9912.2 9912.2
1|65|34 Z=X+F                                   0.9 9913.1 9913.1
0.9 9913.1 9913.1
1|66|37 Z=X*F                                   0.9 9914.0 9914.0
0.9 9914.0 9914.0
1|67|89 If (X<=>F)                              0.4 9914.4 9914.4
0.4 9914.4 9914.4
1|68|89 If (X<=>F)                              0.4 9914.8 9914.8
0.4 9914.8 9914.8
1|69|30 Z=F                                     0.3 9915.1 9915.1
0.3 9915.1 9915.1
1|70|95 End                                     0.2 9915.3 9915.3
0.2 9915.3 9915.3
1|71|95 End                                     0.2 9915.5 9915.5
0.2 9915.5 9915.5
1|72|56 Saturation Vapor Pressure               4.2 9919.7 9919.7
4.2 9919.7 9919.7
1|73|37 Z=X*F                                   0.9 9920.6 9920.6
0.9 9920.6 9920.6
1|74|36 Z=X*Y                                   1.2 9921.8 9921.8
1.2 9921.8 9921.8
1|75|35 Z=X-Y                                   1.1 9922.9 9922.9
1.1 9922.9 9922.9
1|76|3 Pulse                                    6.0 9928.9 9928.9
6.0 9928.9 9928.9
1|77|92 If time is                              0.3 9929.2 9929.2
0.3 9929.2 9929.2
 Output Flag Set @ 177 for Array 100
1|78|80 Set Active Storage Area                 0.2 9929.4 9929.4
0.2 9929.4 9929.4
1|79|77 Real Time                               0.1 9929.5 9929.5
1.0 9930.4 9930.4
 Output Data 2 Values
1|80|71 Average                                12.9 9942.4 9942.4
74.1 10004.5 10004.5
 Output Data 24 Values
1|81|71 Average                                 1.4 9943.8 9943.8
5.1 10009.6 10009.6
 Output Data 1 Values
```

```
1|82|71 Average                        1.4 9945.2
9945.2      5.1 10014.7 10014.7
 Output Data 1 Values
1|83|70 Sample                         0.1 9945.3
9945.3      1.0 10015.7 10015.7
 Output Data 1 Values
1|84|72 Totalize                       1.1 9946.4
9946.4      2.1 10017.8 10017.8
 Output Data 1 Values
1|85|71 Average                        2.4 9948.8
9948.8     11.1 10028.9 10028.9
 Output Data 3 Values
1|86|92 If time is                     0.3 9949.1
9949.1      0.3 10029.2 10029.2
 Output Flag Set @ 186 for Array 200
1|87|80 Set Active Storage Area      0.2 9949.3
9949.3      0.2 10029.4 10029.4
1|88|77 Real Time                      0.1 9949.4
9949.4      1.0 10030.4 10030.4
 Output Data 2 Values
1|89|71 Average                        1.4 9950.8
9950.8      5.1 10035.5 10035.5
 Output Data 1 Values

Program Table 1 Execution Interval   60.000 Seconds

Table 1 Estimated Total Program Execution Time in
msec 9950.8 w/Output 10035.5

Table 1 Estimated Total Final Storage Locations used
per day 3268.0


---------- Table 2 ----------
2|1|96 Serial Out                      0.2    0.2
0.2      0.2    0.2    0.2

Program Table 2 Execution Interval   60.000 Seconds

Table 2 Estimated Total Program Execution Time in
msec    0.2 w/Output    0.2

Table 2 Estimated Total Final Storage Locations used
per day    0.0


Estimated Total Final Storage Locations used per day
3268.0
```

Final Storage Label File for: CR710702.CSI
Date: 10/1/2002
Time: 12:06:05

100 Output_Table 15.00 Min
1 100 L
2 Day_RTM L
3 Hour_Minute_RTM L
4 IRTE_1_AVG L
5 IRTE1_POL_AVG L
6 IRTE_2_AVG L
7 IRTE2_POL_AVG L
8 IRTA_1_AVG L
9 IRTA1_BOD_AVG L
10 IRTA1_POL_AVG L
11 IRTA_2_AVG L
12 IRTA2_BOD_AVG L
13 IRTA2_POL_AVG L
14 Inet_1_AVG L
15 Inet_2_AVG L
16 Is_AVG L
17 WindmV_1_AVG L
18 WindmV_2_AVG L
19 U_AVG L
20 Winddirec_AVG L
21 Fsoil_1_AVG L
22 Fsoil_2_AVG L
23 empity_AVG L
24 Theta_V_AVG L
25 Theta_m_AVG L
26 Theta_o_AVG L
27 Tair_AVG L
28 RH001_AVG L
29 vpd_kPa_AVG L
30 RH L
31 Rain_TOT L
32 Tsoilave1_AVG L
33 Tsoilave2_AVG L
34 Tsoilave3_AVG L

200 Output_Table 1440.00 Min
1 200 L
2 Day_RTM L
3 Hour_Minute_RTM L
4 Vbattery_AVG L

Estimated Total Final Storage Locations used per day
3268.0

APPENDIX 4.2

Program used for the calibration of IRTs

```
;{21X}
;
*Table 1 Program
  01: 10.000    Execution Interval (seconds)

1: Batt Voltage (P10)
 1: 1       Loc [ Vbatt    ]

2: Internal Temperature (P17)
 1: 2       Loc [ Tpanel   ]

3: Thermocouple Temp (DIFF) (P14)
 1: 1       Reps
 2: 1       5 mV Slow Range
 3: 1       DIFF Channel
 4: 1       Type T (Copper-Constantan)
 5: 2       Ref Temp (Deg. C) Loc [ Tpanel   ]
 6: 3       Loc [ TC       ]
 7: 1.0     Mult
 8: 0.0     Offset

4: Volt (Diff) (P2)
 1: 2       Reps
 2: 5       5000 mV Slow Range
 3: 2       DIFF Channel
 4: 4       Loc [ IRTE_1   ]
 5: 1.0     Mult
 6: 0.0     Offset

5: Thermocouple Temp (DIFF) (P14)
 1: 2       Reps
 2: 1       5 mV Slow Range
 3: 4       DIFF Channel
 4: 3       Type K (Chromel-Alumel)
 5: 2       Ref Temp (Deg. C) Loc [ Tpanel   ]
 6: 6       Loc [ IRTA_1   ]
 7: 1.0     Mult
 8: 0.0     Offset

6: Thermocouple Temp (DIFF) (P14)
 1: 2       Reps
 2: 1       5 mV Slow Range
 3: 6       DIFF Channel
 4: 3       Type K (Chromel-Alumel)
 5: 2       Ref Temp (Deg. C) Loc [ Tpanel   ]
 6: 8       Loc [ IRTA_2   ]
 7: 1.0     Mult
 8: 0.0     Offset

7: If time is (P92)
 1: 0       Minutes into a
 2: 15      Minute Interval
 3: 10      Set Output Flag High

8: Set Active Storage Area (P80)
 1: 1       Final Storage
 2: 100     Array ID

9: Real Time (P77)
 1: 1220    Year,Day,Hour/Minute (midnight = 2400)

10: Average (P71)
 1: 9       Reps
 2: 3       Loc [ TC       ]

11: If time is (P92)
 1: 0       Minutes into a
 2: 1440    Minute Interval
 3: 10      Set Output Flag High

12: Set Active Storage Area (P80)
 1: 1       Final Storage
 2: 200     Array ID

13: Average (P71)
 1: 1       Reps
 2: 1       Loc [ Vbatt    ]

*Table 2 Program
  02: 0.0000    Execution Interval (seconds)

1: Serial Out (P96)
 1: 30      SM192/SM716/CSM1

*Table 3 Subroutines


End Program

-Input Locations-
1 Vbatt     1 1 1
2 Tpanel    1 2 1
3 TC        1 1 1
4 IRTE_1    5 1 1
5 IRTE_2    17 1 1
6 IRTA_1    5 1 1
7 IRTA1_BOD 17 1 1
8 IRTA_2    5 1 1
9 IRTA2_BOD 17 1 1
10 IRTA2_2  1 1 1
11 _________ 1 1 1
12 _________ 1 0 1
13 _________ 1 0 1
14 _________ 1 0 1
15 _________ 1 0 1
16 _________ 17 0 1
17 _________ 1 0 0
18 _________ 1 0 0
19 _________ 0 0 0
20 _________ 0 0 0
21 _________ 0 0 0
22 _________ 0 0 0
23 _________ 0 0 0
24 _________ 0 0 0
25 _________ 0 0 0
26 _________ 0 0 0
27 _________ 0 0 0
28 _________ 0 0 0
-Program Security-
0
0000
0000
```

Program Trace Information File for:
CALIBRA.CSI
T = Program Table Number
N = Sequential Program Instruction Location Number
Instruction = Instruction Number and Name

Inst ExTm = Individual Instruction Execution Time
Block ExTm = Cumulative Execution Time for program block,
i.e., subroutine
Prog ExTm = Cumulative Total Program Execution Time

```
Output Flag High

Inst  Block   Prog     Inst  Block
Prog

ExTm   ExTm   ExTm     ExTm   ExTm
ExTm
T|N|Instruction
(msec) (msec) (msec)   (msec) (msec)
(msec)
---------------                    ---
--- ------ ------   ------ ------ ---
---
1|1|10 Batt Voltage
7.6    7.6    7.6      7.6    7.6
7.6
1|2|17 Internal Temperature
14.0   21.6   21.6     14.0   21.6
21.6
1|3|14 Thermocouple Temp (DIFF)
81.9  103.5  103.5     81.9  103.5
103.5
1|4|2 Volt (Diff)
21.6  125.1  125.1     21.6  125.1
125.1
1|5|14 Thermocouple Temp (DIFF)
124.6  249.7  249.7    124.6  249.7
249.7
1|6|14 Thermocouple Temp (DIFF)
124.6  374.3  374.3    124.6  374.3
374.3
1|7|92 If time is
0.3  374.6  374.6      0.3  374.6
374.6
 Output Flag Set @ 17 for Array 100
1|8|80 Set Active Storage Area
0.2  374.8  374.8      0.2  374.8
374.8
1|9|77 Real Time
0.1  374.9  374.9      1.0  375.8
375.8
 Output Data 3 Values
1|10|71 Average
5.4  380.3  380.3     29.1  404.9
404.9
 Output Data 9 Values
1|11|92 If time is
0.3  380.6  380.6      0.3  405.2
405.2
 Output Flag Set @ 111 for Array 200
1|12|80 Set Active Storage Area
0.2  380.8  380.8      0.2  405.4
405.4
1|13|71 Average                    1.4
382.2  382.2      5.1  410.5  410.5
 Output Data 1 Values

Program Table 1 Execution Interval   10.000
Seconds
```

Table 1 Estimated Total Program Execution Time in msec 382.2 w/Output 410.5

Table 1 Estimated Total Final Storage Locations used per day 1250.0

---------- Table 2 ----------
2|1|96 Serial Out 2.0 2.0 2.0 2.0 2.0 2.0

Program Table 2 Execution Interval 0.000 Seconds

Table 2 Estimated Total Program Execution Time in msec 2.0 w/Output 2.0

Table 2 Estimated Total Final Storage Locations used per day 0.0

Estimated Total Final Storage Locations used per day 1250.0

```
Final Storage Label File for:
CALIBRA.CSI

100 Output_Table  15.00 Min
1 100 L
2 Year_RTM  L
3 Day_RTM  L
4 Hour_Minute_RTM  L
5 TC_AVG  L
6 IRTE_1_AVG  L
7 IRTE_2_AVG  L
8 IRTA_1_AVG  L
9 IRTA1_BOD_AVG  L
10 IRTA_2_AVG  L
11 IRTA2_BOD_AVG  L

200 Output_Table 1440.00 Min
1 200 L
2 Vbatt_AVG  L


Estimated Total Final Storage Locations
used per day 1250.0
```

APPENDIX 4.3

Program used for the calibration of Vaisala CS500 Air temperature and Relative humidity probe (MJ Savage, 2001)

```
;{21X}
;c:\campbell\logprog\LI610\vaiscal5.csi
;for routine calibration - for five CS500
;Vaisalas - dewpoint incremented by 1 °C every 30 min
;data collected for the last 5 min of each 30 min cycle
;When dewpoint is 1.5 °C below the airstream
temperature, dewpoint
;is reset to 0 °C

;c:\campbell\logprog\LI610\vaiscat5.csi
;for quick testing - for five CS500
;Vaisalas - dewpoint incremented by 10 °C every 2 min
;data collected for the last 1 min of each 2 min cycle
;When dewpoint is 3 °C below panel temperature,
dewpoint
;is reset to 0 °C

;Program: vaiscal5.csi M J Savage 17 October 2001
;Program to calibrate five Vaisala T/RH probes
;using a LI-COR 610 dewpoint generator
;
;Program sets LI-COR 610 Tdp at 0 °C for 30 min. All
sensor measurements
;are made in the last 5 min of a 30 min period - means
are output.
;LI-COR 610 Tdp is then increased by 1 °C. This
process continues until
;the Tdp is greater than the panel temperature less 3 °C.
When this happens,
;the Tdp of the LI-COR 610 is set to 0 °C and the
process starts all over
;again.

;Caps of the Vaisala's were removed to reduce the lag
time of the
;changes in relative humidity

;The Bev-a-line tubing from the LI-COR 610 was
inserted in the top of a
;narrow (about 50 mm diameter) plastic tubing. The two
Vaisala's were pushed
;into the tubing (sensor cap off). A TC was also
inserted. The tube partially
;sealed at the other end.

;Sensor connections are as follows:
;Vaisala #1 (CSI old wiring): Black 1H; brown 1L
;       red 12 V line
;       all other wires to ground
;The newer CS500 sensors have:
;       Brown 1H; black 1L
;       red 12 V line
;       all other wires to ground
;The sensors directly from Vaisala (50Y or 50YC)
;have the following wiring:
;       Brown 1H; black 1L
;       yellow 12 V line
;       all other wires to ground
;Some of the sensors directly from Vaisala (50YC)
;have the following wiring:
;       Violet 1H; brown 1L
;       yellow 12 V line
;       all other wires to ground
;
;LI-COR 610 dewpoint generator connection: analogue
output from
;       generator connected to 7H and 7L
;       command input to generator connected to CAO 1 and
ground
;

;Copper-constantan placed close to sensor region of Vaisala's
connected
;       to 6H and 6L

*Table 1 Program
  01: 1.0      Execution Interval (seconds)

1: Internal Temperature (P17)
  1: 1       Loc [ Tpanel   ]

2: Volt (SE) (P1)
  1: 1       Reps
  2: 5       5000 mV Slow Range
  3: 1       SE Channel
  4: 8       Loc [ TairV1   ]
  5: 0.1     Mult
  6: -40     Offset

3: Volt (SE) (P1)
  1: 1       Reps
  2: 5       5000 mV Slow Range
  3: 2       SE Channel
  4: 9       Loc [ RHVal_1  ]
  5: 0.1     Mult
  6: 0.0     Offset

4: Saturation Vapor Pressure (P56)
  1: 8       Temperature Loc [ TairV1   ]
  2: 10      Loc [ eV1      ]

5: Z=X*Y (P36)
  1: 9       X Loc [ RHVal_1  ]
  2: 10      Y Loc [ eV1      ]
  3: 10      Z Loc [ eV1      ]

6: Z=X*F (P37)
  1: 10      X Loc [ eV1      ]
  2: 0.01    F
  3: 10      Z Loc [ eV1      ]

7: Volt (SE) (P1)
  1: 1       Reps
  2: 5       5000 mV Slow Range
  3: 3       SE Channel
  4: 11      Loc [ TairV2   ]
  5: 0.1     Mult
  6: -40     Offset

8: Volt (SE) (P1)
  1: 1       Reps
  2: 5       5000 mV Slow Range
  3: 4       SE Channel
  4: 12      Loc [ RHVal_2  ]
  5: 0.1     Mult
  6: 0.0     Offset

9: Saturation Vapor Pressure (P56)
  1: 8       Temperature Loc [ TairV1   ]
  2: 13      Loc [ eV2      ]

10: Z=X*Y (P36)
  1: 12      X Loc [ RHVal_2  ]
  2: 13      Y Loc [ eV2      ]
  3: 13      Z Loc [ eV2      ]
```

```
11: Z=X*F (P37)
 1: 13      X Loc [ eV2      ]
 2: 0.01    F
 3: 13      Z Loc [ eV2      ]

12: Volt (SE) (P1)
 1: 1       Reps
 2: 5       5000 mV Slow Range
 3: 5       SE Channel
 4: 14      Loc [ TairV3     ]
 5: 0.1     Mult
 6: -40     Offset

13: Volt (SE) (P1)
 1: 1       Reps
 2: 5       5000 mV Slow Range
 3: 6       SE Channel
 4: 15      Loc [ RHVal_3    ]
 5: 0.1     Mult
 6: 0.0     Offset

14: Saturation Vapor Pressure (P56)
 1: 14      Temperature Loc [ TairV3    ]
 2: 16      Loc [ eV3        ]

15: Z=X*Y (P36)
 1: 15      X Loc [ RHVal_3  ]
 2: 16      Y Loc [ eV3      ]
 3: 16      Z Loc [ eV3      ]

16: Z=X*F (P37)
 1: 16      X Loc [ eV3      ]
 2: 0.01    F
 3: 16      Z Loc [ eV3      ]

17: Volt (SE) (P1)
 1: 1       Reps
 2: 5       5000 mV Slow Range
 3: 7       SE Channel
 4: 17      Loc [ TairV4     ]
 5: 0.1     Mult
 6: -40     Offset

18: Volt (SE) (P1)
 1: 1       Reps
 2: 5       5000 mV Slow Range
 3: 8       SE Channel
 4: 18      Loc [ RHVal_4    ]
 5: 0.1     Mult
 6: 0.0     Offset

19: Saturation Vapor Pressure (P56)
 1: 17      Temperature Loc [ TairV4    ]
 2: 19      Loc [ eV4        ]

20: Z=X*Y (P36)
 1: 18      X Loc [ RHVal_4  ]
 2: 19      Y Loc [ eV4      ]
 3: 19      Z Loc [ eV4      ]

21: Z=X*F (P37)
 1: 19      X Loc [ eV4      ]
 2: 0.01    F
 3: 19      Z Loc [ eV4      ]

22: Volt (SE) (P1)
 1: 1       Reps
 2: 5       5000 mV Slow Range
 3: 7       SE Channel
 4: 20      Loc [ TairV5     ]
 5: 0.1     Mult
 6: -40     Offset

23: Volt (SE) (P1)
 1: 1       Reps
 2: 5       5000 mV Slow Range
 3: 8       SE Channel
 4: 21      Loc [ RHVal_5    ]
 5: 0.1     Mult
 6: 0.0     Offset

24: Saturation Vapor Pressure (P56)
 1: 20      Temperature Loc [ TairV5    ]
 2: 22      Loc [ eV5        ]

25: Z=X*Y (P36)
 1: 21      X Loc [ RHVal_5  ]
 2: 22      Y Loc [ eV5      ]
 3: 22      Z Loc [ eV5      ]

26: Z=X*F (P37)
 1: 22      X Loc [ eV5      ]
 2: 0.01    F
 3: 22      Z Loc [ eV5      ]

27: Thermocouple Temp (DIFF) (P14)
 1: 1       Reps
 2: 1       5 mV Slow Range
 3: 6       In Chan
 4: 1       Type T (Copper-Constantan)
 5: 1       Ref Temp Loc [ Tpanel    ]
 6: 6       Loc [ TairTC     ]
 7: 1       Mult
 8: 0       Offset

28: Z=X (P31)
 1: 6       X Loc [ TairTC     ]
 2: 23      Z Loc [ TairTCcal ]

29: Z=X+F (P34)
 1: 2       X Loc [ TairTC1p5 ]
 2: 0       F
 3: 2       Z Loc [ TairTC1p5 ]

30: IF (X<=>F) (P89)
 1: 2       X Loc [ TairTC1p5 ]
 2: 1       =
 3: 1       F
 4: 30      Then Do

31: Z=F (P30)
 1: -250    F
 2: 4       Z Loc [ Vdewpoint ]

32: Else (P94)

;For testing make this 1 min into a 2 min interval
33: If time is (P92)
 1: 0       Minutes into a
 2: 20      Minute Interval
 3: 30      Then Do

;For testing use an increment of 10 oC (1000 mV)
;For routine calibration, use 1 oC increment (100 mV)
34: Z=X+F (P34)
 1: 4       X Loc [ Vdewpoint ]
 2: 100     F
 3: 4       Z Loc [ Vdewpoint ]

35: End (P95)

36: End (P95)

37: Analog Out (P21)
 1: 1       CAO Chan
 2: 4       mV Loc [ Vdewpoint ]

;Dew point calibrator sensor connects to input channel 7
(differential)
```

```
38:  Volt (Diff) (P2)
 1: 1       Reps
 2: 5       5000 mV Slow Range
 3: 7       In Chan
 4: 5       Loc [ Tdpcalibr ]
 5: 0.01    Mult
 6: 0       Offset

39:  Z=X*F (P37)
 1: 4       X Loc [ Vdewpoint ]
 2: 0.01    F
 3: 7       Z Loc [ Tdewptin  ]

40:  Saturation Vapor Pressure (P56)
 1: 5       Temperature Loc [ Tdpcalibr ]
 2: 25      Loc [ ecal     ]

41:  Saturation Vapor Pressure (P56)
 1: 23      Temperature Loc [ TairTCcal ]
 2: 24      Loc [ RHcal    ]

42:  Z=X/Y (P38)
 1: 25      X Loc [ ecal     ]
 2: 24      Y Loc [ RHcal    ]
 3: 24      Z Loc [ RHcal    ]

43:  Z=X*F (P37)
 1: 24      X Loc [ RHcal    ]
 2: 100     F
 3: 24      Z Loc [ RHcal    ]

;Previously used 3 oC below panel temperature
44:  Z=X+F (P34)
 1: 23      X Loc [ TairTCcal ]
 2: -1.5    F
 3: 2       Z Loc [ TairTC1p5 ]

45:  IF (X<=>Y) (P88)
 1: 5       X Loc [ Tdpcalibr ]
 2: 3       >=
 3: 2       Y Loc [ TairTC1p5 ]
 4: 30      Then Do

;This was -500 (for -5 oC)
46:  Z=F (P30)
 1: 0       F
 2: 4       Z Loc [ Vdewpoint ]

47:  End (P95)

;For testing, make this 1 min into a 2 min interval
48:  If time is (P92)
 1: 25      Minutes into a
 2: 30      Minute Interval
 3: 10      Set Output Flag High

49:  Set Active Storage Area (P80)
 1: 1       Final Storage
 2: 100     Array ID

50:  Resolution (P78)
 1: 1       high resolution

51:  Real Time (P77)
 1: 1110    Year,Day,Hour/Minute

52:  Average (P71)
 1: 1       Reps
 2: 1       Loc [ Tpanel    ]

53:  Average (P71)
 1: 22      Reps
 2: 4       Loc [ Vdewpoint ]

*Table 2 Program
 01: 0.0      Execution Interval (seconds)

*Table 3 Subroutines

End Program

-Input Locations-
1 Tpanel     1 2 1
2 TairTC1p5  1 1 1
3 _________  1 2 1
4 Vdewpoint  1 4 3
5 Tdpcalibr  5 3 1
6 TairTC     1 1 1
7 Tdewptin   1 0 1
8 TairV1     1 2 1
9 RHVal_1    1 1 1
10 eV1       1 3 3
11 TairV2    1 0 1
12 RHVal_2   1 1 1
13 eV2       1 3 3
14 TairV3    1 1 1
15 RHVal_3   1 1 1
16 eV3       1 3 4
17 TairV4    1 1 1
18 RHVal_4   1 1 1
19 eV4       1 3 3
20 TairV5    1 1 1
21 RHVal_5   1 1 1
22 eV5       1 3 3
23 TairTCcal 1 2 1
24 RHcal     1 2 3
25 ecal      1 1 1
26 _________ 1 0 0
27 _________ 0 0 0
28 _________ 0 0 0
29 _________ 0 0 0
-Program Security-
0
0000
0000
```

Program Trace Information File for: VAISCAL5.CSI
T = Program Table Number
N = Sequential Program Instruction Location Number
Instruction = Instruction Number and Name

Inst ExTm = Individual Instruction Execution Time
Block ExTm = Cumulative Execution Time for program block,
i.e., subroutine
Prog ExTm = Cumulative Total Program Execution Time

Output Flag High

T|N| Instruction	Inst ExTm (msec)	Block ExTm (msec)	Prog ExTm (msec)
1|1|17 Internal Temperature	14.0	14.0	14.0
1|2|1 Volt (SE)	12.1	26.1	26.1
1|3|1 Volt (SE)	12.1	38.2	38.2
1|4|56 Saturation Vapor Pressure	4.2	42.4	42.4
1|5|36 Z=X*Y	1.2	43.6	43.6
1|6|37 Z=X*F	0.9	44.5	44.5
1|7|1 Volt (SE)	12.1	56.6	56.6
1|8|1 Volt (SE)	12.1	68.7	68.7
1|9|56 Saturation Vapor Pressure	4.2	72.9	72.9
1|10|36 Z=X*Y	1.2	74.1	74.1
1|11|37 Z=X*F	0.9	75.0	75.0
1|12|1 Volt (SE)	12.1	87.1	87.1
1|13|1 Volt (SE)	12.1	99.2	99.2
1|14|56 Saturation Vapor Pressure	4.2	103.4	103.4
1|15|36 Z=X*Y	1.2	104.6	104.6
1|16|37 Z=X*F	0.9	105.5	105.5
1|17|1 Volt (SE)	12.1	117.6	117.6
1|18|1 Volt (SE)	12.1	129.7	129.7
1|19|56 Saturation Vapor Pressure	4.2	133.9	133.9
1|20|36 Z=X*Y	1.2	135.1	135.1
1|21|37 Z=X*F	0.9	136.0	136.0
1|22|1 Volt (SE)	12.1	148.1	148.1
1|23|1 Volt (SE)	12.1	160.2	160.2
1|24|56 Saturation Vapor Pressure	4.2	164.4	164.4
1|25|36 Z=X*Y	1.2	165.6	165.6
1|26|37 Z=X*F	0.9	166.5	166.5
1|27|14 Thermocouple Temp (DIFF)	81.9	248.4	248.4
1|28|31 Z=X	0.5	248.9	248.9
1|29|34 Z=X+F	0.9	249.8	249.8
1|30|89 If (X<=>F)	0.4	250.2	250.2
1|31|30 Z=F	0.3	250.5	250.5
1|32|94 Else	0.2	250.7	250.7
1|33|92 If time is	0.3	251.0	251.0
1|34|34 Z=X+F	0.9	251.9	251.9
1|35|95 End	0.2	252.1	252.1
1|36|95 End	0.2	252.3	252.3
1|37|21 Analog Out	10.5	262.8	262.8
1|38|2 Volt (Diff)	14.7	277.5	277.5
1|39|37 Z=X*F	0.9	278.4	278.4
1|40|56 Saturation Vapor Pressure	4.2	282.6	282.6
1|41|56 Saturation Vapor Pressure	4.2	286.8	286.8
1|42|38 Z=X/Y	2.7	289.5	289.5
1|43|37 Z=X*F	0.9	290.4	290.4
1|44|34 Z=X+F	0.9	291.3	291.3
1|45|88 If (X<=>Y)	0.6	291.9	291.9
1|46|30 Z=F	0.3	292.2	292.2
1|47|95 End	0.2	292.4	292.4
1|48|92 If time is	0.3	292.7	292.7
Output Flag Set @ 148 for Array 100			
1|49|80 Set Active Storage Area	0.2	292.9	292.9
1|50|78 Resolution	0.4	293.3	293.3
1|51|77 Real Time	0.1	293.4	293.4
1.0 294.3 294.3			
Output Data 3 Values			
1|52|71 Average	1.4	294.8	294.8
5.1 299.4 299.4			
Output Data 1 Values			
1|53|71 Average	11.9	306.7	306.7
68.1 367.5 367.5			
Output Data 22 Values			

Program Table 1 Execution Interval 1.000 Seconds

Table 1 Estimated Total Program Execution Time in msec 306.7 w/Output 367.5

Table 1 Estimated Total Final Storage Locations used per day 2592.0

Estimated Total Final Storage Locations used per day 2592.0

Final Storage Label File for:
VAISCAL5.CSI

100 Output_Table 30.00 Min
1 100 L
2 Year_RTM H
3 Day_RTM H
4 Hour_Minute_RTM H
5 Tpanel_AVG H
6 Vdewpoint_AVG H
7 Tdpcalibr_AVG H
8 TairTC_AVG H
9 Tdewptin_AVG H
10 TairV1_AVG H
11 RHVal_1_AVG H
12 eV1_AVG H
13 TairV2_AVG H
14 RHVal_2_AVG H
15 eV2_AVG H
16 TairV3_AVG H
17 RHVal_3_AVG H
18 eV3_AVG H
19 TairV4_AVG H
20 RHVal_4_AVG H
21 eV4_AVG H
22 TairV5_AVG H
23 RHVal_5_AVG H
24 eV5_AVG H
25 TairTCcal_AVG H
26 RHcal_AVG H
27 ecal_AVG H

Estimated Total Final Storage Locations
used per day 2592.0